ASSAY DESIGN FOR IMMUNOLOGICAL RESPONSES ON POLYMER CAPSULES

DESIGNING CELL- AND PROTEIN-BASED IN VITRO ASSAYS AS MODELS FOR FIBROTIC RESPONSES TO IMPLANTED HYDROGEL CAPSULES

By SERGIO RAEZ-VILLANUEVA, B.SC.

A Thesis Submitted to the School of Graduate Studies in Partial Fulfilment of the Requirements for the Degree Master of Science

McMaster University MASTER OF SCIENCE (2022) Hamilton, Ontario (Medical Sciences)

TITLE: Designing Cell- and Protein-Based in vitro Assays as Models for Fibrotic Responses to Implanted Hydrogel Capsules. AUTHOR: Sergio Raez-Villanueva, B.Sc. (McMaster University) SUPERVISOR: Dr. A.C. Holloway NUMBER OF PAGES: xix, 104

Lay Abstract

In North America, one in eleven adults, or about 415 million people, have diabetes. It is projected that by 2030, around 8% of the world population will be diagnosed with this disease. A common form of treatment is through the frequent injection of insulin, but this is costly, requires multiple daily interventions, and cannot prevent regular excursions from the ideal blood glucose range. Cell-based therapies have a lot of promise in treating several chronic diseases including diabetes. Donor and stem-cell derived islets can be implanted into patients with type 1 diabetes and have been shown to function for over a year, albeit at the price of systematic immune suppression. Alternatively, cells that produce insulin can be placed inside immune-evasive capsules and implanted, potentially providing continuous blood glucose regulation without the need for daily insulin injections. However, this novel form of treatment is limited by the encapsulated cells' survival once implanted. Cell survival can be affected by the body's response to a foreign body (the capsule), causing deposition of protein or cells on the capsule surface which can limit the oxygen supply to cells in the capsule and the ability of insulin to leave the capsule in a timely fashion. The goal of this project is to develop assays to screen new capsule formulations. This can advance research by using capsules more readily accepted by the body, leading to a more promising and long-term treatment of diabetes.

Abstract

It is projected that, by 2030, 8% of all adults in the world will have diabetes mellitus and treatment will account for 10% of the total healthcare budget in many countries. Polymeric biomaterial research has led to the design of robust polymer hydrogel capsules to develop curative cell-based therapies for chronic disorders such as diabetes mellitus. Encapsulation of insulin-producing beta cells within synthetic, semi-permeable polymer hydrogels can avoid host immune rejection including fibrotic responses, and thus holds the promise of a long-term curative treatment of this disease. There is a paucity of literature regarding methods available for standardized *in vitro* screening of synthetic polymer hydrogel capsules to predict host responses *in vivo*. Thus, the focus of this thesis was to design *in vitro* assays able to screen for subsequent *in vivo* fibrotic responses. Two dimensional ('2D') (cell attachment to thin film hydrogel coatings) and three dimensional ('3D') (cell attachment and protein adsorption to hydrogel capsules) *in vitro* experiments were designed and tested in an iterative process to assess fibrotic responses to a diverse group of polymer hydrogels. Cell attachment assays included fibroblast (NIH 3T3) and macrophage (RAW 264.7) cell lines, and protein adsorption assays included proteins used to model fibrosis including fibrinogen and lysozyme. For some formulations, *in vitro* assays were compared with *in vivo* data on pericapsular cellular overgrowth (PCO) after being implanted into mice. A binomial logistic regression model was designed and validated to assess whether the '3D' *in vitro* assays correlated with *in vivo* PCO responses. It was found that the RAW 264.7 cell attachment assay was significantly correlated with PCO outcomes *in vivo*, demonstrating

for the first time a simple, cost-effective, and rapid *in vitro* cell-based approach to screen and select capsules with lower fibrotic potential to be further tested in animals.

Multimedia Abstract

For a lay summary of the thesis presented in a 1-minute video format, visit the following link: https://www.youtube.com/watch?v=VhLzt_tEz-s

This video was uploaded to the McMaster School of Graduate Studies' YouTube Channel as a Gradflix submission to showcase my MSc research. This video was ranked 2nd place overall by a panel of judges at McMaster University; it was also awarded the Dean's Award for Excellence in Communicating Graduate Research.

Acknowledgements

One of my favourite parts about partaking in projects is the nature of collaborations and learning from so many individuals – a thesis project is no different. The conception, experimental design, delivery, editing, and writing of my thesis would not have been possible without the support and feedback from so many dedicated people including fellow scientists and researchers throughout my two years of my MSc. First, I would like to thank the Mitacs Accelerate Program and the Natural Sciences & Engineering Research Council (NSERC) for the funding opportunities that made my research possible. A huge thank you to all past and present staff and students from the Allarta Life Science Inc team who welcomed me since day one, inviting me into R&D meetings and having fruitful discussions. I have felt a part of the team from the very beginning, from talking science, to talking about games, or enjoying together the ever-delicious hot dogs from the hot dog roller. A very special thank you to Carl Ellis, Samantha Ros, Alison Stewart, Nick Burke, Mitchell Johnson, Nicole Mangiacotte, Elody Julien, Carina Yan, Yichen Zhou, Nadia Al-Banna, Felix Gross, Tobias Fuehrmann, and Roopali Chaudhary for all their support throughout my time at the company. From organizing meetings, to discussing about my project and offering ideas along the way, to keeping the lab looking beautiful and operational with supplies, to putting time aside from their own busy schedules to provide me with materials to be able to do my experiments, to being awesome people to work with…the list goes on, but it must be stated that without you this thesis would not be done! Saying ‘thank you’ is a very big understatement! Thank you from the bottom of my heart to Harald Stover and Maria

Antonakos for allowing me to work in their company and allowing me to learn so many new skills and making some wonderful memories along the way! Harald, please know your guidance and expertise in polymer chemistry is inspiring and, as a biochemist myself, I am inspired by you to learn more deeply about the "chemistry and polymer world," and about German culture!

Huge thanks to Jeremy Hirota, a member of my committee and an instructor for one of my graduate courses which provided me a thorough understanding of the immense (and complex) field that immunology has to offer.

To all my colleagues and lab mates in the Holloway lab, a great big hug, and best wishes as some of you wrap up your studies, some are halfway through the grind (keep it up!), or some are just beginning their journey in the great adventures that science offers. Please know that our many years, laughs, and conversations together have shaped who I am as a person and researcher. A big hug too to Alison Holloway, for allowing me to develop as a scientist for so many years now – supporting me not only academically and professionally but also caring for me as a person trying to get through the many ups and downs that life offers – I am grateful for all the guidance and dedication that you have given towards the members of your lab. It has been wonderful to work together, get to know you and your many diverse projects, and work for a fantastic supervisor since 2015.

Finally, a great kiss and hug (or how we say in Spanish, "un gran beso y abrazo") to my girlfriend, Lauren Negrazis, and my dear Peruvian family. For anyone else that helped me along the way and that I have not mentioned here, please know that I appreciate your support, no matter how big or small – thank you all for being you.

Table of Contents

List of Figures

List of Tables

List of all Abbreviations and Symbols

Abbreviation/Symbol	Definition
µ	Micro-
2D	Two dimensional
3D	Three dimensional
ACN	Acetonitrile
AM	Acetoxymethyl
ANOVA	Analysis of variance
APA	Alginate-PLL-alginate
APC	Antigen presenting cell
APTES	(3-aminopropyl)triethoxysilane
ATP	Adenosine triphosphate
Ba^{2+}	Barium ion
CA	Calcium alginate
Ca^{2+}	Calcium ion
cAMP	Cyclic adenosine monophosphate
$CD4^{+}$	Cluster of differentiation 4 protein positive
$CD8^{+}$	Cluster of differentiation 8 protein positive
CLSM	Confocal laser scanning microscope
d	Deci-
dH_2O	Deionized water
ELISA	Enzyme-linked immunosorbent assay
EtOH	Ethanol
FITC	Fluorescein isothiocyanate
GLUT1	Glucose transporter 1
g	Gram
HBS	HEPES-buffered saline
HEPES	4-(2-hydroxyethyl)-1-piperazineethanesulfonic acid
IFNγ	Interferon gamma
IIT	Intensive insulin therapy
IL1	Interleukin 1
IL6	Interleukin 6
iNOS	Inducible nitric oxide synthase
INS	Insulin
IP	Intraperitoneal
IRS	Insulin receptor substrate
K^{+}	Potassium ion
kDa	Kilodalton
L	Litre
m	Milli- or Metre
M	Molar (moles/L)
NaAlg	Sodium alginate

NFE2L2	Nuclear factor, erythroid 2 like 2
NSF	N-ethylmaleimide-sensitive factor
PCO	Pericapsular cellular overgrowth
PDE3B	Phosphodiesterase 3B
PI3K	phosphoinositide-3-kinase
PLL	Poly-L-lysine
PMM	poly(methyl vinyl ether-alt-maleic anhydride)
PY	Proprietary
RFU	Relative fluorescent units
ROS	Reactive oxygen species
SNARE	Soluble NSF attachment protein receptor
TBC1D4	Tre-2/USP6, BUB2, cdc16 domain family member 4
TMTD	Triazole–thiomorpholine dioxide
TNFα	Tumor necrosis factor alpha

Declaration of Academic Achievement

All capsules tested in this thesis were generated by employees of Allarta Life Science Inc (Allarta). The *in vivo* PCO data used in the logistic regression model was collected and curated by employees of Allarta. All other experiments, imaging, and subsequent analyses were performed by the author of this thesis.

1 Introduction

1.1 Diabetes Mellitus Overview

It is projected that, by 2030, between 4.4% to 7.7% of all adults in the world will have diabetes mellitus (Shaw et al., 2010; Wild et al., 2004). Some estimates are as high as 10.4% by 2040 (Ogurtsova et al., 2017), with significant rates of increase in developing countries (Shaw et al., 2010; Smyth & Heron, 2006). While the cause of diabetes has been linked with genetic defects, environmental stressors, and infections, to name a few (American Diabetes Association, 2008), a strong link between obesity and diabetes has also been found (Smyth & Heron, 2006; Verma & Hussain, 2017). Diabetes and its comorbidities are a significant burden on the healthcare system (Ryan, 2009; Smyth & Heron, 2006); in 2017, the International Diabetes Federation estimated that the treatment of diabetes currently accounts for approximately 14% of the total healthcare expenditure in the U.S. (American Diabetes Association, 2018).

1.1.1 Hyperglycemia

Blood sugar regulation, also known as glucose homeostasis, is an essential process that requires the careful regulation of hormones such as glucagon (raises blood sugar) and insulin (lowers blood sugar). Glucagon is a peptide hormone essential for glucose homeostasis by raising plasma glucose levels in response to insulin, serving as a counterregulatory mechanism (Freychet, 1988; Unger & Orci, 2010; Vidnes & Øyasaeter, 1977). Glucagon promotes hepatic glucose output (gluconeogenesis) and decreases

glycolysis in a concerted fashion via multiple mechanisms in the mitochondria. A thorough discussion of these molecular pathways have been summarized by Jiang & Zhang (2003). Insulin can suppress glucagon through phosphoinositide-3-kinase (PI3K) activity and phosphodiesterase-mediated degradation of cyclic adenosine monophosphate (cAMP) (Elliott et al., 2015; Ravier & Rutter, 2005). In this way, glucagon and insulin are tightly regulated, and glucose homeostasis can be maintained (Unger & Orci, 2010). Hyperglycemia may occur due to a disruption of this balance, and this condition is diagnosed in humans when blood glucose levels are over 140 mg/dL or 7.8 mM (Moghissi et al., 2009). Chronic hyperglycemia can lead to cardiovascular and kidney disease, blindness, stroke, and, if untreated, death (Bornfeldt & Tabas, 2011). To prevent hyperglycemia, glucose levels in circulation are maintained by insulin secretion from pancreatic beta cells to promote glucose uptake and storage in peripheral tissues.

1.1.2 Insulin Production and Regulation

To limit high glucose levels in the blood, pancreatic beta cells must synthesize and store insulin, and subsequently release it rapidly and as needed in response to increasing glucose levels. In addition, beta cells must act in response to other time-dependent stimuli including overall stress and physical exercise. The insulin gene (*INS*) is first transcribed into mRNA and translated into pre-proinsulin, which contains an N-terminal signal sequence which allows it to be transported into the rough endoplasmic reticulum (Boland et al., 2017; Støy et al., 2021). There, it is cleaved to proinsulin and stabilized by three disulfide bonds (Steiner, 2011). The resulting folded protein is transported to the Golgi

apparatus where immature insulin granules form to be eventually secreted from the beta cells (Boland et al., 2017; Fu et al., 2013) in response to increasing blood glucose levels. The most studied mechanistic pathway in insulin secretion revolves, unsurprisingly, around glucose. In humans, glucose is transported into beta cells through glucose transporter 1 (GLUT1). Glucokinase, a glucose-phosphorylating enzyme, metabolizes glucose into glucose-6 phosphate, providing adenosine triphosphate (ATP) that leads to the closure of ATP-sensitive potassium ion (K^+) channels in the cell membrane (Ashcroft et al., 1984; Cook & Hales, 1984). Since K^+ can no longer diffuse out of the cells, the potential difference across the cell membrane becomes more positive, or depolarized, leading to the opening of voltage gated calcium ion (Ca^{2+}) channels (MacDonald et al., 2001; Xia et al., 2008) embedded in the cell membrane and the diffusion of Ca^{2+} into the cell (Ashcroft et al., 1994). Vesicles containing insulin within beta cells are then able to fuse with the plasma membrane thanks to the Ca^{2+} influx, mediated by soluble N-ethylmaleimide-sensitive factor (NSF) attachment protein receptor (SNARE) proteins. The contents of these secretory granules can then enter the bloodstream and insulin is finally delivered in the circulation to promote the uptake of glucose by other organs (MacDonald et al., 2005).

Circulating insulin binds to insulin receptor substrate (IRS) receptors in skeletal muscle cells and activate PI3K, which lead to the subsequent activation of protein kinase B, also known as Akt. Akt phosphorylates and inhibits the Rab-GAP activating protein tre-2/USP6, BUB2, cdc16 domain family member 4 (TBC1D4). (Klip et al., 2014;

O'Neill, 2013; Petersen & Shulman, 2018). Overall, insulin-induced TBC1D4 phosphorylation releases glucose transporter 4 (GLUT4) from intracellular compartments; GLUT4 is then translocated to the plasma membrane to facilitate glucose uptake into the cell (Ishikura & Klip, 2008; Sano et al., 2003). From there, glucose is used by the cell in metabolic processes to produce glycogen and provide energy requirements for normal function.

Insulin sensitivity refers to how well cells respond to insulin released by beta cells. There have been several methods proposed to study insulin sensitivity (Gutch et al., 2015); these are usually based on measuring glucose levels in the body and how effectively cells uptake glucose in response to insulin. While the ability for insulin to allow glucose uptake by GLUT4 translocation into the plasma membrane is one of the best studied functional effects of insulin in muscle, other pathways and markers are also involved in other cell types. These pathways, including those involved in adipocytes and hepatocytes, are described in more detail by Petersen & Shulman (2018). For example, in white adipocytes, insulin also activates PI3K but, in addition to stimulating glucose uptake in a similar fashion as in muscle cells, it also suppresses lipolysis by activating phosphodiesterase 3B (PDE3B) which degrades cAMP and finally supresses pro-lipolytic processes in the cell. In liver and skeletal muscle cells, Akt activation by insulin is also known to assist in the intracellular production of glycogen by inhibiting glycogen synthase kinase 3, thereby promoting glycogen synthase activity (O'Neill, 2013). In addition to these pathways, several adipokines such as leptin, adiponectin, and vaspin

produced in the liver and in adipose tissue are some examples of mediators affecting insulin sensitivity (Nicholson et al., 2018). These mediators can cause effects including direct responses to insulin such as glucose uptake as well as other indirect responses like hepatic glucose production (Petersen & Shulman, 2018).

1.1.3 Types of Diabetes Mellitus and Pathologies

Diabetes mellitus is characterized by defects in insulin secretion, insulin action, or both, leading to chronic hyperglycemia (American Diabetes Association, 2004). The two most common forms of diabetes mellitus are type 1 and type 2 diabetes. Type 1 diabetes, accounting for 5 to 10% of all diabetes cases, results from the autoimmune destruction of beta cells in the pancreas. Individuals affected by this disease depend on an exogenous source of insulin (American Diabetes Association, 2004; Smyth & Heron, 2006). Chronic hyperglycemia in type 2 diabetes can result from insulin resistance with normal insulin production/secretion, normal insulin sensitivity at peripheral tissues but impaired insulin production/secretion through a loss of beta cell function or number, or both insulin resistance and impaired beta cell function (American Diabetes Association, 2004). Individuals with type 2 diabetes may be able to keep their blood glucose concentration at normal levels through careful diet and exercise, although some others may require anti-diabetic medications (Piya et al., 2010) or exogenous insulin treatment (Smyth & Heron, 2006).

In type 1 diabetes, beta cell destruction occurs with insulitis activating antigen presenting cells (APCs). APCs activate cluster of differentiation 4 protein positive ($CD4^+$) helper-T cells, leading to cytokine release. These cytokines activate cluster of differentiation 8 protein positive ($CD8^+$) cytotoxic–T cells (Feau et al., 2012), which lead to the destruction of beta cells (Tomita, 2017). Additionally, cytokines can alter intracellular Ca^{2+} levels by depleting Ca^{2+} in the endoplasmic reticulum and consequently increasing Ca^{2+} influx. The cytokine interleukin 1 (IL1) causes an increase in the expression of inducible nitric oxide synthase (iNOS) in beta cells which may lead to immune-mediated beta cell destruction (Corbett & McDaniel, 1995; Yasuda et al., 2009). As such, cytokine-induced calcium disruptions may lead to beta cell death and reduce insulin release in both type 1 and type 2 diabetes (Ramadan et al., 2011). Obesity can also increase the risk of developing type 2 diabetes. Obesity has been linked with increased secretion of adipokines, fatty acids, and proinflammatory cytokines by adipocytes; changes in circulating levels of all these factors have been shown to play a role in beta cell failure in type 2 diabetes (Kahn et al., 2006; Nicholson et al., 2018). For instance, while fatty acids can enhance insulin secretion, they can be lipotoxic and lead to beta cell dysfunction or death (Boden, 2005; Ježek et al., 2018; Orci et al., 1973). Moreover, adiposity can further recruit more cytokines as a positive feedback loop through macrophage recruitment leading to inflammation and additional cytokine recruitment (Shoelson, 2006). These proinflammatory cytokines from adipose tissue such as tumor necrosis factor alpha (TNFα), interleukin 6 (IL6), transforming growth factor beta (TGFβ), and interferon gamma (IFNγ) can also adversely affect beta cell survival and

insulin secretion once they enter into circulation (Agrawal, 2014; Ramadan et al., 2011). Insulin sensitivity is also essential to maintain glucose tolerance, which can in part be mediated by beta cell function: a hyperbolic relationship has been described between beta cell function and insulin sensitivity (Kahn et al., 1993), highlighting the necessity of the proper function of beta cells to ameliorate the insulin resistance present in diseases like type 2 diabetes (Chiasson & Rabasa-Lhoret, 2004; Kahn, 2003). High glucose levels may also overstimulate beta cells and thus lead to beta cell dysfunction; with chronic hyperglycemia insulin stores may be depleted and persistent elevation of cytoplasmic Ca^{2+} may trigger apoptosis, participating in long-term irreversible deterioration of beta cell function (Cnop et al., 2005; Grill & Björklund, 2001).

The interrelation between insulin secretion and insulin sensitivity creates difficulties to directly and reliably measure beta cell function (Cernea & Dobreanu, 2013; Ferrannini & Mari, 2004). Although glucose is the principal stimulus and regulator of beta cell function via ATP-sensitive K^+ channels and voltage gated Ca^{2+} channels, a number of other pathways also regulate insulin exocytosis from the beta cells (Lang, 1999; MacDonald et al., 2005). For instance, insulin release from beta cells has also been documented in pathways independent of K^+ channel (Sato & Henquin, 1998) and Ca^{2+} channel activity (Komatsu et al., 1997). Likewise, there is evidence to suggest that the IRS family of proteins can also regulate beta cell differentiation, growth, survival, and insulin secretion (Burks & White, 2001; Lavin et al., 2016; White, 2006). Further still, antioxidant upregulation of nuclear factor, erythroid 2 like 2 (NFE2L2) to prevent

reactive oxygen species (ROS) buildup may play a paradoxical role in protecting beta cells from oxidative damage but also in reducing insulin secretion by glucose-triggered ROS signalling (Pi et al., 2010; Shoelson, 2006). Overall, diabetes mellitus occurs due to the body's inability to regulate glucose homeostasis through a variety of mechanisms, resulting in chronic hyperglycemia. Treatments for diabetes mellitus thus focus on improving insulin sensitivity, increasing insulin secretion, or inhibiting glucose production.

1.2 Diabetes Mellitus Treatments

1.2.1 Traditional Treatments

Currently, drug therapy, in particular insulin administration, remains the national and international standard for the treatment of type 1 diabetes (Piya et al., 2010). Treatment for type 1 diabetes is focused on blood monitoring for glucose levels by patients and using multiple daily injections of insulin as required, or through continuous subcutaneous insulin infusion using an automated insulin pump (Barnard et al., 2007). Oral agents such as biguanides (e.g., metformin) (Foretz et al., 2019) and thiazolidinediones (also called glitazones) (Thangavel et al., 2017) are administered to reduce blood glucose levels and improve insulin sensitivity in type 2 diabetes. Other oral treatments also include meglitinides and sulfonylureas, able to stimulate insulin release by beta cells in the pancreas (Grant & Graven, 2016; Lamos et al., 2013; Lebovitz & Melander, 2015). Yet another treatment includes dipeptidyl-peptidase 4 inhibitors, reducing the release of glucose by the liver and stimulating insulin secretion when blood

glucose levels rise (Stonehouse et al., 2012). Additional studies (Dowarah & Singh, 2020; Gökçay Canpolat & Şahin, 2020) discuss other recent diabetes treatments including α-glucosidase inhibitors, G protein-coupled receptor agonists, and sodium-glucose co-transporter inhibitors. However, when anti-diabetic medications fail to control blood glucose levels, insulin therapy is used for glycemic control even in type 2 diabetes patients.

The treatments for both type 1 and type 2 diabetes are long-term and indefinite. Moreover, the drugs (including insulin) used for the treatment of diabetes are expensive in the long run for both the patient and the healthcare system (American Diabetes Association, 2008). Some additional disadvantages of insulin administration include frequent daily injections which come with the associated risk of hypoglycemia (Censi et al., 2018) and the fact that insulin treatments do not always preserve beta cell function (Piya et al., 2010). Eventually, loss of beta cells worsens a patient's ability to maintain glycemic control and, in a vicious cycle, the patient requires even more insulin to prevent hyperglycemia (Rachdaoui, 2020). Moreover, because insulin dosage and administration in ever-changing physiological conditions depends heavily on blood monitoring, treatment with exogenous insulin is unable to fully avoid the long-term problems of hyperglycemia in patients who are not able to strictly control their blood glucose levels (Efrat, 2002). A newer approach termed intensive insulin therapy (IIT) wherein newly diagnosed type 2 diabetics are treated with a course of aggressive exogenous insulin is thought to take some of the demand away from the declining native beta cells and give

them a chance to recover. IIT may prolong the function of the remaining native beta cells and delay onset of full insulin dependence by years (Shah et al., 1989), with a more recent study suggesting advances in this form of therapy (McInnes et al., 2020). However, insulin administration for the treatment of both type 1 and type 2 diabetes is an important component of clinical practice. Since beta cells are the major source of insulin production in the body, and because diabetes is considered a disease of beta cell failure (Eizirik et al., 2020) it is not surprising that there has been considerable research interest in the utility of developing beta cell-based therapies as a treatment for diabetes.

1.2.2 Islet Transplantation

Islet transplantation methods were first introduced in 1972 when it was found that these implanted islets could cure chemically induced diabetes in rats (Ballinger & Lacy, 1972). During the 1970s, however, insulin treatment was still the only treatment for this disease in humans (Srinivasan et al., 2007). It was only in the 1980s where advancements in immunosuppression made transplantations a clinical reality (Srinivasan et al., 2007). Islet allotransplantation refers to harvesting islets from the pancreas of deceased donors and placing them in patients with diabetes (Health Quality Ontario, 2015). Some attempts took place throughout the 1980s to accomplish successful clinical islet transplantations in humans, with some patients managing to achieve insulin independence (Largiadèr et al., 1980; Scharp et al., 1990). However, these transplants only functioned for a short-time (approximately 9 months) before there was host rejection (Largiadèr et al., 1980; Scharp et al., 1990). Throughout the 1990s, more than 450 islet transplantation procedures were

made to achieve insulin independence, but unfortunately less than 10% of those attempts had patients maintain insulin independence only up to a year (Bretzel et al., 1996). Most islet transplantation trials failed or were short-lived due to immunological rejection of transplanted beta cells by the host; this issue is still relevant in present times. In 2000, however, the Edmonton Protocol introduced a steroid-free immunosuppression regimen for islet transplantation, guidelines in collecting more islets from multiple donors to collect a larger number of viable islets, and better techniques in islet isolation and purification as well as storage techniques prior to islet transplantation (Shapiro et al., 2000). The introduction of the Edmonton Protocol achieved insulin independence more consistently and for longer times (up to 1 year) in patients with diabetes (Shapiro et al., 2000). The Edmonton Protocol's founding guidelines have led to further improved techniques including evolving immunosuppression protocols that contain different cocktails of medications to optimize graft success and reduce the immunological rejection of beta cells (Health Quality Ontario, 2015). Likewise, more improvements have been made, such as using exenatide to promote insulin secretion in type 1 diabetes after islet transplantations (Ghofaili et al., 2007). Exenatide is an analog of glucagon-like peptide-1 hormone which increases glucose induced insulin secretion (Hering, 2005) by acting directly on beta cells (and transplanted beta cells) (Fung et al., 2006). A main issue, however, is that most of the conventional immunosuppressive agents used during and after transplantation (e.g., sirolimus and tacrolimus (Couriel et al., 2005; Nir et al., 2007)) are toxic to beta cells and compromise their survival and proper function (Chatenoud, 2008; Nir et al., 2007; Shapiro et al., 2005). Further advances in immunosuppressive

protocols are still needed to improve their safety and reduce adverse effects on beta cells. A key objective in islet transplantation research is to accomplish total unresponsiveness (tolerance) of an islet transplant without the need for chronic immunosuppression (Dolgin, 2014; Nanji & Shapiro, 2004). Whether this is possible without compromising beta cell function remains elusive.

The limited availability of donor pancreases for transplantation and the need for immunosuppressive therapy are the main limiting factors of islet transplantation (Efrat, 2002; Health Quality Ontario, 2015). In fact, the rate of donation from deceased donors remains poor in Canada, with most donated pancreases not being suitable for islet extraction (Health Quality Ontario, 2015). For these reasons, alternatives have been sought including xenotransplantation (i.e., islet transplantation from another species) and transdifferentiation (i.e., conversion of one cell type to another) of liver, bile duct, and exocrine pancreatic cells into beta cells (Hatziavramidis et al., 2013). Further options have arisen to tackle the shortage of donors in islet transplantations. These include differentiating beta cells by reversible immortalization (Efrat, 2002; Scharfmann et al., 2019) and obtaining beta cells derived from stem cells (Chen et al., 2020; Efrat, 2002; Maloy et al., 2020; Salib et al., 2022). However, again, even if these techniques were readily available, these implanted beta cells are likely to also require protection from the host immune system. For instance, about 60% of implanted beta cells are destroyed by an inflammatory response in the host within hours (Delaune et al., 2017; Gamble et al., 2018; Paez-Mayorga et al., 2022; Shapiro et al., 2001). These donor-less alternatives may

not be as efficient as the more established islet transplantation procedures from donors followed by the administration of immunosuppressing agents. Nonetheless, the issue of immunological rejection cannot be overstated. One additional, current, and promising area of research may be able to bypass or at least alleviate the problem of immunological rejection of transplanted beta cells: beta cell encapsulation remains an attractive and potential solution to this issue (Carroll et al., 2019).

1.3 Cell Encapsulation Versus Fibrotic Responses

Cell encapsulation has the potential to avoid rejection of the transplanted therapeutic cells by the host's immune system through physical means, reducing the need for pharmacological immunosuppression (Carroll et al., 2019; Dolgin, 2014; Jacobs-Tulleneers-Thevissen et al., 2013; Li et al., 2022; Q. Zhang et al., 2022). The basic principle is that embedding of the transplanted cells within a semi-permeable hydrogel can prevent cell-cell contact-mediated immune responses, and, at the very least, reduce immune responses mediated through soluble factors such as allo or xenogenic proteins expressed by the transplanted cells. Alginate microspheres have received the most research attention as a method for islet encapsulation (Carroll et al., 2019; Jacobs-Tulleneers-Thevissen et al., 2013; Li et al., 2022; Scharp & Marchetti, 2014; Q. Zhang et al., 2022). Alginate is an inexpensive, versatile biomaterial that forms hydrogels in di-cationic aqueous solutions (Ca^{2+}, barium ion (Ba^{2+})) (Lee & Mooney, 2012). Although it also has low cell toxicity, a significant concern is that the hydrogel itself can also give rise to a foreign body response that can trigger fibrosis. Fibrosis is a result of a foreign

body reaction from the complex interaction of monocyte/granulocytes/macrophage attachment, giant cell formation, and crosstalk between macrophages/giant cells and immune/fibroblast cells (Scharp & Marchetti, 2014; Sheikh et al., 2015; Vegas, Veiseh, Gürtler, et al., 2016). The fibrotic response begins as soon as the implanted capsule is introduced to the host, where non-specific proteins adsorb to the capsule's surface (Major et al., 2015; Santos et al., 2010; Tang et al., 1996). Immune cells including macrophages and neutrophils interact with this protein-coated layer and produce chemokines, cytokines, ROS, and other enzymes, further attracting more cells towards the implantation site (Grainger, 2013). Macrophages are considered a first line of response in inflammation, angiogenesis, and fibrosis, being the 'primary cells at the biomaterial-tissue interface' (Witherel et al., 2019). Notably, macrophages secrete other signal molecules like TNFα and TGFβ signaling molecules which further activate more macrophages and recruit fibroblasts, respectively (Major et al., 2015). Fibroblasts are then differentiated by TGFβ into myofibroblasts (Wermuth & Jimenez, 2015; Witherel et al., 2019); these cells contribute to forming a collagenous layer around the capsule by laying down new extracellular matrix, finalizing this fibrotic and inflammatory response (Erathodiyil et al., 2020; Grainger, 2013; Mackie et al., 2019; Major et al., 2015; Santos et al., 2010)(Erathodiyil et al., 2020; Grainger, 2013; Mackie et al., 2019; Major et al., 2015; Santos et al., 2010). A summary of these processes is shown in Figure 1. It is important to note that the fibrotic response is not stepwise but is instead a matrix of many of these components happening at a given time. Immortal fibroblast cell lines such as NIH 3T3 cells as well as immortal macrophage cell lines such as RAW 264.7 cells are

used to study fibrotic responses *in vitro* (Godek et al., 2004; Goonoo et al., 2019; Morin & He, 2017). Table 1 shows some differences and similarities between these cells.

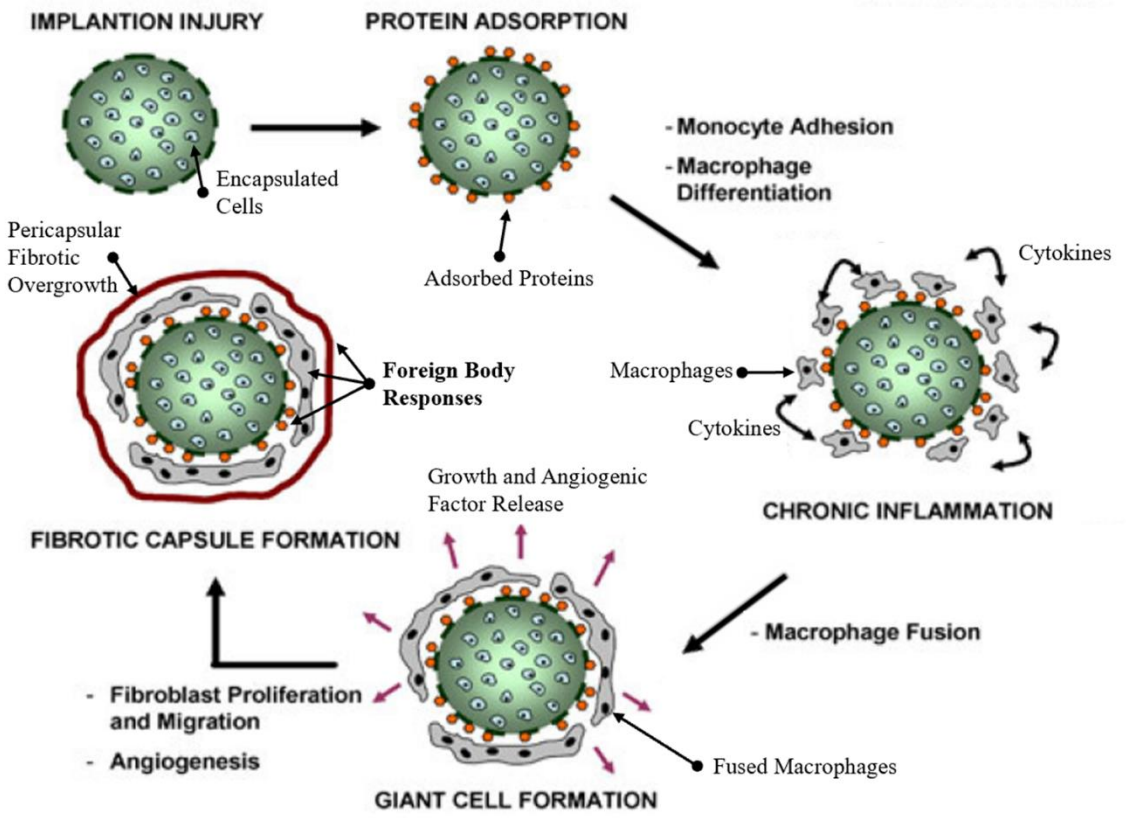

Figure 1: Stages of immune attack for a capsule implant. Foreign body responses include but are not limited to protein adsorption, macrophage recruitment, cytokine upregulation, and fibroblast recruitment. Chronic inflammation occurs after prolonged acute inflammation (not depicted). Adapted from Santos et al., 2010.

Table 1: Differences and similarities between NIH 3T3 and RAW 264.7 cells.

	NIH 3T3	**RAW 264.7**
Description	Embryonic fibroblast cells derived from Swiss albino mice	Macrophage-like, Abelson leukemia virus-transformed cell line derived from BALB/c mice
Morphology	Adherent, fibroblastic	Monocyte/macrophage (round). Mostly adherent
Doubling time	20-26 hours	~15 hours
Adherence	Adheres to tissue culture-grade plastic through cation-dependent integrin receptors and other cation-independent receptors	Adheres to tissue culture-grade plastic through cation-dependent integrin receptors and other cation-independent receptors

Fibrosis in implanted hydrogels has been observed in non-human primates (Bochenek et al., 2018) and rodents (King et al., 2001). Further, in a pilot study where a patient with type 1 diabetes received an islet transplant where the islets were encapsulated in barium alginate, at 5 weeks post-transplant, alginate capsules containing islets were found to be surrounded by fibrotic tissue, aggregated in large clumps (also a sign of fibrosis (Veiseh et al., 2015)). Some possible explanations causing fibrosis in alginate capsules include their high porosity allowing immune components in as well as their overall structural integrity (i.e., prone to gel dissolution). Thus, alginate alone cannot resolve immunological rejection, suggesting that conventional alginate formulations must be chemically modified to enable successful, long-term islet transplantation (Bochenek et al., 2018; Jacobs-Tulleneers-Thevissen et al., 2013; Vlahos & Sefton, 2018). Chemically modified alginates, bearing groups such as triazole–thiomorpholine dioxide (TMTD)

(Vegas, Veiseh, Doloff, et al., 2016) and zwitterionic (i.e., possessing both positively and negatively charged groups) carboxy- or sulfobetaines (Liu et al., 2019), have been shown to reduce fibrotic responses after implantation. Using an anti-fibrotic, TMTD-modified alginate derivate (known as Z1-Y15) as the encapsulation material in a non-human primate, long-term protection of viable and glucose-responsive allogeneic islets was achieved without the need for immunosuppressive agents (Bochenek et al., 2018). This, however, only occurred when implanted in the omental bursa rather than the more common site of implantation, the general intraperitoneal (IP) area. Further, sometimes rather than changing the alginate/capsule composition, the capsule can be coated with a membrane. For instance, coating calcium alginate (CA) beads with poly-L-lysine (PLL) and then with polyanionic alginate creates semipermeable membranes known as alginate-PLL-alginate (APA) capsules. APA capsules have been shown to reduce blood glucose levels in chemically induced diabetic mice to normal levels for 6 months after transplantation, posing no harmful effect on beta cell survival (Dusseault et al., 2008). However, PLL-coated capsules have been shown to cause fibrosis and cell overgrowth around coated capsules after being retrieved from animals (Lopez-Mendez et al., 2021; Safley et al., 2008; Strand et al., 2001). Microsphere size can also affect the immunological/fibrotic responses to implanted capsules in addition to capsule aggregation. Larger alginate capsules (~1.5 mm) have been found to decrease fibrosis and capsule aggregates post-implantation compared to smaller capsules (Bochenek et al., 2018; Vegas, Veiseh, Doloff, et al., 2016; Veiseh et al., 2015), though this has been questioned (Barkai et al., 2016; Vlahos & Sefton, 2018).

Considering all these factors, methods of beta cell encapsulation for long-term treatment of diabetes is a complex problem. The alginate modifications and coatings, the area of implantation, and the size of the capsule are a few aspects that must be thought out carefully for a successful implantation where success is defined as the maintenance of beta cell function and survival as well as immunological tolerance from the host. Beta cells also require an abundant supply of oxygen and nutrients for survival, metabolism, and function; their encapsulation may compromise the accessibility of these resources into the capsule as well as proper insulin secretion out of the capsule (Barkai et al., 2016; Efrat, 2002; Vlahos & Sefton, 2018). Thankfully, several studies seem to suggest that these potential drawbacks are not as severe in practice, as many alginate derivative encapsulations do not alter implanted islet function or their ability to secrete insulin (Bochenek et al., 2018; Dusseault et al., 2008; Jacobs-Tulleneers-Thevissen et al., 2013; Vegas, Veiseh, Doloff, et al., 2016). Regardless, it is imperative to verify these aspects in any new chemical compositions/coatings during exploratory research. Although beta cell encapsulation poses procedural challenges, it may provide a treatment for diabetes without the costly reliance on insulin and other drugs needed in its traditional treatment, or intense dependence on immunosuppressive agents required in non-encapsulated islet transplantations. The potential of beta cell encapsulation and transplantation for the long-term treatment of diabetes has great promise for the treatment of this disease.

1.4 Screening Tests for Hydrogels and Cell Responses

The growing interest in developing polymeric biomaterials has led to the design of robust polymer hydrogel capsules to enable a wide range of cell-based therapies. A key focus is on developing curative cell-based therapies for chronic disorders such as diabetes mellitus. Synthetic polymers are valuable in designing robust implantable capsules that can protect therapeutic cells from host immune rejection while allowing good metabolic exchange, in particular for oxygen, nutrients, and therapeutic actives such as insulin (Paez-Mayorga et al., 2022). However, as mentioned previously, such implanted capsules can themselves elicit strong foreign body responses that can lead to fibrosis with asphyxiation of any encapsulated cells (Delaune et al., 2017; Paez-Mayorga et al., 2022). Encapsulation of insulin-producing beta cell clusters, whether donor or stem cell derived, within synthetic, semi-permeable polymer hydrogels, has the potential to avoid host immune rejection and thus holds the promise of long-term curative treatment of this disease (Dolgin, 2014; Jacobs-Tulleneers-Thevissen et al., 2013; Nanji & Shapiro, 2004). However, there is a paucity of literature regarding standardized *in vitro* methods to screen and test the diverse types of synthetic polymer hydrogel capsules now accessible to modern polymer science for their suitability for cell encapsulation. Some attempts have been performed including measuring protein adsorption through fluorescence (Liu et al., 2019) and extraction (Vegas, Veiseh, Doloff, et al., 2016) on desired surfaces coated with desired polymers, but typically these simplify or modify the material. Thus, the focus of this thesis is to design and validate *in vitro* assays able to screen polymers for subsequent

in vivo immune responses. Further in this project, assays using the identical materials to be used *in vivo* were developed to best resemble *in vivo* implanted materials. Developing screening techniques for the testing of synthetic polymers required in cell encapsulation for treatment of chronic diseases like diabetes mellitus will allow for a cost-effective, reliable, and quicker method of testing the likelihood of success for these innovative, long-term, and long-acting treatments. Moreover, being able to screen these polymers *in vitro* to predict their performance *in vivo* will ideally lower the number of animal trials required as only the most promising capsule formulations will be further tested *in vivo*. This study will provide critical information regarding methods to better standardize and better predict polymers' fibrotic and immune responses at early stages in development through benchtop assays.

1.5 Objectives

This thesis work was done in collaboration with Allarta Life Science Inc, a start-up company from the laboratory of Dr. Harald Stover, which has deep expertise in developing charge-balanced and cross-linked polymer hydrogels designed to avoid foreign body responses (i.e., fibrosis) while increasing capsule shell robustness. This project is focused on developing *in vitro* cell-based assays to assess the fibrotic response to novel polymer hydrogels.

The specific aims of this thesis are: (1) to develop and optimize *in vitro* screening assays to assess fibroblast and macrophage cell attachment to novel polymer

formulations; (2) to develop and optimize *in vitro* screening assays to assess protein adsorption to novel polymer formulations, (3) to evaluate these polymer compositions in the cell attachment and protein adsorption assays, and (4) to determine the validity and predictability of these assays by comparing *in vivo* fibrotic responses (i.e., capsule overgrowth) to these same polymers. The results of this project will inform the development of encapsulated cell therapies for chronic diseases like diabetes mellitus.

2 General Methods

2.1 Cell Culture Maintenance

NIH 3T3 mouse embryonic fibroblast cells (ATCC, Manassas, VA) and RAW 264.7 mouse macrophage cells (ECACC, Wiltshire, England) were cultured in Dulbecco's Modified Eagle Medium (DMEM). For NIH 3T3 cells, DMEM contained 4.5 g/L D-glucose, L-glutamine, and 110 mg/L sodium pyruvate (Gibco, Grand Island, NY) supplemented with 10% (v/v) bovine calf serum (Thermo Fisher Scientific, Waltham, MA). For RAW 264.7 cells, DMEM contained 4.5 g/L D-glucose, L-glutamine, and 110 mg/L sodium pyruvate (Gibco) supplemented with 10% (v/v) heat-inactivated fetal bovine serum (Gibco). The media for both cell lines were further supplemented with 100 μg/mL penicillin streptomycin (Gibco). Both cell lines were grown at 37 °C in a humidified atmosphere of 95% O_2 and 5% CO_2. Unless otherwise noted, experiments using DMEM contained this supplementation for each respective cell line and incubations were done under these conditions. Experiments were performed with cells between

passage numbers 25-55 for NIH 3T3 cells and passage numbers 10-40 for RAW 264.7 cells.

2.2 Hydrogel/Capsule Coating Treatment Groups

This work was done in collaboration with Allarta and as a result some of the formulations discussed in this thesis have been coded as polycation X1, polycation X2, proprietary (PY) capsules 1-1.3, 2-2.3, 3-3.3, and 4-4.3. The polymers used for the capsules were evaluated in two forms, termed two dimensional ('2D') and three dimensional ('3D'). In the '2D' approach, one or more of the polymers were coated onto a glass surface prior to analysis, while in the '3D' approach, the polymers were coated onto different capsule cores including calcium alginate (CA) cores. The '2D' approach has the potential to allow rapid screening but may not provide an accurate representation of the actual capsules.

The polycations used for coating were Poly-L-lysine hydrobromide (PLL; 15-30 kDa; Sigma-Aldrich, St. Louis, MO) and several proprietary polycations. Some of the polycation-coated capsules were coated with PMM_{50}, which is partially hydrolyzed poly(methyl vinyl ether-alt-maleic anhydride) (PMM). It was used for the high reactivity of its anhydride groups with nucleophiles (Rätzsch, 1988) both to drive the spontaneous cross-linking during layer-by-layer assembly of thin films on glass (Goujon et al., 2015), and to covalently and electrostatically bind to PLL-coated CA capsules. This covalent crosslinking improves longevity of the capsules in the face of slow calcium loss to serum

(Gardner et al., 2010). Each cross-linking reaction also consumes a cationic amine group while generating an anionic carboxylate, and the rapid hydrolysis ($t_{1/2}$ = 2.5 minutes) of all residual anhydrides ensures absence of residual reactive anhydride groups shortly after coating. CA, PLL, and PLL-PMM_{50} were used for optimization trials, where PLL and PLL-PMM_{50} were coatings added to the CA core capsule. Hence, CA capsules are also referred to as uncoated (i.e., CA Uncoated), 0.1% PLL as having CA coated with PLL (i.e., CA (0.1% PLL)), and 0.1% PLL-0.2% PMM_{50} as having CA coated with PLL and then PMM_{50} (i.e., CA (0.1% PLL-0.2% PMM_{50})). A summary and description of the polymers used in optimization and experimental trials are presented in Table 2. Some of these polymers were used in '2D' experiments as hydrogels, whereas for '3D' experiments, hydrogel capsules prepared as described elsewhere (Gardner et al., 2012; Hastings & Stöver, 2019) were stored at 4 °C once synthesized and were suspended at a concentration of about 900 capsules/mL in saline. Prior to any experiments, these suspensions were thoroughly mixed with a transfer pipette before being added to the well or vessel to ensure that roughly equal numbers of capsules were present in each experiment. All capsule formulations with their respective concentrations used in both optimization and experimental trials are listed in Table 3.

Table 2: Experimental polymer compositions used.

Composition Name	**Composition Acronym**	**Polymer Qualities**
Calcium alginate	CA	Core capsule (denoted as CA Uncoated).
Poly-L-lysine hydrobromide	PLL	Highly cationic and commercially available. Coating overlayed on core capsule.
Poly(methyl vinyl ether-alt-maleic anhydride)	PMM_{50}	Outer coating. This final coating is added on to capsules when it is 50% hydrolyzed (PMM_{50}) and is overall anionic.

Table 3: Hydrogel capsule concentrations used across optimization and experimental trials.

3D Hydrogel Capsule Concentrations Used	**Trial**
CA Uncoated	Optimization and experimental
CA (0.1% PLL)	Optimization
CA (0.1% PLL-0.2% PMM_{50})	Optimization
CA (0.05% PLL-0.2% PMM_{50})	Experimental

2.3 In Vivo Pericapsular Cellular Overgrowth

Pericapsular cellular overgrowth (PCO) on retrieved capsules implanted intraperitoneally in immune-competent male C57BL/6j mice were analyzed as described elsewhere (Bochenek et al., 2018; Liu et al., 2019; Tuch et al., 2009; Vaithilingam et al., 2014). Briefly, the degree of cellular overgrowth was calculated by determining how much of the capsule surface area was covered by PCO, using the following categorical variables: 0–25, 25–50, 50–75, 75–100%. Each category was assigned a score from 1 to 4, with 1 representing the lowest (i.e., 0–25%) and 4 representing the highest (i.e., 75–100%) PCO. Then, an overall PCO score for a capsule type was calculated using the

following formula: [(percentage of capsules retrieved within 0-25% PCO x 1) + … + (percentage of capsules retrieved within 75-100% PCO x 4)] ÷ 100. The same experimental capsules used in the *in vitro* blind trials were assessed (see Table 3).

2.4 Statistical and Image Analysis

All assays involving images were analyzed using ImageJ unless otherwise noted. All statistical analyses were performed using SigmaPlot (v.11.2, Systat Software, San Jose, CA) unless otherwise noted. The results are expressed as mean ± SEM. Data were tested for outliers (Grubbs' test), normality, and equal variance. Data that failed normality or equal variance were analyzed by Kruskal–Wallis one-way analysis of variance (ANOVA) on ranks unless otherwise noted. For protein adsorption optimization, data that failed normality or equal variance were analyzed using Mann-Whitney rank sum test, otherwise they were compared using a two-tailed unpaired t-test. All other outcome measures were compared by one-way ANOVA unless otherwise noted. When significance was detected ($p < 0.05$), appropriate post hoc tests were performed to find any differences for all the groups tested.

R version 3.6.2 (R Core Team, 2019) was used with the glm package to perform binomial logistic regression to create a model for classification and prediction assessing whether an *in vivo* outcome (i.e., PCO data) will be “0-50%” (i.e., PCO score lower than 2) PCO or “50-100% (i.e., PCO score greater than 2) PCO based on *in vitro* assays described in the next sections. A training set consisting of 75% of the data for each

capsule was used to create the models. Following model generation, the remaining 25% of the data (i.e., testing set) for each capsule was used to assess misclassification rate. Odds ratios and 95% confidence intervals were also calculated from these models.

3 Methods and Results for Optimizing ('2D') Trials

3.1 Thin Film Well Coating Validation

Synthetic polymers have the potential to be coated as '2D' thin film cell scaffolds (Kleinberger et al., 2016) that could be used to test how their distinct surfaces may affect, for instance, cytotoxicity and cell attachment (Goujon et al., 2015). To validate that the coatings were able to create a surface prior to assaying cells, polymers were tagged with fluorescein isothiocyanate (FITC) as previously described (Ros et al., 2015) and plated on 96-well glass bottom plates with high performance (1.5H) cover glass (Cellvis, Sunnyvale, CA). Although this procedure has been used previously to assess coatings on glass coverslips (Goujon et al., 2015), in this thesis I chose to perform the assay in 96-well glass bottom plates instead of glass coverslips in order to increase the number of polymers that could be screened in a single run.

Briefly, glass bottom 96-well plates were first washed with 95% ethanol (EtOH). Then, for groups where the coating was applied directly on glass, 0.1% (w/v) of FITC-labelled polymers dissolved in 7.4 pH 4-(2-hydroxyethyl)-1-piperazineethanesulfonic acid (HEPES)-buffered saline (HBS) were coated directly onto the wells and left overnight at room temperature. For coatings not applied directly on glass, the wells were

first coated with 2% (v/v) solution of (3-aminopropyl)triethoxysilane (APTES) in 95% EtOH for 2 minutes, and then washed with 95% EtOH prior to adding the FITC-labelled polymer. APTES allows for amine groups to be introduced onto the surface of the glass, allowing covalent bonding between the glass and the first PMM layer and preventing film delamination (Goujon et al., 2015). 0.2% PMM was deposited from acetonitrile (ACN) solution and left for 5 minutes before being washed with ACN.

The next day, all wells were washed with deionized water (dH_2O) and left to dry prior to adding HBS. To ensure that the coatings were also present after being incubated with cells and media, after the wash with dH_2O, NIH 3T3 cells were seeded in additional wells with DMEM at 2,500 cells/well and incubated for three days. To prove that the fluorescence was due to the newly formed films, all films were scratched with an 18-gauge needle prior to imaging. Pictures were taken at 10X magnification with a Zeiss LSM 510 confocal laser scanning microscope (CLSM) fitted with air-cooled argon and HeNe lasers (LASOS; LGK 7628-1) and running LSM Image Browser software. Fluorescent thin film hydrogel coatings were visible in all polymer surface coatings tested after overnight incubation without cells (Fig. 2) and after a three-day incubation with cells (Fig. 3), although at varying levels of intensity. Some coatings were not uniformly fluorescent, creating more of a patchy surface (e.g., Fig. 2D) rather than a uniform polycation coating on top, as more clearly seen in the images of the glass-polycation surfaces (Fig. 2B and Fig. 3B). The scratches confirm that the thin film surfaces are present and that cells can attach to them (Fig. 3). Surprisingly, the glass-polycation (Fig.

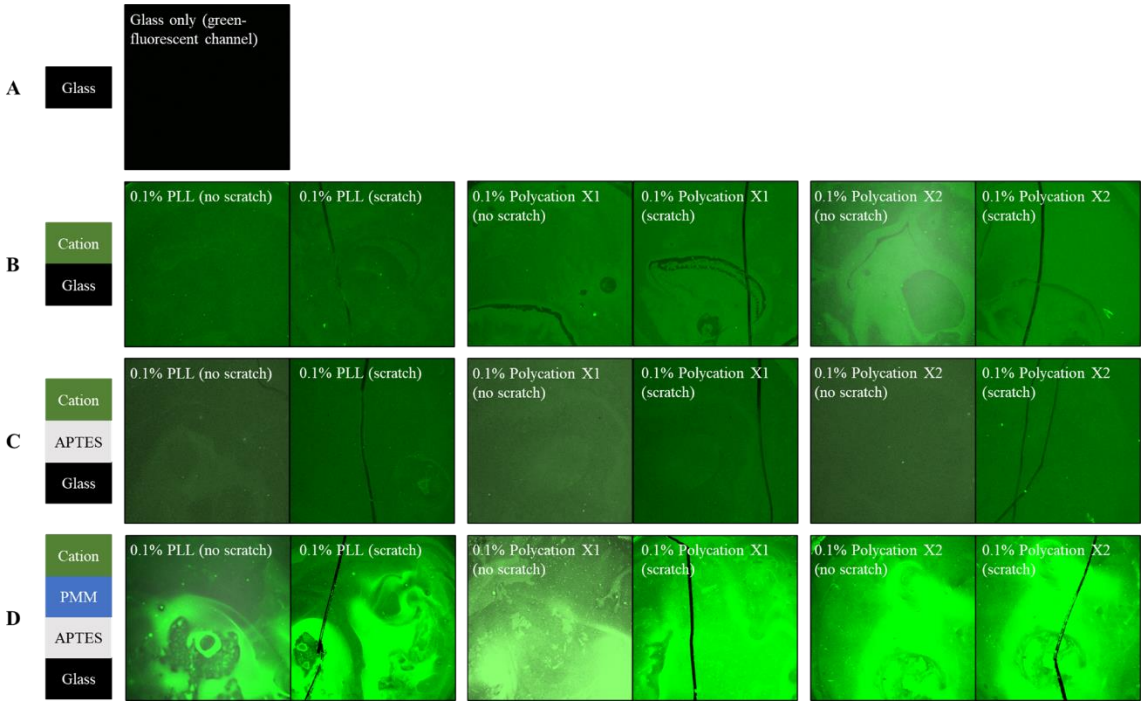

Figure 2: Green-fluorescent microscopy images of thin film ('2D') coatings after one day of incubation before and after scratching. The surface layering is (A) glass only, (B) glass-0.1% polycation, (C) glass-2% APTES-0.1% polycation, and (D) glass-2% APTES-0.2% PMM-0.1% polycation. The polycations tested were PLL (left), Polycation X1 (middle), and Polycation X2 (right). The polycation-on-PMM images show a surface that was coated with PMM (anhydride form) for its eventual hydrolysis.

2B and Fig. 3B) and the glass-2% APTES-polycation (Fig. 2C and Fig. 3C) showed a fluorescent layer even though we did not expect the coating to adhere; it has been suggested that the polycations would not be able to bind efficiently to glass without the anionic surface that PMM provides (Kleinberger et al., 2016). In other words, the presence of fluorescence shows that these coatings were still effectively binding to the glass even without an anionic surface. Furthermore, this assay must be performed with extreme care as the multiple washes performed once the thin film has been formed can lead to disruption to the thin film itself. A clear example can be observed in the glass-

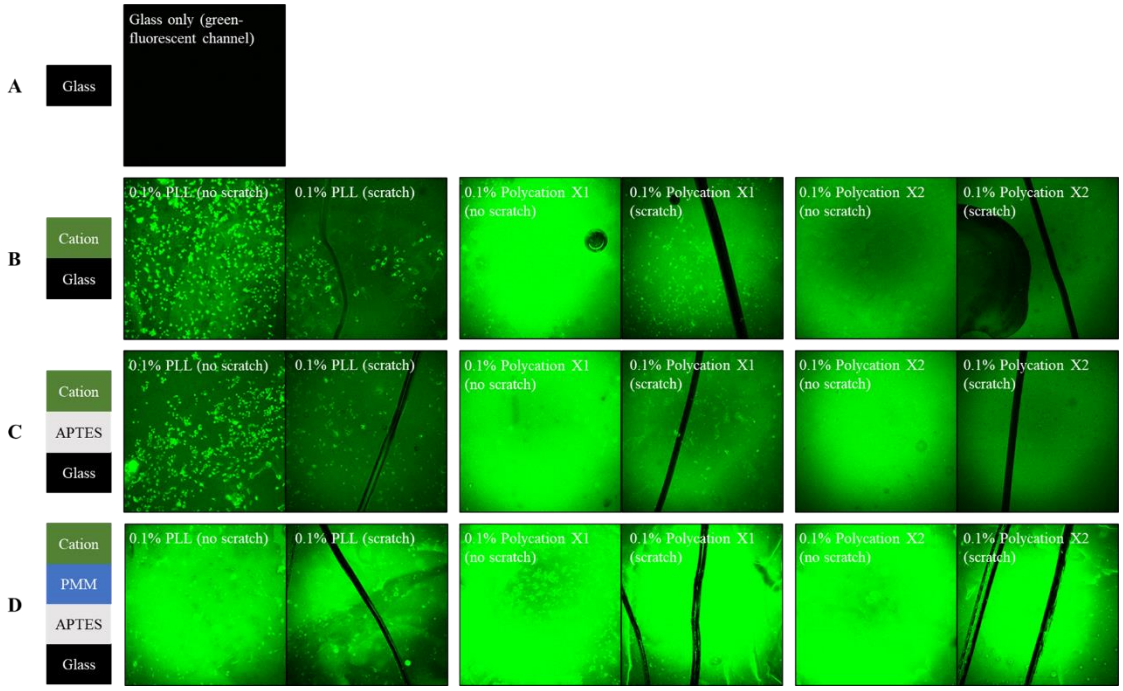

Figure 3: Green-fluorescent microscopy images of NIH 3T3 cells on thin film ('2D') coatings after three days of incubation before and after scratching. The surface layering is (A) glass only, (B) glass-0.1% polycation, (C) glass-2% APTES-0.1% polycation, and (D) glass-2% APTES-0.2% PMM-0.1% polycation. The polycations tested were PLL (left), Polycation X1 (middle), and Polycation X2 (right). The polycation-on-PMM images show cell attachment on a surface that was coated with PMM (anhydride form) for its eventual hydrolysis.

polycation group for Polycation X2 (Fig. 3B), which shows that a substantial portion of the layer was absent, likely because of a mechanical error like a pipette disrupting the thin film while adding/removing the washes. In addition, even though the cells were not fluorescently labelled, the fluorescent polymers from some of the thin films must have been absorbed by some cells, as observed especially for the PLL group where the cells were also fluorescent.

3.2 Thin Film Cell Attachment

Once I confirmed that the coatings were present in the wells, non-FITC labelled hydrogel coatings were applied and assessed in quadruplicate for cell surface coverage with NIH 3T3 cells (N = 10-16 independent experiments). An additional group, sodium alginate (NaAlg) for thin film ('2D') experiments, was utilized as a control (glass-alginate layer), representing the most basic, uncoated, capsule formulation. Prior to coating, all polymers were filtered using a 0.22 μm syringe filter (FroggaBio, Toronto, ON), and the thin films were formed and applied similarly as described in section 3.1. NIH 3T3 cells in supplemented DMEM were then seeded in all wells at a density of 2,500 cells/well and incubated for three days. Prior to imaging, a live-dead stain (Thermo Fisher Scientific) consisting of green-fluorescent calcein-acetoxymethyl (AM) (to indicate intracellular esterase activity) and red-fluorescent ethidium homodimer-1 (to indicate loss of plasma membrane integrity) was added to each well at 2 μM and 4 μM, respectively. After addition of the dyes, the plate was incubated for 30 minutes prior to imaging. One image per well was taken at the centre of the well. CellProfiler software (Broad Institute, Cambridge, MA) was used to quantify fluorescence of the cells against the total area of the image to obtain percent cell surface coverage.

Cell surface coverage for each thin film was assayed. The surfaces tested were those coated with polycation (glass-polycation) (i.e., the most simple and direct surface) (Fig. 4A), and those coated with 2% APTES with an additional coating of 0.2% PMM and a polycation (glass-2% APTES-0.2% PMM-polycation) surface (Fig. 4B). This last

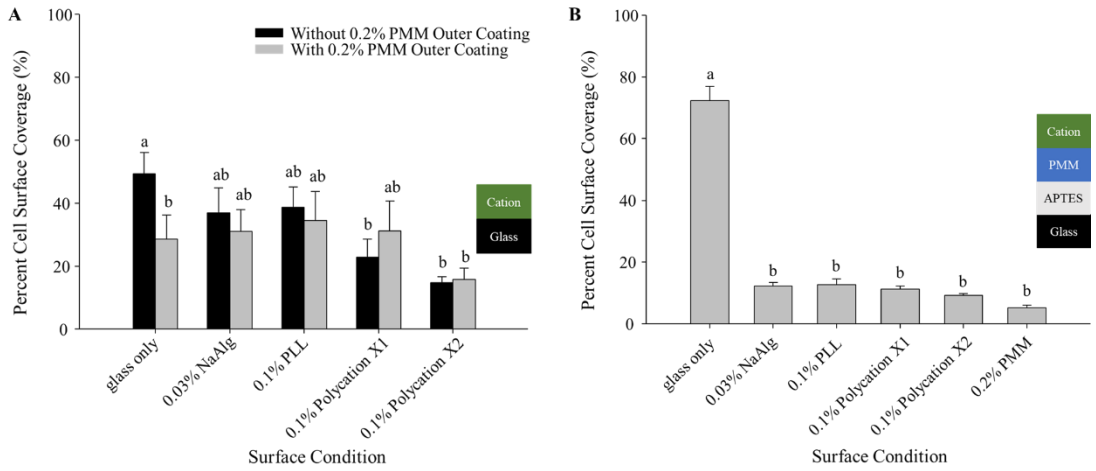

Figure 4: Percent cell surface coverage of NIH 3T3 cells on thin film ('2D') coatings after three days of incubation. The surface layering is (A) glass-polymer and (B) glass-2% APTES-0.2% PMM-polymer except for the 0.2% PMM group in the latter as it did not have a polycation coated on top. Data represented as mean ± SEM, N = 10-16 independent experiments (in quadruplets). Values with different letters are significantly different from one another, $p < 0.05$.

surface was included as it was previously evaluated by our group (Kleinberger et al., 2016). An additional treatment group was explored by coating the glass-polycation surfaces with PMM as the final outer surface to model PLL-coated CA capsules, and to allow comparison for groups without PMM at the outer coating. We compared the different surfaces via two-way ANOVA with (1) surface type (e.g., glass only, 0.1% PLL, etc.) and (2) presence of 0.2% PMM outer coating as the main effects. Based on the 2-way ANOVA, there was no main effect on presence of 0.2% PMM outer coating ($p = 0.354$); there was also no significant interaction between the main factors ($p = 0.345$). Surface type was statistically significant ($p = 0.020$), and a Tukey post-hoc test was used to identify these differences. The 0.2% PMM coating reduced cell coverage only in the glass surface (uncoated) group compared to the glass only group without 0.2% PMM.

Further, both the 0.1% Polycation X1 (without 0.2% PMM) and 0.1% PolycationX2 (with and without 0.2% PMM) surfaces decreased cell coverage compared to the glass only group (Fig. 4A). On the other hand, there were no statistically significant differences between the PLL, PolycationX1, and Polycation X2 hydrogel groups for the glass-2% APTES-0.2% PMM-polycation layered coating (Fig. 4B). This was surprising since we expected that the PLL coating should allow for higher cell attachment and coverage as reported elsewhere (Strand et al., 2001), especially compared with the 0.2% PMM group whose anionic surface should discourage cell attachment as opposed to PLL's cationic surface.

3.2.1 Thin Film Conclusion

The thin film ('2D') approach, although quick to implement, may be difficult to accurately replicate based on the disruption to the thin film surfaces created due to the matrix of substances being used and/or due to the washes. The more direct glass-polycation surfaces may be better indicators to predict cell attachment to these surfaces than the layered glass-2% APTES-0.2%-PMM-polycation surfaces. This conclusion is supported by the observation that the cell coverage in glass-0.1% Polycation X1 and glass-Polycation X2 surfaces result in lower cell coverage than glass. This follows what was expected as the Polycation X1 and X2 copolymers have reduced cationic charge density compared to glass-PLL which is highly cationic. Other approaches may be able to discriminate cell attachment properties of different polymer hydrogels, such as coating on cover slips or changing cell concentration/timepoints to test the percent cell coverage.

Alternatively, total cell number remaining on the well instead of cell coverage could be tested. In addition, the thin coatings on a hard substrate may not be a very good model for surface coatings of CA capsules, which are much softer, more porous, and highly hydrated However, given the fact that (1) the current thin film ('2D') approach did not yield a large percent cell surface coverage for the PLL group, (2) the layering of these hydrogels was difficult to consistently replicate, and that (3) it was difficult to quantify cells attached with auto-fluorescent cells, this '2D' assay was deemed not viable for further development.

4 Methods and Results for Optimizing ('3D') Cell-Based Trials

4.1 Capsule Monolayer Static Model

Instead of a '2D' thin film layer, the next model chosen to assess was a '3D' capsule attachment assay. In this model, glass bottom 96-well plates were seeded with NIH 3T3 cells in DMEM at 2,500 cells/well. Immediately after seeding, using a sterile transfer pipette, 1 drop of a capsule suspension was added to each well (~45 capsules/well) for a 3-day incubation. The capsules tested in this assay included (1) CA Uncoated capsules, (2) CA (0.1% PLL) capsules, and (3) CA (0.1% PLL-0.2% PMM_{50}) capsules. In addition, I also tested the ability of the cells to attach to the capsules when the capsules were added to the well followed by the cells. After the 3-day incubation, a live-dead stain (Thermo Fisher Scientific) was added to each well as described in section 3.2, and the plates were incubated and imaged. A z-stack of images at 4X magnification were taken at the middle of each well ranging in 10 μm increments from bottom to top of

the capsules. The fluorescent settings on the confocal microscope (i.e., for green channel a laser line of 488 nm and power of 10, and for the red channel a laser line of 561 nm and power of 1) were consistent throughout all pictures.

Unfortunately, this method did not yield any quantifiable results as the cells settled to the bottom of the well without interacting with the capsule, or at least most of the capsule surface, for all capsules tested (Fig. 5). The results rendered this attempt to artificially attach cells on a capsule by simply seeding them on a 96-well plate as unusable to properly model cell-capsule interaction and attachment. As such, a different approach was explored.

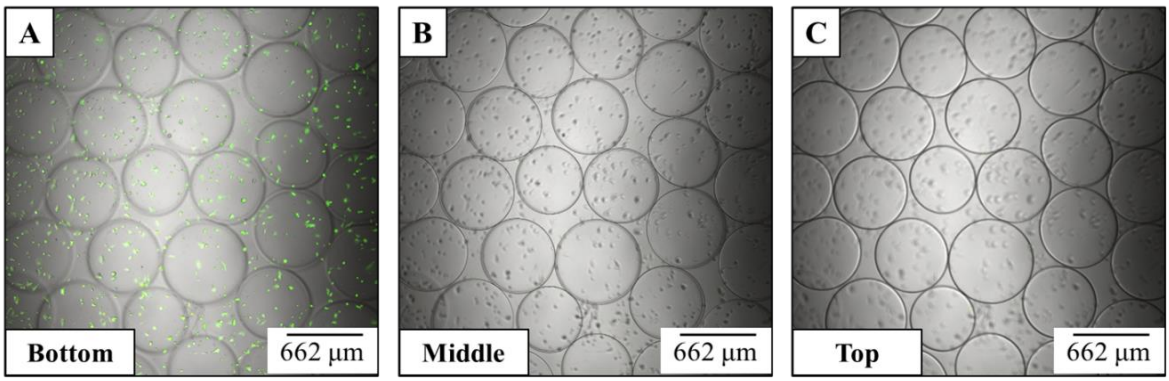

Figure 5: Representative images of NIH 3T3 cells seeded with CA (0.1% PLL) capsules after three days of incubation in a static approach, regardless if cells were seeded first and then capsules, and vice versa. The fields of view (4X magnification) of the images are (A) bottom of the well and capsules, (B) middle of the capsules, and (C) top of the capsules. Similar observations were observed in CA Uncoated capsules and with CA (0.1% PLL-0.2% PMM_{50}) capsules.

4.2 Establishing a Capsule Spinning Hybridizer Suspension Model

To allow for capsules and cells to interact, a suspension model was pursued. Disposable 20 mL borosilicate glass scintillation vials (VWR, Mississauga, ON) were washed with 10 mL 95% EtOH, aspirated, and left to air dry. For each glass vial, NIH 3T3 cells in DMEM at 100,000 and 350,000 cells/mL were added to the vial in 10 mL volumes. Using a sterile transfer pipette, 50 drops (from a ~900 capsules/mL stock) of CA Uncoated capsules, CA (0.1% PLL) capsules, and CA (0.1% PLL-0.2% PMM_{50}) capsules suspended in saline were placed into the glass vials already containing media and cells (final concentration of ~180 capsules/mL in the glass vial). The glass vials were placed in a UVP HB-1000 hybridization incubator (Thermo Fisher Scientific) and left spinning at ~8 rpm at 37 °C for different timepoints (2, 4, 20, and 70 hours). Culture of the NIH 3T3 cell line in suspension for at least three days (i.e., 72 hours) retain a regular cell cycle and cell function once the suspended cells reattach to a surface (Otsuka & Moskowitz, 1976). This added reassurance that our hybridizer suspension model was not adversely affecting the cell viability or function while the cells were in suspension. At each timepoint, glass vials in the hybridizer were removed and 1 drop (~9 capsules/well) was removed from each vial and was placed into a 96-well plate containing 0.2 mL prewarmed DMEM using a transfer pipette (4 wells/treatment condition) for imaging. Then, a live-dead stain (Thermo Fisher Scientific) was added as described in section 3.2, and the plates were incubated and imaged with the fluorescent settings described in section 4.1. A z-stack of images at 10X were taken for each capsule ranging in 10 μm

increments from bottom to top of the capsules. A total of 4-6 capsules were imaged per group; each day of capsule incubation and imaging is considered an independent experiment and, unless otherwise noted, I performed a minimum of N = 3 independent experiments for each capsule formulation.

To first test out the approach, a concentration of 100,000 cells/mL was assayed after a 2-hour spinning incubation, showing a slight improvement in the assay's ability to cause cell attachment than in a more static approach (Fig. 5), as seen by some cells being detected on the 'top' field of view (Fig. 6). This was especially promising given the shorter 2-hour incubation time compared to three days to the capsule monolayer static model ('3D'). Subsequently, to identify whether the assay performance could be improved at higher cell densities or longer incubation times, we tested 350,000 cells/mL for 7-, 20-, and 70-hour incubation times (Fig. 7). A limitation of the hybridizer spinning approach is the sealed vial that prevents replenishment of the 5% CO_2 environment,

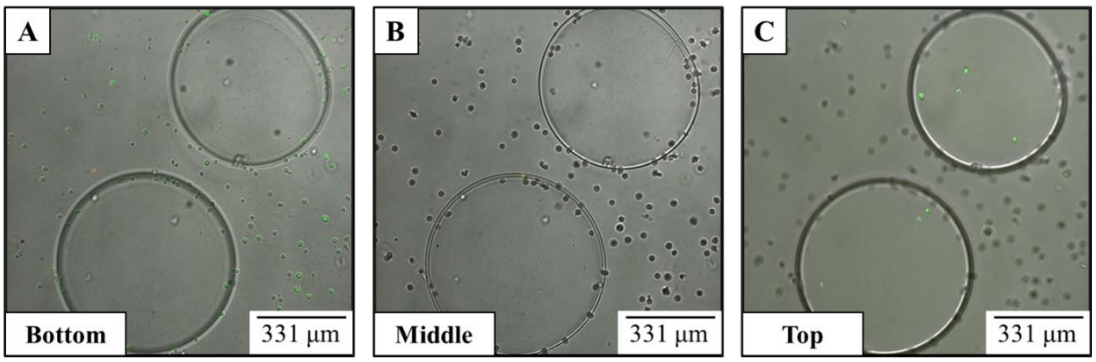

Figure 6: Representative images of NIH 3T3 cells seeded with CA (0.1% PLL) capsules after 2 hours of incubation at 100,000 cells/mL while spinning in a hybridizer. The fields of view (10X magnification) of the images are (A) bottom of the well and capsule, (B) middle of the capsule, and (C) top of the capsule. Similar observations were observed in CA Uncoated capsules and CA (0.1% PLL-0.2% PMM_{50}) capsules.

which will adversely affect the cells' long-term survival. After 20 hours of incubation, the media colour in the vials had turned yellow (phenol red is a pH indicator in the media) indicating a change in pH to a more acidic environment versus the normal red colour of

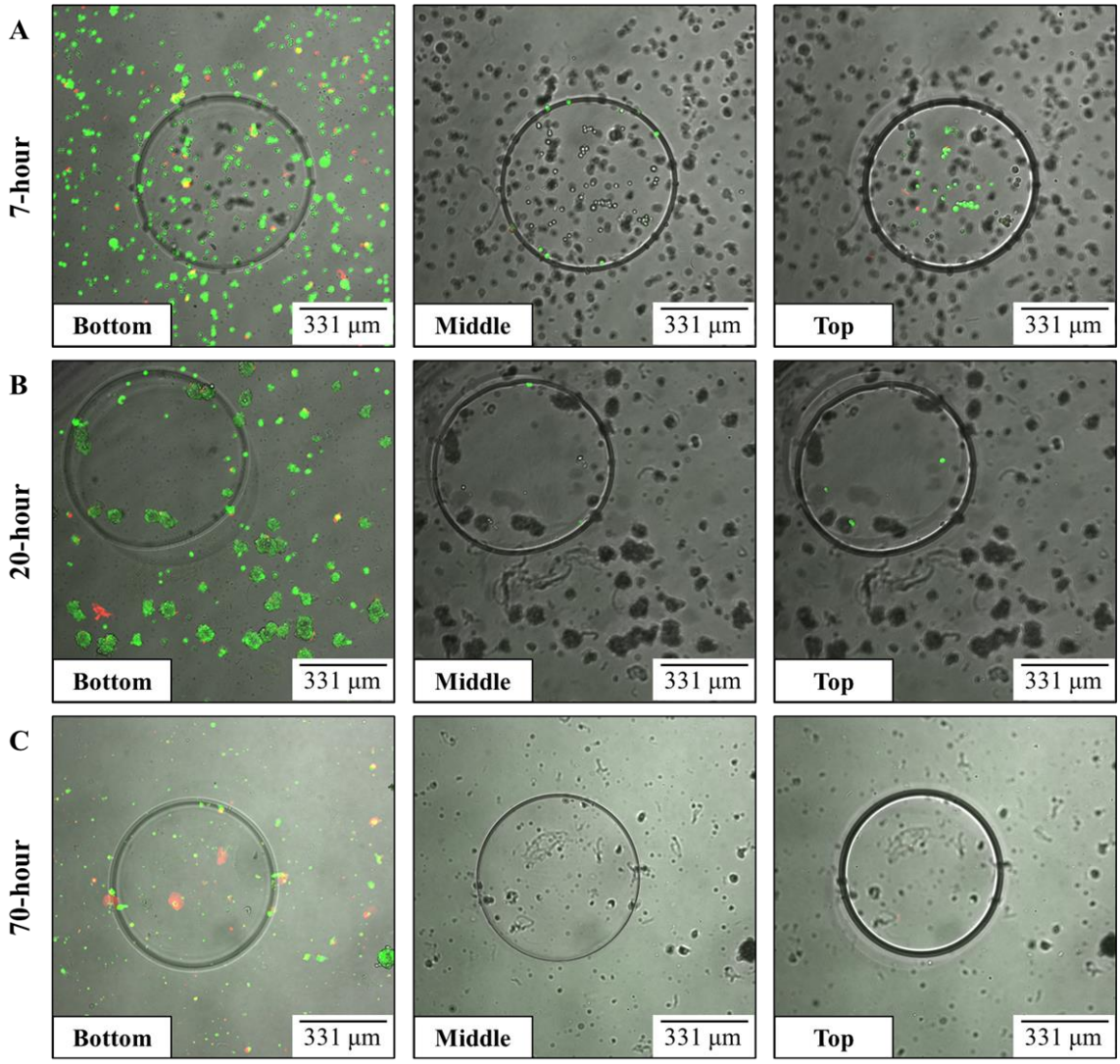

Figure 7: Representative images of NIH 3T3 cells seeded with CA (0.1% PLL) capsules after (A) 4 hours, (B) 20 hours, and (C) 70 hours of incubation at 350,000 cells/mL while spinning in a hybridizer. The fields of view (10X magnification) of the images are shown for the bottom of the well and capsule (left), the middle of the capsule (middle), and the top of the capsule (right). Similar observations were observed in CA Uncoated capsules and CA (0.1% PLL-0.2% PMM_{50}) capsules.

media at physiological pH (i.e., pH 7.4) (Pansu & Gautheyrou, 2006, Chapter 15). After 7 hours of incubation, there were no visible changes in the colour of the media suggesting that the buffering capacity of the media was maintaining pH in the physiological range. After 20 and 70 hours of incubation, cells were clumping (Fig. 7B) and appeared to have decreased attachment to the capsule (Fig. 7B and 7C) compared to the 7-hour timepoint (Fig. 7A). Indeed, the most promising timepoints to maximize cell attachment and to be able to quantitatively compare cell attachment across different capsule formulations appears to be roughly around 7 hours of incubation or less. This was a promising start to determine an ideal time and cell concentration to maximize cell attachment, which is explored further in section 4.3.

4.3 NIH 3T3 Cell Density and Timepoint for Capsule Spinning Hybridizer Suspension Model

To further determine an optimal timepoint and cell concentration for the capsule spinning hybridizer suspension model (‘3D’), the same assay was performed with concentrations of 175,000, 350,000, 700,000, and/or 1,000,000 cells/mL at 4-, 8-, and 12-hour timepoints in 20 mL vials (Fig. 8A). Only the CA (0.1% PLL) capsule was used for the rest of this optimization as it was expected to cause the highest cell attachment based on reports that CA (0.1% PLL) capsules lead to high cell overgrowth and fibrosis (Strand et al., 2001). Acquired z-stack images at 10X magnification were analyzed in ImageJ to identify and quantify the number of cells attached to each capsule. Briefly, the fluorescently labelled live cells with calcein-AM (from the live-dead staining described in

section 3.2) were manually counted across the z-stack and normalized to the surface area of the capsule to account for variation in capsule sizes. Thus, values were reported in cells/mm^2 and compared across timepoints and concentrations.

Interestingly, in 20 mL glass vials (Fig. 8A), at the 4-hour timepoint, the 700,000 cells/mL density had the highest number of NIH 3T3 cells attached to the CA (0.1% PLL) capsules compared to the other cell densities tested, and this number remained constant throughout the 8- and 12-hour timepoints (~100 cells/mm^2). This consistency across timepoints was also seen for the 175,000 cells/mL and 350,000 cells/mL groups, although at lower values (~20 and ~40 cells/mm^2, respectively). The average cell attachment in the 1,000,000 cells/mL group only matched that of the 700,000 cells/mL density at the 12-hour timepoint. Considering this difference in cell attachment, the 700,000 cells/mL

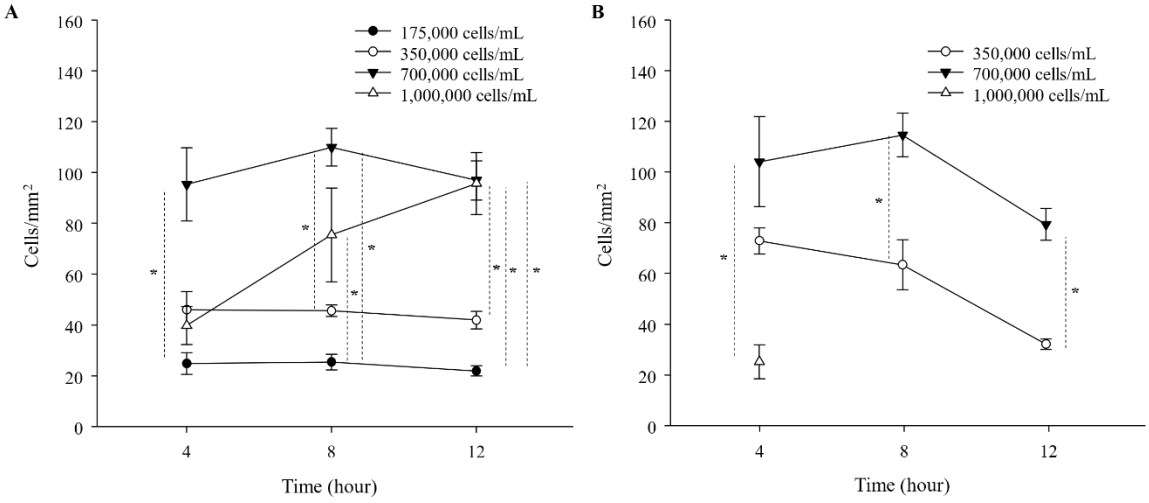

Figure 8: Number of attached NIH 3T3 cells normalized to CA (0.1% PLL) capsule's surface area (cells/mm^2) at various cell densities (175,000, 350,000, 700,000, and/or 1,000,000 cells/mL) after 4, 8, or 12 hours spinning in a hybridizer in (A) 20 mL and (B) 4 mL glass vials. Data represented as mean ± SEM, N = 2-3 independent experiments. Values with asterisks (*) are significantly different from one another, $p < 0.05$.

density seemed promising as a starting concentration to maximize cell attachment in the shortest timepoint possible.

To further test the assays' reproducibility and suitability as a high-throughput screening assay, a similar experiment was performed using 4 mL glass vials (Fig. 8B) instead of the original 20 mL glass vials to save on material resources and reagents. The conditions for this experiment were scaled down by a factor of 5 compared to the 20 mL glass vial experiment as stated in section 4.2. Briefly, a 2 mL volume of NIH 3T3 cells at different cell concentrations were added in DMEM. Using a sterile transfer pipette, 10 drops of capsules were added into this mix for a total suspension of ~180 capsules/mL in the glass vial left to spin in the hybridizer. The steps for image analysis were the same as described above. Only the intermediate cell densities (350,000, 700,000 cells/mL) were tested, with a higher emphasis on the 4-hour timepoint which was the only time point where we had data for the 1,000,000 cells/mL group.

Like the 20 mL glass vials at the 4-hour timepoint, the 4 mL glass vials also had the highest cell attachment (~100 cells/mm^2) at an incubation density of 700,000 cells/mL (Fig. 8B). Interestingly, at a density of 1,000,000 cells/mL the cell attachment was lowest at this timepoint. There was also a clear distinction between the cell attachment of the 350,000 and 700,000 cells/mL groups as time progressed, where the latter density had almost double the amount of cell attachment than the former group. Overall, like in the 20 mL glass vial experiments, the 4 mL glass vial was able to yield similar results by using fewer resources. In conclusion, following this set of experiments, I chose to use a cell

density of 700,000 cells/mL in a 4 mL glass vial for 4 hours as the experimental conditions to further optimize for this assay.

4.4 Optimizing the NIH 3T3 Cell Capsule Spinning Hybridizer Suspension Model

4.4.1 Interrater Variability

To further validate the capsule spinning hybridizer suspension model ('3D'), the quantification method and way in which cells were counted had to be validated across different users. Utilizing a pilot trial using CA Uncoated capsules, CA (0.1% PLL) capsules, and CA (0.1% PLL-0.2% PMM_{50}) capsules, two different users were given the same set of pictures (blinded labels) to analyze. User 1 had experience analyzing previous pictures whereas user 2 was inexperienced and was given a written protocol to follow. It was found that a manual counting system introduces bias and is not reproducible or consistent across different users. Although the manual counts were statistically similar between two different users for CA Uncoated, user 1's manual count significantly differed with user 2's manual count for the CA (0.1% PLL) and CA (0.1% PLL-0.2% PMM_{50}) capsules (Fig. 9D). To address this, an automatic macro was developed in ImageJ to standardize counts across users. The automatic macro requires the user to manually identify and select the region(s) of interest (i.e., capsule(s)) and ensure the z-stacks of the images start at the bottom of the well. Once this is done, the automatic macro will create a fluorescent 'maximum projection' image from all the z-stacks (ignoring the first 15 z-stacks to avoid counting cells attached to the bottom of the well), displaying all the dyed cells. Then, it will identify the cells as individual dots and count

the number of cells within each pre-selected region (i.e., the capsule), and return the image that it creates from it ('macro-output'). The automatic macro went through three versions changing settings to identify the cells more accurately before being tested with the users. These settings included how large/small a fluorescent signal must be to be counted as a cell, and how accurately cell clusters can be distinguished and accurately counted. By using this finalized automatic macro, the results from the two users were

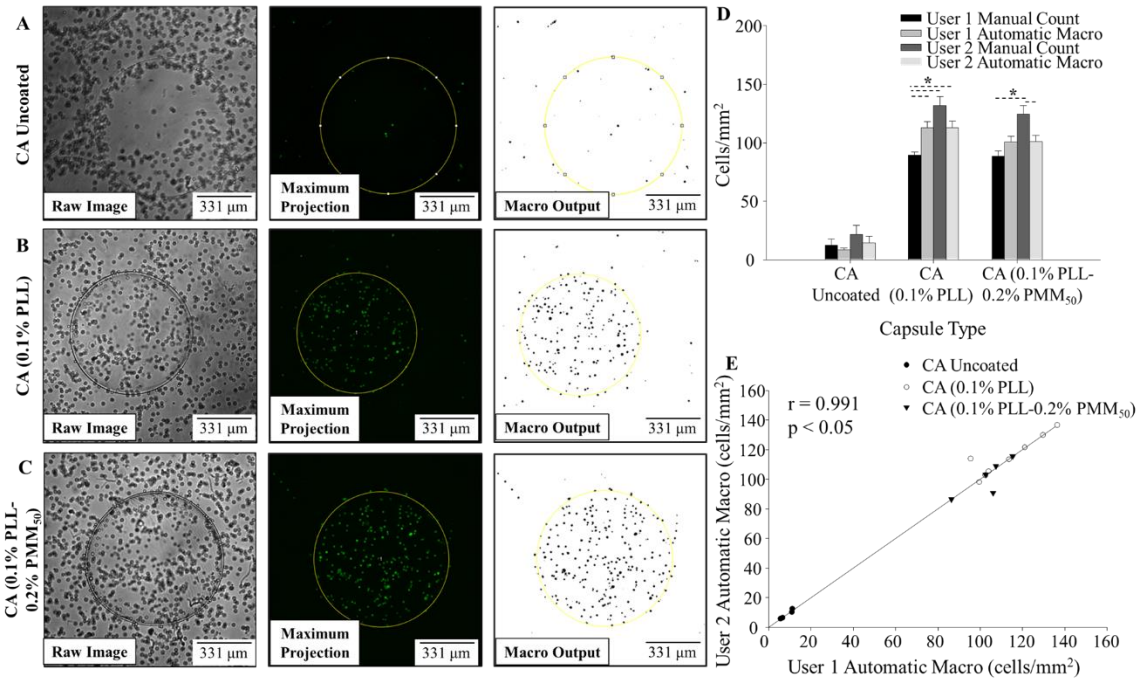

Figure 9: Representative confocal images of NIH 3T3 cells with (A) CA Uncoated, (B) CA (0.1% PLL), and (C) CA (0.1% PLL-0.2% PMM_{50}) capsules after 4 hours of incubation at 700,000 cells/mL while spinning in a hybridizer. The fields of view (10X magnification) of the images are shown at the middle of the capsule for the raw image (left), green-fluorescent maximum z-stack projection (middle), and the image analyzed by the automatic macro (right). Cells attached to capsules were counted manually or automatically with a macro by two different users. Normalized counts to capsule size were compared (D) between manual/automatic counts by the two users across each capsule type. Data represented as mean ± SEM, N = 5-6 capsules per group. Values with asterisks (*) are significantly different from one another, $p < 0.05$. The automatic counts done by each user with the macro were (E) correlated for all capsule types tested ($r = 0.991$, $p < 0.05$).

almost identical despite any type of capsule analyzed, as highlighted by a significant and strong, positive correlation between the two users' automatic macro approach counts (Fig. 9E). Moreover, the automatic macro count falls in between the counts done by the two users. Evidently, utilizing an automated approach rather than a manual count can standardize the results amid different users and provide more consistent counts overall. As such, moving forward, the remaining experiments for this assay were analyzed with the automatic macro instead of manually.

4.4.2 Confocal Magnification and Washing Step

Up to this point, the capsule spinning hybridizer suspension model ('3D') was imaged at 10X magnification on a confocal microscope. This only allowed for 1-2 capsules to be imaged at a time with each z-stack taking 4-6 min to setup and acquire. Because 4-6 capsule replicates were imaged per group (N = 1 independent experiment), this required over 15 minutes of imaging time per capsule type. Since the purpose of this *in vitro* assay is to image multiple capsule compositions/coatings (> 6 capsule types) in one session, the time to take images for all capsules could be lengthy (> 1.5 hours). As the cells are at room temperature from the start of the imaging session, a long wait until the cells are imaged could compromise cell viability and thus influence the amount of cell attachment to each capsule type. Therefore, the feasibility of using 4X magnification for imaging instead of the 10X magnification was examined. By using a 4X magnification, 4-6 capsules can be captured in a single image (~5 minutes), which reduces overall imaging time by a third.

As the objective of this experiment is to determine the degree to which cells are strongly attached to the capsule surface, the current protocol was further optimized to remove those cells that were only lightly attached or simply resting on the capsule. This could potentially bias results and make reproducibility more difficult. To account for this, a washing step was introduced prior to imaging the capsules where, after incubating with the live/dead stain for 15 minutes, 0.2 mL media was removed, and the capsules were washed with 0.2 mL HBS once. This volume was then removed, and 0.2 mL HBS was readded, and the capsules were then imaged as described before in section 4.2.

In general, the washing step significantly decreased cell attachment on CA Uncoated, both in the 10X magnification (washed) and 4X magnification (washed) analyses when compared to the 10X magnification (unwashed) group. This downward trend was also seen for the CA (0.1% PLL) and CA (0.1% PLL-0.2% PMM_{50}) capsules, although not statistically significant (Fig. 10D). Most importantly, regardless of the magnification used, or if the washing step was performed, the results were the same; namely, CA Uncoated capsules had a significantly lower cell attachment than the CA (0.1% PLL) and the CA (0.1% PLL-0.2% PMM_{50}) capsules (Fig. 10D). However, the cell attachment for CA (0.1% PLL) and the CA (0.1% PLL-0.2% PMM_{50}) capsules were statistically the same. Overall, therefore, to significantly save time and ensure that strong cell attachment was being measured, the 4X magnification and washing approach were used moving forward.

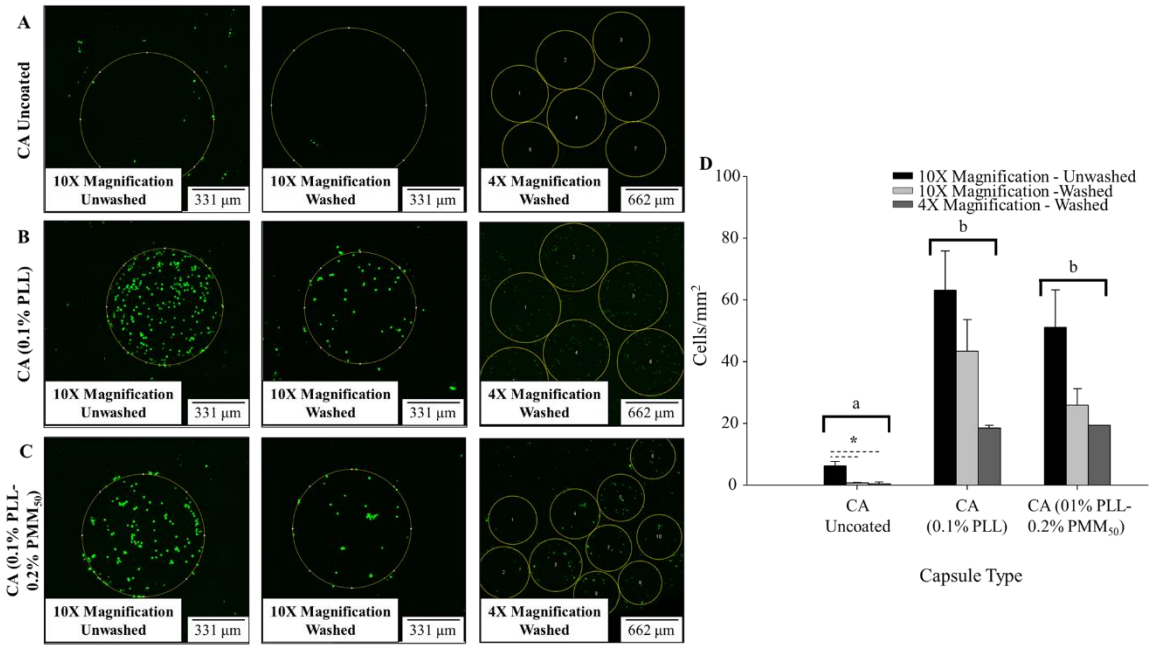

Figure 10: Representative confocal images of NIH 3T3 cells with (A) CA Uncoated, (B) CA (0.1% PLL), and (C) CA (0.1% PLL-0.2% PMM_{50}) capsules after 4 hours of incubation at 700,000 cells/mL while spinning in a hybridizer. The green-fluorescent maximum z-stack projection of the images are shown for images taken at 10X magnification without a washing step (left), at 10X magnification with a washing step (middle), and at 4X magnification with a washing step (right). Cells attached to capsules were counted automatically with a macro. Normalized counts to capsule size were compared (D) between magnification type and presence of washing step. Data represented as mean ± SEM, N = 7-8 independent experiments. Values with asterisks (*) are significantly different from one another between magnification/washing groups, $p < 0.05$. Values with different letters are significantly different from one another between capsule type regardless of magnification/washing, $p < 0.05$.

4.4.3 Conclusion

Overall, the capsule spinning hybridizer suspension model (‘3D’) has been optimized for the cell attachment assay by using a 700,000 cells/mL NIH 3T3 cell concentration, spinning in a hybridizer for 4 hours in a 4mL vial, introducing a washing step after the spinning incubation, and imaging with a 4X magnification on the confocal

microscope. For image analysis, the automated macro should be utilized to assess cell attachment counts. A summary of all these conditions can be found in Table 4.

Table 4: Optimized cell attachment assay parameters for NIH 3T3 cells.

Parameter	**Optimized Option**	**Reason**
Cell concentration	700,000 cells/mL	Maximizes cell attachment
Incubation time	4 hours	Maximizes cell attachment, minimizes experiment duration
Counting method	Automated macro	Improves interrater variability
Ensuring cells are attached	Introduce a washing step	Lowers variability and improves reproducibility
Confocal magnification	4X	Images more capsules at a time and speeds up imaging time

4.5 Cytokine Response for NIH 3T3 Cell Capsule Spinning Hybridizer Suspension Model

In addition to measuring cell attachment for NIH 3T3 cells after spinning in hybridizer with capsules for 4 hours at 700,000 cells/mL, we assessed levels of TNFα and IL6 in the media at the end of the 4-hour incubation period. Both TNFα (Cayman Chemical, Ann Arbor, MI) and IL6 (Enzo Life Sciences, Farmingdale, NY) levels were quantified by performing ELISAs on the spent media according to the manufacturer's instructions. Absorbance was read using a Synergy H4 Hybrid Reader (BioTek, Winooski, VT), and cytokine concentrations were determined from a standard curve by a four-parameter logistic regression using software provided by the manufacturer for TNFα

(ELISA Double, Cayman Chemical) or an online analysis tool for IL6 (www.myassays.com). To normalize between different experimental days, values were standardized to CA (0.1% PLL) for each trial (i.e., CA (0.1% PLL) was set as 100%, and other capsule cytokine concentrations were calculated relative to this). We selected to standardize to CA (0.1% PLL) because the highly cationic property of PLL, as seen in the optimization of the cell attachment experiments (Fig. 10), allowed for reliably high cell attachment compared to CA Uncoated. As such, CA (0.1% PLL) offers a consistent positive control across multiple experiments to standardize other capsules tested within the same batch. Cytokine concentrations are thus (1) reported in absolute values (i.e., pg/mL) across all different experimental trials, and (2) expressed as a percent of CA (0.1% PLL) to normalize data between trials.

Although the absolute concentrations of both the TNFα and IL6 cytokine concentrations were not statistically significant between the capsules tested (Fig. 11A and 12A), when standardized to CA (0.1% PLL) for each individual experiment, TNFα secretion for CA Uncoated was increased (almost by double) compared to CA (0.1% PLL) and for CA (0.1% PLL-0.2% PMM_{50}) (Fig. 11B). When standardized to CA (0.1% PLL) for each individual experiment, IL6 media concentration for CA (0.1% PLL-0.2% PMM_{50}) was also reduced compared to CA Uncoated (Fig. 12B).

IL6 signaling drives fibrosis in unresolved inflammation (Fielding et al., 2014). Similarly, TNFα leads to foreign body responses and inflammation (Zelová & Hošek, 2013). The mannuronic acid component in CA has been found to increase levels of TNFα

(Kulseng et al., 1996), and the increased TNFα and IL6 levels found in this assay fit this pattern, although no other pattern was observed between CA (0.1% PLL) and CA (0.1% PLL-0.2% PMM_{50}). Overall, however, although a cytokine profile could be valuable to assess and contrast how distinct capsule types elicit cytokine responses, collecting supernatant to measure cytokines from the capsule spinning hybridizer suspension model ('3D') may not be specific enough to confidently contrast these capsule types. This is clear when assessing similarities found for IL6 between CA (0.1% PLL) and CA Uncoated capsules. In fact, CA Uncoated capsules have been found to reduce the secretion of TNFα and IL6 more than its CA-PLL counterpart when in human blood (Ørning et al., 2016), which we did not observe. As such, determining a cytokine profile

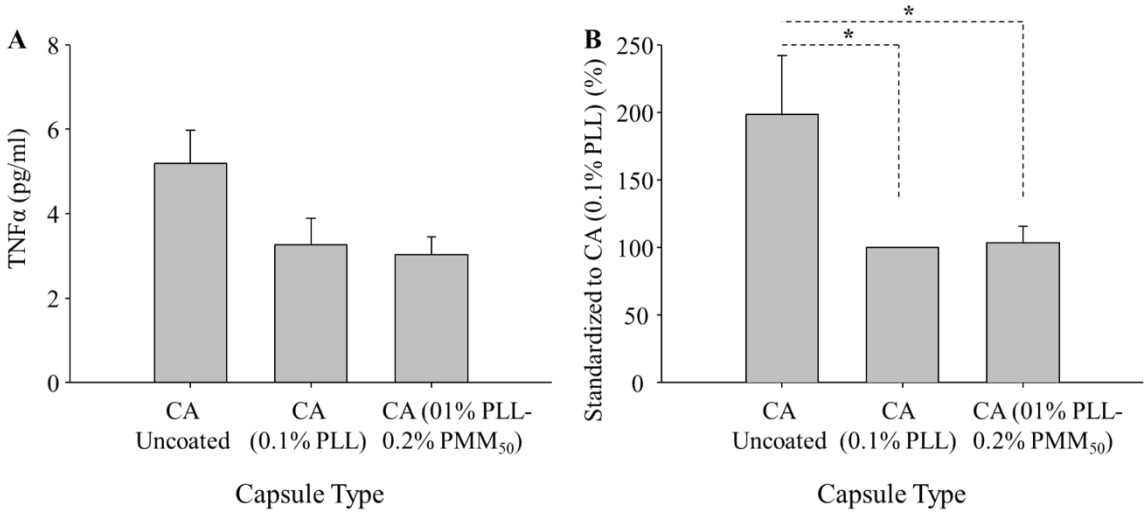

Figure 11: TNFα concentration from media collected after 4 hours of incubation while spinning in a hybridizer with 700,000 NIH 3T3 cells/mL with CA Uncoated, CA (0.1% PLL), and CA (0.1% PLL-0.2% PMM_{50}) capsules. Values are shown as (A) absolute values for TNFα and (B) standardized to CA (0.1% PLL) per experiment. Data represented as mean ± SEM, N = 10-11 independent experiments. Values with asterisks (*) are significantly different from one another, $p < 0.05$.

within these experiments to assess and compare different capsules' fibrotic potentials was not pursued further.

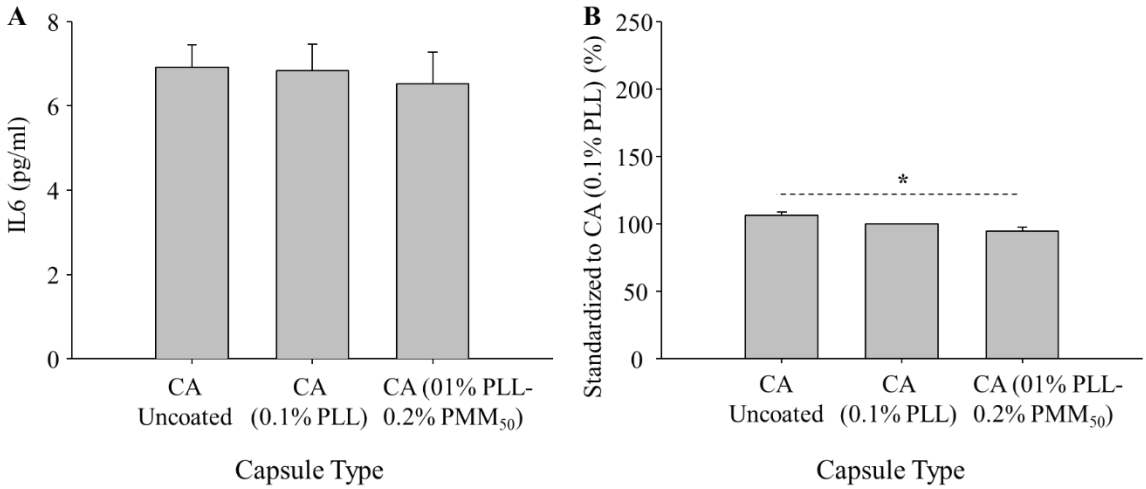

Figure 12: IL6 concentration from media collected after 4 hours of incubation while spinning in a hybridizer with 700,000 NIH 3T3 cells/mL with CA Uncoated, CA (0.1% PLL), and CA (0.1% PLL-0.2% PMM_{50}) capsules. Values are shown as (A) absolute values for IL6 and (B) standardized to CA (0.1% PLL) per experiment. Data represented as mean ± SEM, N = 7-11 independent experiments. Values with asterisks (*) are significantly different from one another, $p < 0.05$.

4.6 Optimizing the RAW 264.7 Cell Capsule Spinning Hybridizer Suspension Model

In addition to the NIH 3T3 cell line discussed in the previous sections, the RAW 264.7 macrophage cell line was also used in the capsule spinning hybridizer suspension model ('3D') since these cells are also used to study fibrotic responses *in vitro* (Godek et al., 2004; Goonoo et al., 2019; Morin & He, 2017). Macrophages are considered a first line of response in inflammation, angiogenesis, and fibrosis (Witherel et al., 2019). From already established parameters for NIH 3T3 cells, we kept the same incubation time (4 hours), counting method (automated macro), washing step introduction, and confocal

magnification (4X). The cell concentration was the final variable to be optimized. Since 700,000 cells/mL was the concentration that maximized the NIH 3T3 cell attachment, cell numbers of 50,000, 175,000, 350,000, 700,000, and 1,000,000 cells/mL were tested for RAW 264.7 cells. CA Uncoated and CA (0.1% PLL) capsules were used for the optimization of the assay with RAW 264.7 cells.

It was found that cell attachment kept increasing past the 1,000,000 cells/mL range (data not shown). As such, an additional experiment was performed adding a concentration of 2,000,000 cells/mL (Fig. 13). This cell concentration had a significantly higher cell attachment range, being almost 4 times higher than the cell attachment for the 1,000,000 cells/mL group. Regardless of the cell density used, CA Uncoated capsules had a significantly lower cell attachment than the CA (0.1% PLL) capsules. Thus, the capsule spinning hybridizer suspension model (‘3D’), originally optimized for NIH 3T3 cells at 700,000 cells/mL, has now also been optimized to yield the highest number for cell attachment by using a 2,000,000 cells/mL RAW 264.7 cell concentration. This will allow for a larger range to be able to compare different capsule types, as portrayed by CA and CA (0.1% PLL) in this experiment.

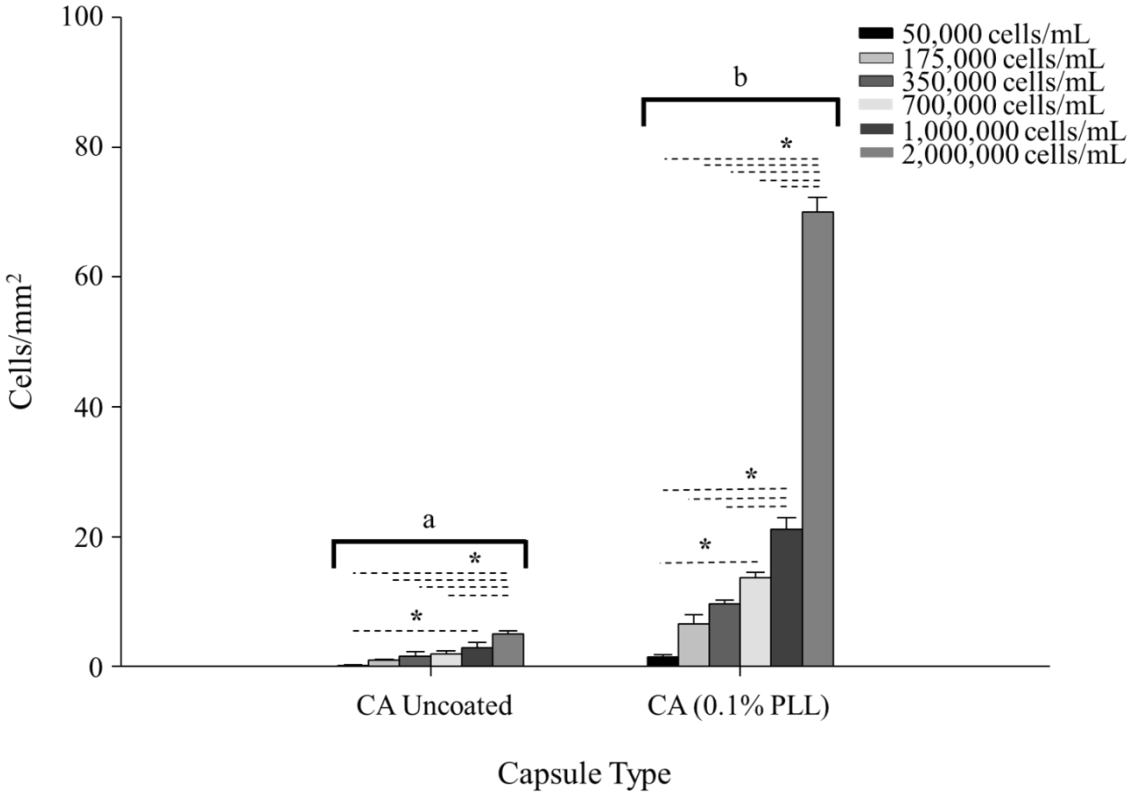

Figure 13: Cell attachment for CA Uncoated and CA (0.1% PLL) capsules after 4 hours of incubation while spinning in a hybridizer with 50,000, 175,000, 350,000, 700,000, 1,000,000, and 2,000,000 RAW 264.7 cells/mL. Cells attached to capsules were counted automatically with a macro. Normalized counts to capsule size were compared between the cell densities tested. Data represented as mean ± SEM, N = 3-5 capsules per group. Values with asterisks (*) are significantly different from one another between cell densities, $p < 0.05$. Values with different letters are significantly different from one another between capsule type regardless of cell density, $p < 0.05$.

4.7 Optimization of Cell-Based Trials Conclusion

In vitro assays to assess cell attachment are not new with studies in the literature reporting cell attachment to surface hydrogels (Diba et al., 2021; Schneider et al., 2004) or microparticles/microcapsules/microcarriers (Dias et al., 2017; Nifontova et al., 2019; Smith et al., 2019). We opted for a '3D' model as the thin film ('2D') approach proved to

be variable and difficult to interpret. “Micro-” experiments are done statically (Dias et al., 2017) or in shaking bioreactors (Smith et al., 2019). However, an important difference to note is that the majority of these ‘3D’ entities are small, most ranging from 125-250 µm in diameter. This is vastly smaller than the capsules for cell encapsulation that we are proposing to screen. While up to this point the optimizing experiments have been performed in capsules ranging from 900-1100 µm, other capsule sizes may be 500-600 µm, all still larger than the microspheres assayed for cell attachment *in vitro* across the literature (Dias et al., 2017; Nifontova et al., 2019; Smith et al., 2019). Thus, none of these experiments account for larger capsule sizes or are designed to compare several capsule compositions at a time, which is one of this thesis’ objectives. The capsule monolayer static model (‘3D’), proved to be ineffective for these larger capsule sizes as the cells settled to the bottom of the wells and did not interact with the capsule surface. As a result, this led to the development and optimization of the capsule spinning hybridizer suspension model (‘3D’). Overall, the most optimal parameters for attempting this assay for NIH 3T3 cells are spinning a 4 mL glass vial for 4 hours in a hybridizer with a cell density of 700,000 cells/mL at a 2 mL volume adding 10 drops of capsules into this mix for a total suspension of ~180 capsules/mL (see Table 4 for summary). For RAW 264.7 cells, we used the same parameters except for cell density; for the RAW 264.7 cells a density of 2,000,000 cells/mL was found to be optimal. It was also determined that using an automatic macro to count the cells attached to the capsules reduced bias and produced more accurate results across users as opposed to manually counting the cells during the analysis process. Using a 4X magnification in a confocal

microscope rather than a 10X magnification was also more time effective; introducing a washing step also ensured cells that were fully attached to capsule surfaces were the only ones being counted.

CA Uncoated, being negatively charged, had significantly lower cell attachment than CA (0.1% PLL) and CA (0.1% PLL-0.2% PMM_{50}) (about 20 times lower). With this range, the assay can detect differences across other capsules that may fall in between that range, making this assay the first model of its kind to reliably suspend cells with capsules (the same capsules that would be tested *in vivo*) *in vitro* to measure cell attachment. Although CA (0.1% PLL)'s cationic surface was expected to allow for the greatest cell attachment, the cell attachment was also similar with CA (0.1% PLL-0.2% PMM_{50}). This was unexpected since PMM_{50} is an anionic outer coating and should have in theory countered or be tightly bound by the cationic surface provided by PLL (Gardner et al., 2011) to stabilize the charges and reduce cell attachment. Yet, in this cell attachment assay, similar with the thin film ('2D') assay, 0.2% PMM_{50} does not seem to reduce cell attachment when added in conjunction with 0.1% PLL. This may be due, in part, to the fact that 0.2% PMM_{50} may not have a high enough concentration to interact with all the polycationic charges present in CA coated with 0.1% PLL. As such, a lower concentration of PLL or a higher concentration of PMM_{50} could be implemented to assess how cell attachment differs for this assay with these changes. However, in HeLa cells, strong cell attachment has been found on either highly cationic or anionic surfaces (Ishihara et al., 2015). Similarly, concerning PLL-PMM, Kleinberger et al. (2016) also

found that a PMM coating, although generating a more anionic surface (as opposed to PLL's highly cationic surface), did not decrease *in vitro* cell attachment but in fact improved it for NIH 3T3 cells. Regardless, moving forward, the capsule spinning hybridizer suspension model ('3D') offers a way to compare capsules' cell attachment responses and will be utilized for additional capsule compositions in section 6.1.

5 Methods and Results for Optimizing ('3D') Protein-Based Trials

5.1 Establishing a Capsule Spinning Hybridizer Protein Adsorption Model

Protein adsorption is one of the first steps in the foreign body response that leads to fibrotic responses (Major et al., 2015; Tang et al., 1996). As such, an assay was developed to measure protein adsorption on capsules' surfaces to be able to compare protein adsorption across different compositions. Fibrinogen is a large (340 kDa), blood plasma protein that strongly adsorbs to hydrophobic surfaces that is commonly used as a model for sticky serum proteins. Lysozyme is a small (14 kDa), positively charged protein often used as a standard for electrostatic interactions of proteins with surfaces. Both of these are considered model proteins for their well characterized adsorption behaviours (Kim & Somorjai, 2003; Liu et al., 2019) and as such were selected for this thesis.

Using a sterile transfer pipette, 3 drops of CA Uncoated capsules, CA (0.1% PLL) capsules, and CA (0.1% PLL-0.2% PMM_{50}) capsules suspended in saline at ~180 capsules/mL were placed into 1.7 mL microcentrifuge tubes. A 0.2 mL volume of

fluorescently labelled fibrinogen (Thermo Fisher Scientific) or lysozyme (Nanocs, Boston, MA) was added to each tube for a final concentration of 0.1 mg/mL (i.e., 0.3 µM for fibrinogen and 7 µM for lysozyme). The primary goal of this assay is to quantify and compare the fluorescence of proteins adsorbed to the surface of a capsule. The tubes containing capsules and fluorescently labelled protein were placed in a UVP HB-1000 hybridization incubator (Thermo Fisher Scientific) and left spinning at 8 rpm at 37 °C for 2 and 24 hours. At the end of each incubation period, tubes in the hybridizer were removed and the capsules were left to settle to the bottom of the tube. Using a syringe and needle, the supernatant (i.e., saline and unbound protein mix) was removed, and remaining capsules were washed with 1 mL HBS to remove any excess protein. This wash step was repeated 2 times for a total of 3 washes. Following the last wash step, capsules were resuspended in 1 mL fresh HBS. Then, using a transfer pipette, 2 drops of this mix (~9 capsules/well) were placed into a 96-well plate; the contents of each tube were tested in triplicate. Pictures of each well were taken at 4X magnification with a Zeiss LSM 510 confocal laser scanning microscope (CLSM) fitted with air-cooled argon and HeNe lasers (LASOS; LGK 7628-1) and running LSM Image Browser software. The fluorescent settings on the confocal microscope (i.e., for green channel a laser line of 488 nm and power of 10) were consistent throughout all pictures for each protein. Around 4-6 capsules were imaged per capsule type by taking a single image per well focusing on the middle (or equatorial) section of the capsules. Images were initially analyzed by taking the mean fluorescence intensity of the entire capsule after subtracting for background

manually (i.e., obtaining the mean fluorescence intensity of 3-4 regions in the image where there were no capsules present).

5.1.1 Pilot Trials

An initial pilot experiment was performed to assess how fluorescence intensity differed after 2 hours of incubation with fibrinogen and lysozyme using an open pinhole (250 µm) on the confocal microscope. The open pinhole maximizes fluorescence intensity at the expense of spatial resolution. This pilot was also done to assess the mean fluorescence intensity from the entire capsule. Unfortunately, using 0.1 mg/mL of protein, the mean fluorescence intensity was under 200 relative fluorescent units (RFU), which was very close to background levels (i.e., ~60 RFU). Moreover, the results from the analysis did not seem conclusive or reliable when comparing the pictures to the data. For instance, Figure 14A shows the CA (0.1% PLL) capsule as being visually brighter than the CA (0.1% PLL-0.2% PMM_{50}) capsule when incubated with fibrinogen. However, in the results (Fig. 14B) these two capsules appear to have similar fluorescence intensities. This mismatch in the data, along with the low levels of fluorescence closely resembling background levels for both fibrinogen and lysozyme (Fig. 14B and 14D), prompted a new experimental design with a higher protein concentration to assess different methods of analysis. Lastly, the CA Uncoated capsules were difficult to analyze as their fluorescence was hard to detect at times on the green channel (i.e., no apparent capsules could be seen), and sometimes extremely bright in a separate trial (image not shown). Further, when observed on the brightfield channel, the CA Uncoated capsules were at times either

broken or dissolved and difficult to image. This was not unexpected as CA beads can lose calcium ions with each solution change (e.g., wash), leading to a weakening of the CA gel that results in swelling and then dissolution. The lack in consistency in their fluorescence, their integrity, and their ease of visibility to analyze them at the early stages of this protocol's development resulted in the decision to remove the CA Uncoated group from the next stages of assay optimization.

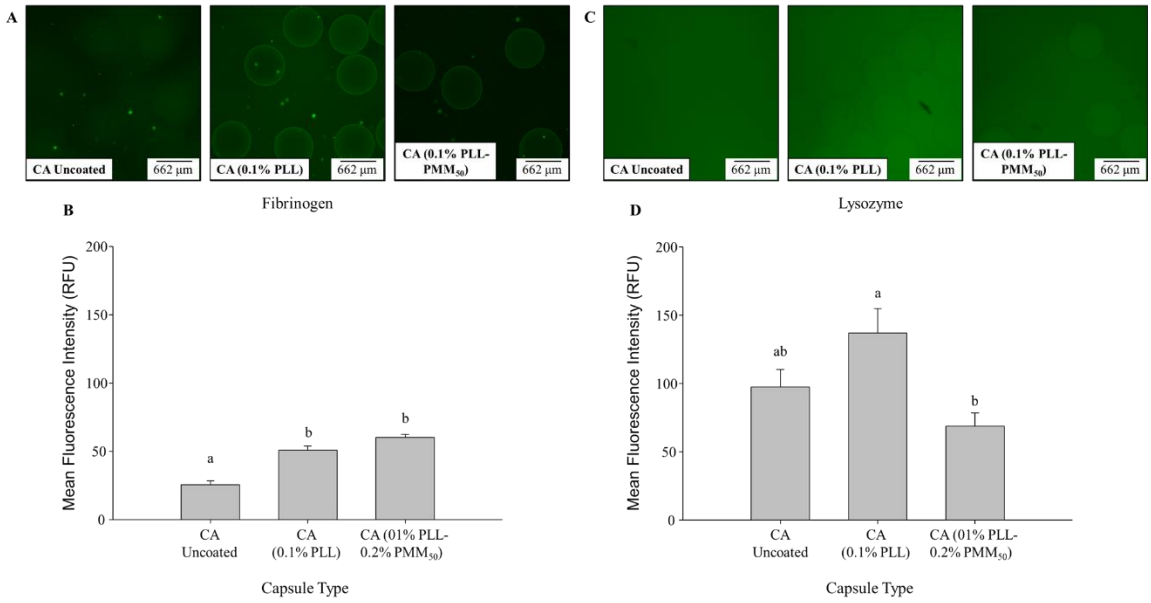

Figure 14: Representative images and mean fluorescence intensity in relative fluorescent units (RFU) of CA Uncoated, CA (0.1% PLL), and CA (0.1% PLL-0.2% PMM_{50}) capsules after being incubated for 2 hours with 0.1 mg/mL (A, B) fibrinogen and (C, D) lysozyme while spinning in a hybridizer. Pictures were taken at a 4X magnification using a confocal microscope (open pinhole, 250 µm) after the capsules were washed twice with HBS. Images shown are in the green-fluorescent channel and have been brightened by 100% for viewing. Data represented as mean ± SEM, N = 18-38 capsules per group. Values with different letters are significantly different from one another, $p < 0.05$.

5.1.2 Standardizing a Method of Analysis

In addition to using a higher protein concentration (1 mg/mL), a smaller pinhole (30 µm) was also used during confocal microscopy analysis to accentuate the edges of the capsule and potentially decrease the noise from the background. During the incubation stage, a 10-minute wait time was added after each wash with HBS to allow for protein equilibration between the inside and the outside of the capsule. All other conditions were left unchanged from the first pilot trial, and only fibrinogen was attempted for this trial. In total, four different types of analyses were performed in ImageJ after taking the images (Fig. 15). These were (1) the 'entire capsule' method (as performed previously in Fig. 14), (2) the 'band' method, (3) the 'line profile' method, and (4) the 'maximum line profile' method. The 'entire capsule', the 'band', and the 'line profile' methods subtracted the background manually from each image based on areas where there were not any capsules, whereas the 'maximum line profile' method subtracted the background from each image automatically using ImageJ's "subtract background" feature with a rolling ball radius of 50 pixels and with the drawn lines having a width of 10 units (this width was selected to capture the least curvature on the capsule as opposed to a thinner line). Briefly, the 'entire capsule' method obtained the mean fluorescence intensity from the whole capsule (inside and outside) (Fig. 15A). The remaining methods focused on the capsule surface only, with the notion that fibrosis takes place on the surface (outside) of the capsule. The 'band' method obtained the mean fluorescence intensity from only the edge of the capsule (Fig. 15B). The 'line profile' method obtained the mean fluorescence

intensity from the edge of the capsule by drawing 3 lines across the entire capsule (Fig. 15C) and obtaining the values only for the edges. Finally, the 'maximum line profile' method had a similar approach to the 'line profile' method, except that instead of 3 long lines, it had 6 smaller lines being drawn around the capsule (Fig. 15D) (the lines being on

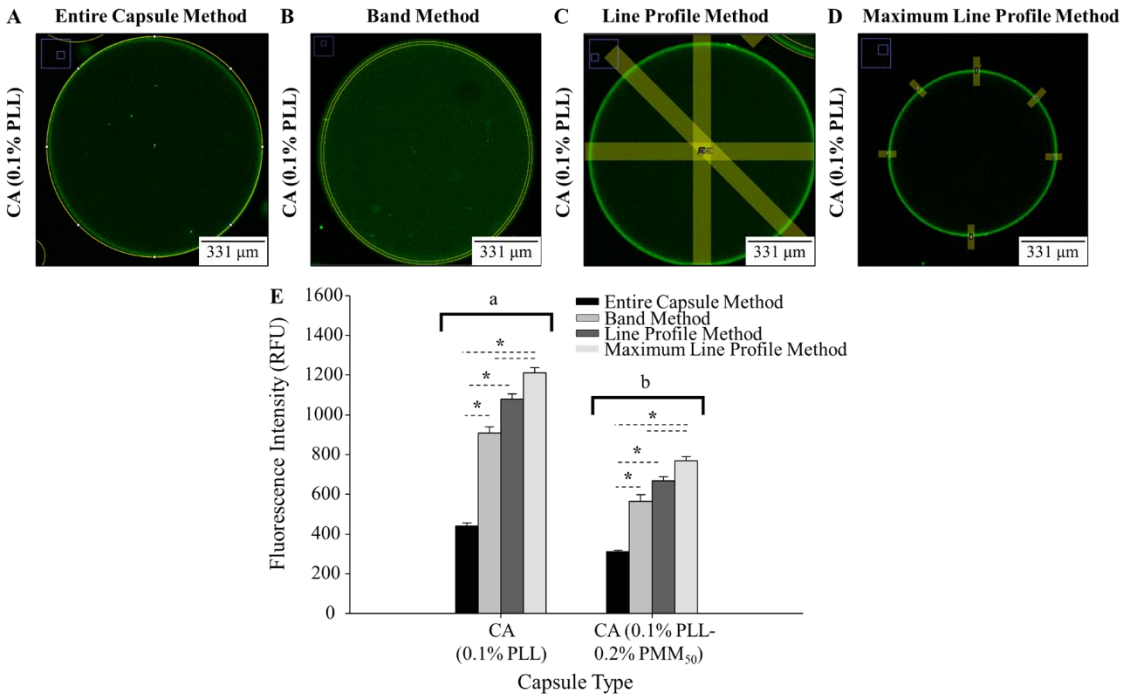

Figure 15: Representative images for CA (0.1% PLL) capsules after being incubated for 2 hours with 1 mg/mL fibrinogen while spinning in a hybridizer. Images were analyzed with the (A) entire capsule method, (B) band method, (C) line profile method, or (D) maximum line profile method, and values were compared through their calculated (E) fluorescence intensity in relative fluorescent units (RFU) for CA (0.1% PLL) and CA (0.1% PLL-0.2% PMM_{50}) capsules. Pictures were taken at a 4X magnification using a confocal microscope (small pinhole, 30 µm) after the capsules were washed twice with HBS (10-minute wait time between each wash). Images shown are in the green-fluorescent channel and have been zoomed in. Data represented as mean ± SEM, N = 9-38 capsules per group. Values with asterisks (*) are significantly different from one another between methods of analysis within a capsule type, $p < 0.05$. Values with different letters are significantly different from one another between capsule type regardless of method of analysis, $p < 0.05$.

the top, bottom, left, right, top left, and top right of the capsule), and using the maximum fluorescence intensity as the value to compare across capsules instead of mean value.

Overall, the 'entire capsule' method had a significantly lower fluorescence intensity compared to all other methods used. While the fluorescence intensity for the 'maximum line profile' method was also significantly higher than that of the 'band' method, it was not statistically different to that of the 'line profile' method. This holds true for both the CA (0.1% PLL) and CA (0.1% PLL-0.2% PMM_{50}) capsules tested. It is important to note that, out of all the methods tested, the 'maximum line profile' method is the quickest to perform, reducing the number of steps needed to obtain the fluorescence intensity and being less prone to error. This is because the 'maximum line profile' returns values directly by ImageJ once the lines are drawn, whereas the other methods require further refinement to obtain the desired values. Most importantly, regardless of the method of analysis used, the results were the same; namely, CA (0.1% PLL) capsules had a significantly higher fluorescence intensity than the CA (0.1% PLL-0.2% PMM_{50}) capsules (Fig. 15E). Overall, therefore, to considerably save time, avoid errors, and ensure the highest range possible (as seen by a higher fluorescence intensity) while analyzing and comparing values, the 'maximum line profile' method was used moving forward.

5.2 Optimizing the Capsule Spinning Hybridizer Protein Adsorption Model

5.2.1 Inverted Microscopy

After establishing the 'maximum line profile' method of analysis, an additional trial was performed with fibrinogen and lysozyme using both 0.1 and 1 mg/mL concentrations, this time using an inverted microscope instead of a confocal microscope (Fig. 16). This was done to assess imaging procedures and because an inverted microscope would capture the entire lower hemispheres of the capsule in a single image.

Surprisingly, the fluorescence intensities for FITC-fibrinogen at 0.1 and 1 mg/mL deposited onto CA (0.1% PLL) were quite similar, and 0.1 mg/mL fibrinogen showed even higher intensity on CA (0.1% PLL-0.2% PMM_{50}) than 1 mg/mL fibrinogen. CA (0.1% PLL) capsules showed a significantly higher fluorescence intensity after FITC-fibrinogen exposure than CA (0.1% PLL-0.2% PMM_{50}) capsules (Fig. 16C), especially at 1 mg/mL FITC-fibrinogen concentration. FITC-Lysozyme similarly seemed to bind more to CA (0.1% PLL) capsules than to CA (0.1% PLL-0.2% PMM_{50}) capsules regardless of the protein concentration used. More aligned to expectations, however, the fluorescence intensity for 0.1 mg/mL lysozyme was significantly lower compared to 1 mg/mL lysozyme in both capsules tested (Fig. 16F). Lastly, several small but bright fluorescent areas were observed in some images (Fig. 15A, 15B, and 15E). These are attributed to undesirable clusters of insoluble protein which could potentially bias the analysis of some images. To select the most appropriate method for image acquisition, and before pursuing

inverted microscopy further, confocal microscopy was also explored (section 5.2.2).

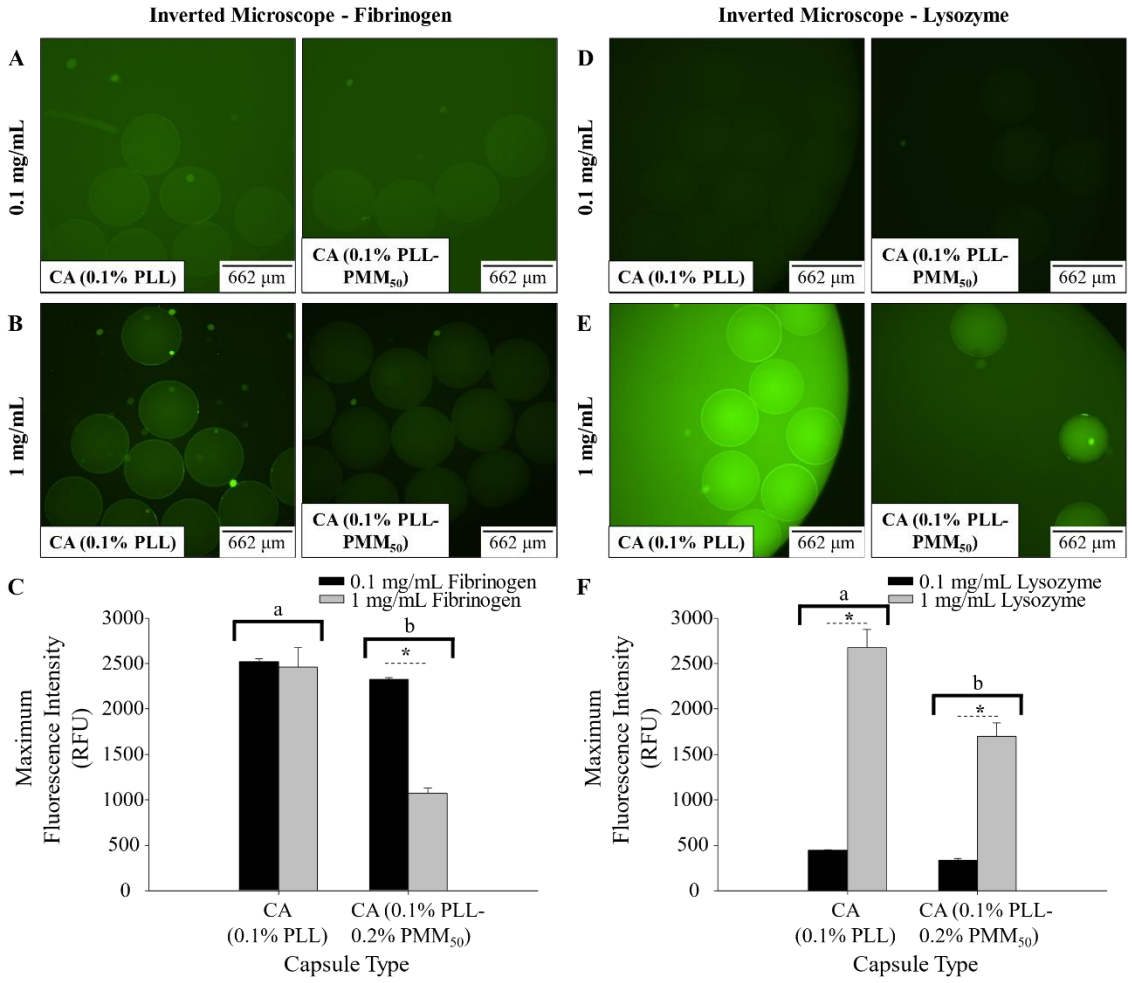

Figure 16: Representative images for CA (0.1% PLL) and CA (0.1% PLL-0.2% PMM_{50}) capsules after being incubated for 2 hours with (A, D) 0.1 and (B, E) 1 mg/mL fibrinogen (left side) or lysozyme (right side) while spinning in a hybridizer. Pictures were taken at a 4X magnification using an inverted microscope after the capsules were washed twice with HBS (10-minute wait time between each wash). Images shown are in the green-fluorescent channel and have been brightened by 100% for viewing. Data calculated as (C, F) maximum fluorescence intensity in relative fluorescent units (RFU), represented as mean ± SEM, N = 13-45 capsules per group. Values with asterisks (*) are significantly different from one another between protein concentration, $p < 0.05$. Values with different letters are significantly different from one another between capsule type regardless of protein concentration, $p < 0.05$.

5.2.2 Confocal Microscopy

The unexpected results for fibrinogen's 0.1 and 1 mg/mL concentrations, in addition to the bright fluorescence clusters of proteins that were being observed through the inverted microscope, led to a final trial comparing 0.1 and 1 mg/mL fibrinogen concentrations on a confocal microscope (Fig. 17). This was done to see if the lower concentration would indeed have a lower fluorescence signal compared to the higher concentration, as seen in lysozyme using an inverted microscope (Fig. 16F), and if the confocal imaging method could decrease the interference by clusters of protein observed. The confocal microscope focuses the laser specifically on a thin section of the capsule in point-by point form as opposed to the entire well area like in an inverted microscope; as such, if there are some protein clusters present even after filtering the protein, they are less prone to interfere in confocal microscopy. The same 'maximum line profile' method of analysis described in section 5.1.2 was used to measure fluorescence intensity.

Indeed, using a confocal microscope, although the protein cluster proteins are still visible (Fig. 17A and 17B), they caused less interference compared to the inverted microscope. As seen by inverted microscopy above (Fig. 16C), CA (0.1% PLL) capsules had a significantly higher fluorescence intensity than the CA (0.1% PLL-0.2% PMM_{50}) capsules regardless of the fibrinogen concentration tested (Fig. 17C). The fluorescence intensity for 0.1 mg/mL fibrinogen was significantly lower compared to 1 mg/mL fibrinogen in both capsules tested (Fig. 17C), as opposed to the analogous comparisons above using an inverted microscope (Fig. 16C). Overall, being able to use images as

cross-section slices makes confocal microscopy more appropriate to assess surface

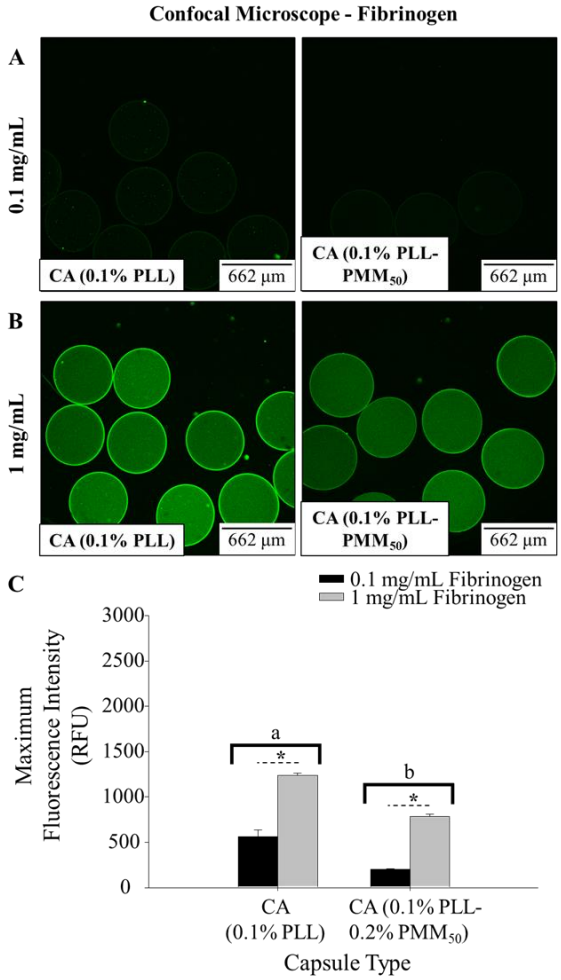

Figure 17: Representative images for CA (0.1% PLL) (left side) and CA (0.1% PLL-0.2% PMM_{50}) (right side) capsules after being incubated for 2 hours with (A) 0.1 and (B) 1 mg/mL fibrinogen while spinning in a hybridizer. Pictures were taken at a 4X magnification using a confocal microscope after the capsules were washed twice with HBS (10-minute wait time between each wash). Images shown are optical cross-sections (10 µm thick, 1024 x 1024 pixels) in the green-fluorescent channel and have been brightened for viewing. Data calculated as (C) maximum fluorescence intensity in relative fluorescent units (RFU), represented as mean ± SEM, N = 15-37 capsules per group. Values with asterisks (*) are significantly different from one another between protein concentration, $p < 0.05$. Values with different letters are significantly different from one another between capsule type regardless of protein concentration, $p < 0.05$.

protein deposition than conventional images from an inverted microscope, especially to avoid potential artifacts including protein clusters. Thus, confocal microscopy was kept as the imaging procedure moving forward. Since the 1 mg/mL concentration proved to consistently yield a higher fluorescence, this concentration was also selected for future experiments.

5.2.3 Protein Volume

Finally, up to this point, the protein adsorption assay had been performed in a 0.2 mL volume of fibrinogen or lysozyme solution. This volume had the potential to be reduced to improve cost-effectiveness, especially when running multiple capsules at a time. Therefore, the next step in the optimization process was to incubate the capsules with 0.05 mL of protein solution versus the original 0.2 mL volume (Fig. 18). Interestingly, using the same number of capsules and using 1 mg/mL fibrinogen with a 0.05 mL volume yielded a slightly but significantly lower fluorescence intensity compared to the 0.2 mL volume for CA (0.1% PLL) capsules, but no change for CA (0.1% PLL-0.2% PMM_{50}) capsules (Fig. 18C). Overall, incubating capsules in 0.05 mL of protein solution versus 0.2 mL had a small effect on the range of the assay and yielded the same conclusions; namely, that the CA (0.1% PLL) capsules had a significantly higher fluorescence intensity than the CA (0.1% PLL-0.2% PMM_{50}) capsules regardless of the fibrinogen volume tested (Fig. 18C). However, there is a significant cost savings realized by reducing the volume of protein solution used in the assay.

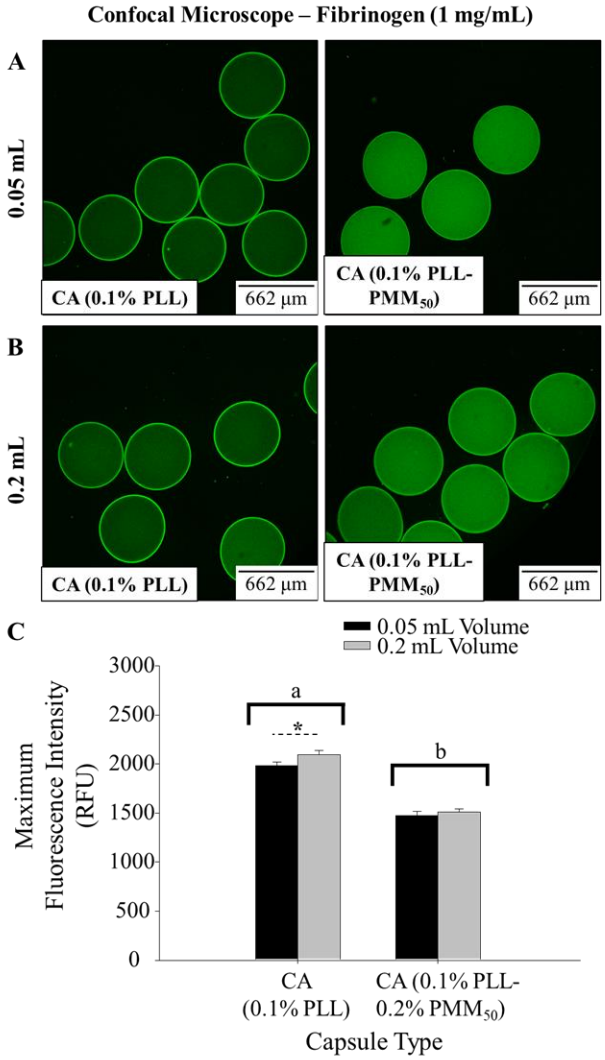

Figure 18: Representative images for CA (0.1% PLL) (left side) and CA (0.1% PLL-0.2% PMM_{50}) (right side) capsules after being incubated for 2 hours with 1 mg/mL fibrinogen at (A) 0.05 and (B) 0.2 mL volumes while spinning in a hybridizer. Pictures were taken at a 4X magnification using a confocal microscope after the capsules were washed twice with HBS (10-minute wait time between each wash). Images shown are optical cross-sections (10 µm thick, 1024 x 1024 pixels) in the green-fluorescent channel and have been brightened for viewing. Data calculated as (C) maximum fluorescence intensity in relative fluorescent units (RFU), represented as mean ± SEM, N = 13-21 capsules per group. Values with asterisks (*) are significantly different from one another between volumes, $p < 0.05$. Values with different letters are significantly different from one another between capsule type regardless of protein concentration, $p < 0.05$.

5.3 Optimization of Protein-Based Trials Conclusion

The capsule spinning hybridizer protein adsorption model is an attractive option as the assay can be performed on any protein desired to investigate its adsorption to the capsules, provided it can be fluorescently tagged. If the proteins bear different fluorophores that are excited at different wavelengths, it might be possible to expose capsules to both proteins in a single, competitive experiment, provided there is no interference. Further, the assay tests the fluorescence of the capsule after exposure to protein in a '3D' environment, rather than a bulk hydrogel (Liu et al., 2019; Swartzlander et al., 2015). Overall, the final parameters optimized for the capsule spinning hybridizer protein adsorption model are using 1.7 mL microcentrifuge tubes incubated for 2 hours in a hybridizer with fluorescently labelled fibrinogen or lysozyme at 1 mg/mL and 3 drops of the desired capsules at ~180 capsules/mL. Thereafter, the capsules are washed twice with HBS (with a 10-minute waiting period in between) and imaged on a confocal microscope at a 4X magnification. The acquired images are then analyzed using the 'maximum line profile' method as described before. A summary of all the optimized parameters used can be found in Table 5. It must be noted that using a line profile measurement has been performed in the past while analyzing fluorescently labelled bovine serum albumin (BSA) (Gardner et al., 2011; Shen et al., 2008), but both the 'line profile' method and the 'maximum line profile' method used in this assay's optimization are faster and more reliable as six edges of a capsule are taken into account as opposed to two, improving the signal/noise.

Table 5: Optimized protein adsorption assay parameters.

Parameter	**Optimized Option**	**Reason**
Method of analysis	'Maximum line profile' method	Less prone to error and more time efficient and consistent
Incubation time	2 hours	More time efficient
Microscope type and magnification	Confocal microscope (4X magnification)	Less variability and more time efficient and consistent
Protein concentration	1 mg/mL	Maximizes assay range
Volume	0.05 mL	More cost-effective

An important outcome from this experiment is the conclusion that the assay should only compare protein fluorescence intensity on the capsule surface. The rationale for this decision stems from the fact that the outside surface of the capsule is most likely responsible for eliciting a foreign body response from the host (Major et al., 2015; Tang et al., 1996). Surface fluorescence intensity was assessed by comparing maximum fluorescence intensity at the edge of a capsule; this maximum lies just below the outermost surface of a capsule and is expected that, when implanted, host tissue likely interacts with this surface. There is an alternative question that involves how the diffusion of these proteins into the capsules compares, and how this porosity may affect capsule integrity and perhaps even fibrosis. It is evident that some capsule types allow more protein in-diffusion. For example, the CA (0.1% PLL) capsules are mostly fluorescent on the edge/outer surface of the capsule, as opposed to CA (0.1% PLL-PMM_{50}) capsules which have fluorescence both on the surface and throughout the interior of the capsule (Fig. 18A and 18B). The current focus is on the exterior of the capsule, but this

experimental design has the potential to also measure protein diffusion into the capsule, and molecular weight cut-offs. Moving forward, the capsule spinning hybridizer protein adsorption model offers a way to compare capsules' protein adsorption responses and will be utilized for additional capsule compositions in section 6.2.

6 Experimental Trials: Unknown Capsule Formulations

After the development of cell attachment assays for NIH 3T3 and RAW 264.7 cells, as well as protein adsorption assays for fibrinogen and lysozyme, a variety of capsules were tested to assess and compare their responses to these assays. Capsule types tested were labelled with a code and not revealed to the investigator until the end of the analysis process (blinded trials). This was done to ensure no bias was present at any point during the experiment, whether in data generation or analysis. Up to this point, only CA had been used as the core base for all capsules used for optimizing experiments, where 0.1% PLL and 0.1% PLL-0.2% PMM_{50} were the outer coatings. It is also important to note that CA Uncoated capsules are not typically suitable for *in vivo* usage because the alginate may incorporate fibrogenic motifs and have low structural integrity at low alginate loading (i.e., they dissolve easily) (see section 1.3).

Every independent trial had CA Uncoated capsules and CA (0.1% PLL) capsules included to serve as internal calibrators. Based on the optimization trials for cell attachment, CA Uncoated capsules always had a lower cell attachment compared to CA (0.1% PLL), and the latter was always consistently higher both in cell attachment and

fluorescence intensity when compared to other capsules like CA (0.1% PLL-0.2% PMM_{50}). Thus, CA Uncoated capsules could be considered 'negative' or 'low' calibrators, and CA (0.1% PLL) capsules could be considered as 'positive' or 'high' calibrators. Further, in addition to reporting data in cells/mm^2 (for cell attachment) or RFU (for protein adsorption fluorescence intensity), data was also expressed as a percent of CA (0.1% PLL) to normalize data between trials.

6.1 Cell Attachment Blind Trials

With all the parameters now optimized for the cell attachment capsule spinning hybridizer suspension model ('3D') using NIH 3T3 or RAW 264.7 cells, 4-6 capsules were imaged per group and averaged (this is a N = 1 independent experiment). There were a minimum of N = 4 independent experiments performed on different days unless otherwise noted. Capsule types tested have a diameter of ~1100 μm unless otherwise noted.

6.1.1 Results for NIH 3T3 Cells

Proprietary formulations, PY, appear to have significantly lower cell attachment than CA (0.1% PLL) CA (0.05% PLL-0.2% PMM_{50}), whether expressed as cells/mm^2 (Fig. 18A) or normalized to CA (0.1%PLL) (Fig. 19B). Overall, PY capsules appeared to have a lower cell attachment compared to CA-coated capsules.

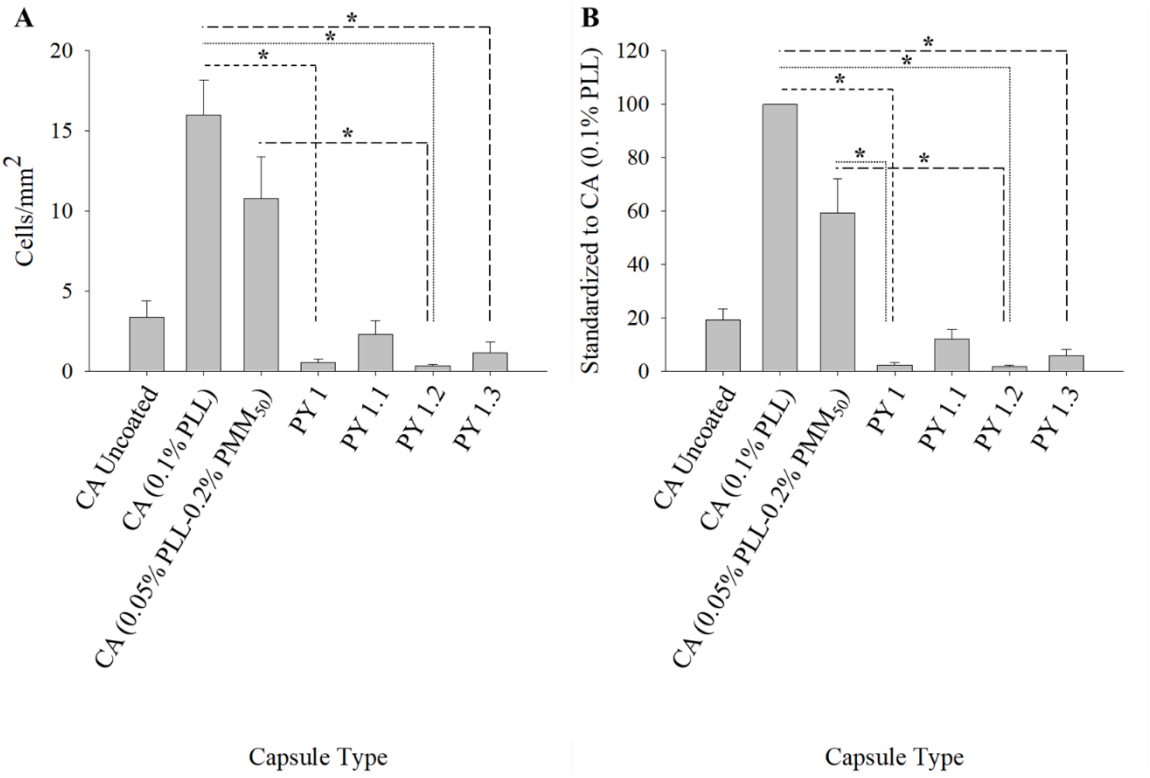

Figure 19: Cell attachment for various capsule types after 4 hours of incubation while spinning in a hybridizer with 700,000 NIH 3T3 cells/mL. Values are shown as (A) cells/mm^2 and (B) standardized to CA (0.1% PLL) per experiment. Data represented as mean ± SEM, N = 4-13 independent experiments. Values with asterisks (*) are significantly different from one another, $p < 0.05$.

6.1.2 Results for RAW 264.7 Cells

Cell attachment was significantly higher in CA (0.1% PLL) when compared against CA Uncoated (Fig. 20). In fact, CA (0.05% PLL-0.2% PMM_{50}), also had a higher cell attachment compared to CA Uncoated but a similar cell attachment to CA (0.1% PLL). Other PY formulations were higher or lower than CA (0.1% PLL), indicating a range of cell interactions were detected by the assay.

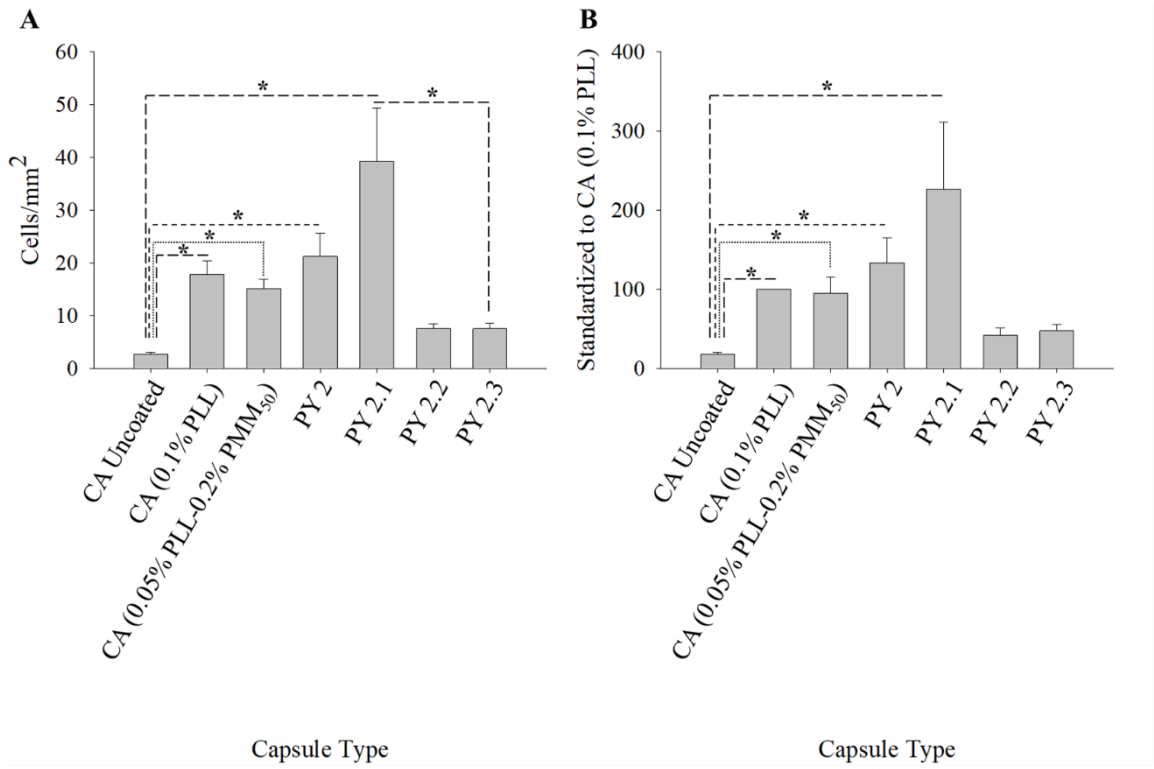

Figure 20: Cell attachment for various capsule types after 4 hours of incubation while spinning in a hybridizer with 2,000,000 RAW 264.7 cells/mL. Values are shown as (A) cells/mm^2 and (B) standardized to CA (0.1% PLL) per experiment. Data represented as mean ± SEM, N = 4-11 independent experiments. Values with asterisks (*) are significantly different from one another, $p < 0.05$.

6.2 Protein Adsorption Blind Trials

With all the parameters now optimized for the capsule spinning hybridizer protein adsorption model, 4-15 capsule replicates performed on a single day (an independent experiment) were imaged per group and averaged.

6.2.1 Results for Fibrinogen Protein

Fibrinogen adsorption on capsules was not statistically different across the capsule types tested, both when measuring the RFU directly (Fig. 21A) or when standardizing experiments to CA (0.1% PLL) (Fig. 21B). There was also no statistically significant trend across capsules, as opposed to the cell attachment experiments. However, a trend worth noting is that fibrinogen adsorption for CA (0.05% PLL-0.2% PMM_{50}) did seem

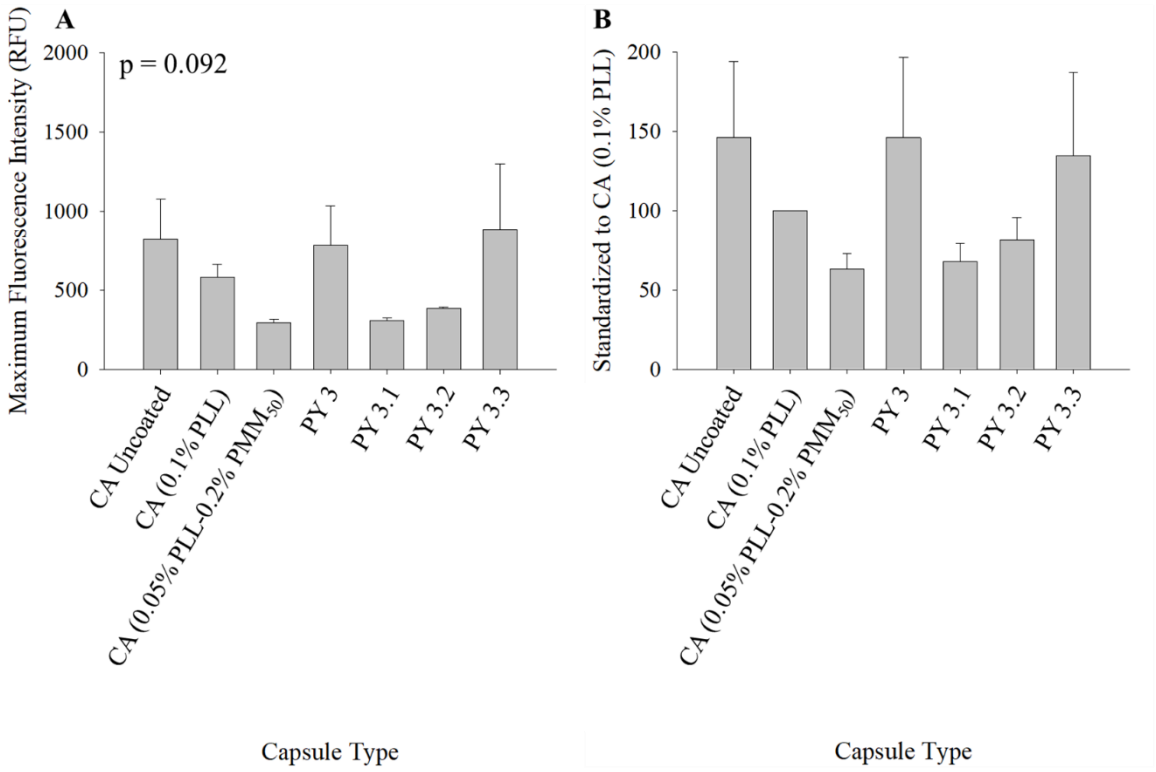

Figure 21: Maximum fluorescence intensity in relative fluorescent units (RFU) for the edges of various capsule types after 2 hours of incubation while spinning in a hybridizer with 1 mg/mL fluorescent fibrinogen. Values are shown as (A) cells/mm^2 and (B) standardized to CA (0.1% PLL) per experiment. Data represented as mean ± SEM, N = 3-5 independent experiments. Values with asterisks (*) are significantly different from one another, $p < 0.05$.

lower than CA Uncoated, CA (0.1% PLL), and some PY compositions; but again, this trend was not statistically significant.

6.2.2 Results for Lysozyme Protein

Contrary to fibrinogen adsorption, for lysozyme adsorption there appeared to be a lower fluorescence trend overall on CA, CA-PLL, and CA-PLL-PMM_{50} capsules compared to the PY formulations. Although this trend could be observed in the RFU

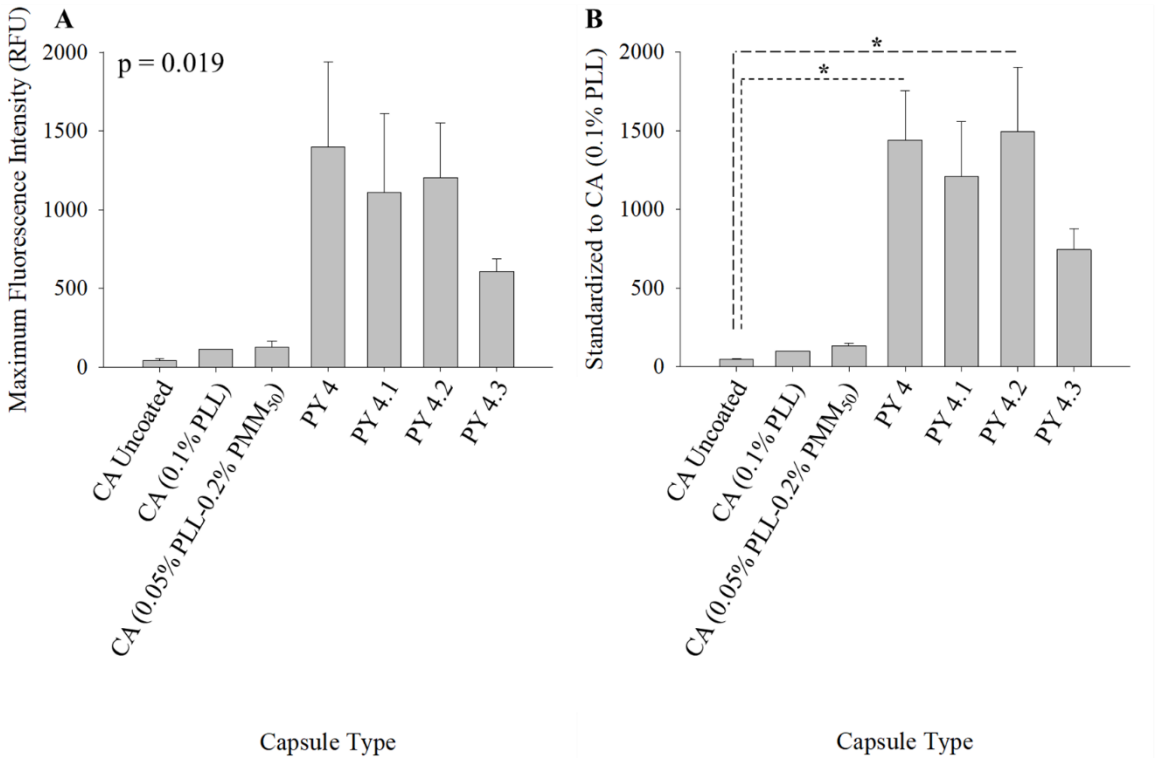

Figure 22: Maximum fluorescence intensity in relative fluorescent units (RFU) for the edges of various capsule types after 2 hours of incubation while spinning in a hybridizer with 1 mg/mL fluorescent lysozyme. Values are shown as (A) cells/mm^2 and (B) standardized to CA (0.1% PLL) per experiment. Data represented as mean ± SEM, N = 3 independent experiments. Values with asterisks (*) are significantly different from one another, $p < 0.05$.

comparison (Fig. 22A), there were no statistically significant differences between any capsule type after post-hoc testing ($p > 0.05$) despite the one-way ANOVA being significant ($p = 0.019$). However, when standardizing experiments to CA (0.1% PLL), two PY formulations achieved significant difference compared to CA Uncoated.

6.3 Predictive Analysis of In Vitro Blind Trials With In Vivo Outcomes

PCO score was modelled using binomial logistic regression (see section 2.4) to assess whether '3D' *in vitro* assay results described in this thesis can predict PCO score *in vivo*. Using the classification categories (of "PCO score lower than 2" (i.e., less than 50% PCO) and "PCO score higher than 2" (i.e., more than 50% PCO)), it was found that *in vitro* cell attachment using RAW 264.7 cells could predict *in vivo* PCO score, either expressed as cells/mm^2 (odds ratio = 1.26, 95% confidence interval [1.06, 1.51], $p = 0.009$) or as a percentage of CA (0.1% PLL) (odds ratio = 1.02, 95% confidence interval [1.01, 1.04], $p = 0.008$). All other outcome measures were not statistically significant and had an odds ratio close to 1. Moreover, *in vitro* cell attachment using RAW 264.7 cells expressed as cells/mm^2 yielded the lowest misclassification rate (16.7%) when using the testing set to assess how well the model created from the training set fitted. Interestingly, protein adsorption using lysozyme as RFU values also had the same misclassification rate, but its effect on the model was not significant (odds ratio = 1.00, 95% confidence interval [0.99, 1.01], $p = 0.12$). Table 6 summarizes the results and assessment of the logistic regression models created.

Table 6: Summary of results and assessment of binomial logistic regression models created for each *in vitro* assay to predict *in vivo* PCO scores.

***In Vitro* Assay**	**Odds Ratio**	**95% Confidence Interval**	**p-value**	**Misclassification Error for Testing Set**
NIH 3T3 cell attachment (expressed as cells/mm^2)	0.72	0.42, 1.22	0.22	22.2%
NIH 3T3 cell attachment (standardized to CA (0.1% PLL))	0.92	0.83, 1.03	0.14	22.2%
RAW 264.7 cell attachment (expressed as cells/mm^2)	1.26	1.06, 1.51	**0.009**	16.7%
RAW 264.7 cell attachment (standardized to CA (0.1% PLL))	1.02	1.01, 1.04	**0.008**	25.0%
Fibrinogen protein adsorption (expressed as RFU)	1.00	0.99, 1.01	0.77	33.3%
Fibrinogen protein adsorption (standardized to CA (0.1% PLL))	1.01	1.00, 1.02	0.45	33.3%
Lysozyme protein adsorption (expressed as RFU)	1.00	0.99, 1.01	0.12	16.7%
Lysozyme protein adsorption (standardized to CA (0.1% PLL))	1.00	0.99, 1.01	0.14	33.3%

7 Discussion for Experimental and Blinded Trials

7.1 Experimental and Blinded In Vitro Trials

Statistical comparisons are key to understanding differences between capsule types, but interesting patterns emerge that are still useful to inform future polymer design even if the results were not statistically different. This section focuses on discussing these trends before moving on to predictive modelling on section 7.2. A summary of the results

standardized to CA (0.1% PLL) from sections 6.1 and 6.2 can be found in Table 7. These assays are meant to be screening tools to compare capsule types with regards to cell attachment and protein adsorption.

Table 7: Experimental trials summary for each capsule type in relation to CA (0.1% PLL) as a reference (set as 100%). Categories are less than 25% ('Low'), 25-66% ('Medium'), and more than 66% ('High'), noting results over 100%.

Capsule Type	**Experimental Trial Outcome**			
	Cell Attachment		**Protein Adsorption**	
	NIH 3T3	**RAW 264.7**	**Fibrinogen**	**Lysozyme**
CA Uncoated	Low	Low	High (>100%)	Medium
CA (0.1% PLL)	Reference (High)	Reference (High)	Reference (High)	Reference (High)
CA (0.05% PLL-0.2% PMM_{50})	Medium	High	Medium	High (>100%)

For cell attachment, in NIH 3T3 cells, CA (0.1% PLL) has a higher cell attachment than CA (0.05% PLL-0.2% PMM_{50}) (Fig. 19), albeit not statistically significant. Although a higher PLL concentration may lead to higher cell attachment, it can also be attributed to PMM_{50}'s anionic properties. In RAW 264.7 cells, this trend is much less apparent as both capsule types have a similar cell attachment (Fig. 20). PLL's highly cationic surface has also been shown to attract cells and lead to cell overgrowth in capsules retrieved from animals, where 0.1% PLL had significantly higher cell overgrowth than 0.05% PLL (Strand et al., 2001). In the optimization experiments with NIH 3T3 cells, CA (0.1% PLL) and CA (0.1% PLL-0.2% PMM_{50}) also had similar cell attachment (Fig. 10), indicating that, even at the same PLL concentration, PMM_{50} may

not be enough to reduce cell attachment. A possible explanation for CA (0.1% PLL) and CA (0.05% PLL-0.2% PMM_{50}) having similar cell attachment in RAW 264.7 cells is that the PLL-PMM_{50} complex may still be cationic enough for cells to attach despite PMM_{50}'s overall anionic surface. Further, cells may also strongly attach to highly charged surfaces, cationic or anionic, as has been reported in HeLa cells (Ishihara et al., 2015) and in NIH 3T3 cells on PLL-PMM surface coatings (Kleinberger et al., 2016). In addition, the strong complexation between PLL and PMM can give a surface that is stiffer and more poorly hydrated (more hydrophobic) than the surface of uncoated capsules.

Figure 19 shows that the CA Uncoated capsules appear to have a higher cell attachment than most of the PY compositions in NIH 3T3 cells, suggesting that PY aids in biocompatibility in general. However, with the RAW 264.7 cells the trend is reversed, with CA Uncoated capsules having lower cell attachment than some of the PY-containing ones, and it was also statistically significantly lower (Fig. 20). It is clear, however, based on the high cell attachment observed with CA (0.1% PLL) capsules overall for both NIH 3T3 and RAW 264.7 cell lines compared to CA Uncoated capsules, that the cell attachment assay can distinguish differences for more "sticky" capsules (in this case, CA Uncoated versus CA (0.1% PLL) capsules). RAW 264.7 cells can offer more range to differentiate cell attachment values compared to NIH 3T3 cells, especially when assessing PY capsule cores, which may prove useful when differentiating performance between these capsule types. Whether the trends observed in NIH 3T3 cells or RAW 264.7 cells (if any) may be more indicative of the cell attachment that occurs *in vivo* due to fibrosis is

discussed further in section 7.2. Importantly, standardizing across different experiments may be crucial to normalize results across different days and allow for proper comparison. Here, we also reported cell attachment standardized to CA (0.1% PLL) as this capsule proved to have constantly high cell attachment (i.e., it was used as a calibrator for being a consistent "positive control"). These results allowed for less variation across experimental days.

Interestingly, the results from the protein adsorption assay were not entirely consistent with the cell attachment assays. For example, when comparing CA and PY capsule cores, there were no differences between fibrinogen adsorption whereas when testing lysozyme many of the CA capsule cores had *lower* fluorescence intensity (as opposed to higher cell attachment) than many of the PY capsules. For fibrinogen, CA Uncoated seem to have higher fibrinogen adsorption than its coated forms (Fig. 21). This is opposite to what is seen with the cell attachment results for NIH 3T3 and RAW 264.7 cells, where CA Uncoated had a lower cell attachment compared to CA (0.05% PLL-0.2% PMM_{50}). More aligned with expectations based on polycation (PLL) loading, fibrinogen adsorption of CA (0.1% PLL) does seem to be higher than CA (0.05% PLL-0.2% PMM_{50}).

Lysozyme's small size and different charge might allow it to deviate from this trend compared to larger proteins like fibrinogen. Indeed, for lysozyme, the CA, CA-PLL, and CA-PLL-PMM_{50} capsules had a much lower fluorescence intensity and hence lower lysozyme adsorption compared to PY capsules (Fig. 22). Nonetheless, both the cell

attachment and protein adsorption experiments have been optimized for the purpose of testing multiple capsules and can offer valuable insight into the properties of these formulations and how they react with NIH 3T3 and RAW 264.7 cell lines and fibrinogen and lysozyme properties. If additional cell lines or properties are desired to be tested, these experiments can be easily modified with little further optimization to obtain additional data for the goal of better predicting *in vivo* responses.

7.2 Predictive Modelling

Logistic regression, a classification tool in machine learning, is a process of modeling the probability of a discrete outcome given an input variable. It is most used for binary outcomes (e.g., yes/no, pass/fail, etc.), but multinomial logistic regression can model scenarios where there are more than two possible discrete outcomes as well. Nonetheless, logistic regression has been used to model and predict whether a foreign body response will be “present” or “not present” based on implant characteristics, implantation site, and/or host (Jeon et al., 2016; Sigler et al., 2014; Watad et al., 2018), whether hydrogel swelling will occur based on hydrogel characteristics and composition (Zheng & Liu, 2021), and whether a disease like cancer or a stroke will “occur” or “not occur” based on inflammatory and/or lipid markers (Ma et al., 2020; J.-J. Zhang et al., 2021). More related with this thesis, logistic regression has also been applied to determine whether an *in vivo* response will be “toxic” or “non-toxic” based on *in vitro* experiments (DiMaggio et al., 2010). In the case of this study, logistic regression was modelled to determine whether an *in vivo* (i.e., PCO) response can be categorized as either having a

"PCO score lower than 2" (i.e., cellular overgrowth lower than 50%) or a "PCO score higher than 2" (i.e., cellular overgrowth higher than 50%) based on *in vitro* experiments (i.e., cell attachment and protein adsorption assays). This modelling was performed on 75% of the data available for each capsule tested (training set) and it was then assessed by checking the misclassification rate on the remaining 25% of the data for each capsule tested (testing set).

It was found that *in vitro* capsule RAW 264.7 cell attachment offered the best results to assess whether a capsule will have *in vivo* cellular overgrowth lower than 50% (i.e., PCO score lower than 2) or higher than 50% (PCO score higher than 2). Further, this classification was most accurate when using the values expressed as cells/mm^2 as opposed to standardizing each independent experimental trial to CA (0.1% PLL), as is shown by having a lower misclassification rate from the testing data set. The odds ratio for RAW 264.7 cell attachment expressed as cells/mm^2 values was 1.26. This can be interpreted as for each one unit increase in cells/mm^2 for RAW 264.7 cell attachment, the odds of a capsule having a PCO score higher than 2 increases by 1.26. It can also be thought as for every unit increase in cells/mm^2, the odds of reaching a PCO score higher than 2 is 1.26 – 1 = 0.26 or 26%. Finally, given this data training set, one can also predict how likely a capsule will reach a PCO score higher than 2 depending on what value we get for an assay (using the logit link function) (Agresti, 2013; McCullagh & Nelder, 2019; Prasetyo et al., 2020). For example, if a value of ~20 cells/mm^2 was obtained when performing a RAW 264.7 cell attachment assay *in vitro*, the calculated probability of that

capsule achieving a PCO score higher than 2 *in vivo* would be ~50%. Further, if a value of ~32 cells/mm^2 was obtained, the calculated probability of that capsule achieving a PCO score higher than 2 would be ~95%. Using the probabilities from a logistic regression model can be attractive when it is difficult to decide what a PCO cut-off 'threshold' may be to screen out a capsule. Alternatively, a simple linear regression model could also be used to predict PCO scores based on the *in vitro* assays, but a decision would have to be made on what score would be used to screen out a capsule (e.g., if the equation to the line of best fits predicts a PCO score higher than 3 based on a given value, then screen the capsule out). Nonetheless, for the purposes of this study and because determining this PCO 'threshold' is in fact difficult to establish, logistic regression and calculated probabilities were used to predict PCO scores based on *in vitro* assay results.

It is important to note that although the other *in vitro* assays used in this thesis were not useful in predicting PCO in this model, they should not be discarded as this predictability may change and be enhanced by using additional capsule compositions. Although assessing more capsules *in vivo* and *in vitro* can further enhance these models and their predictability potential, the modelling results derived from these experiments are a promising first step in using *in vitro* experiments to predict *in vivo* responses. This can allow for a more methodical approach in better selecting and screening future capsule compositions *in vitro* to save time and resources before moving on to *in vivo* experiments.

7.3 Future Steps

All the *in vitro* experiments outlined in this thesis have been performed on empty/blank capsules. An additional question aims to determine if attachment of either NIH 3T3 and/or RAW 264.7 cells (or additional cells) may differ on the surface of the capsules when there are other cells (i.e., beta cells) already encapsulated within the capsules, or if capsules are precoated with proteins prior to attempting the *in vitro* cell attachment experiments. This would, of course, offer an even more realistic scenario of how these capsules are implanted into animals and it would be interesting to compare how cell attachment may differ (if at all) to empty/blank capsules as performed in this thesis. Further, in addition to fibrinogen and lysozyme, testing other proteins' adsorption to a capsule surface, or assessing how a mixture of proteins may affect their adsorption as well could also better resemble the fibrosis progression that occurs *in vivo*. Lastly, co-culturing of cells, like fibroblasts and macrophages, and of proteins, like fibrinogen and lysozyme, and assessing their responses to capsule attachment may also allow for a more realistic model as to what is seen *in vivo*. These additional *in vitro* techniques could also be tested in a model such as logistic regression to predict responses *in vivo*. This study used six different capsule compositions and found that RAW 264.7 cell attachment assays yielded the best results to predict PCO score, but this model can be further improved by adding additional capsule compositions into the model or testing for other assays as described above. The models may also be further refined by creating different categories (e.g., more than two categories instead of only "PCO score lower than 2" and "PCO score

higher than 2") and using multimodal logistic regression, depending on the range available in the PCO data and the number of capsules tested. A limitation in the use of the models for this thesis were that they all were univariate analyses; that is, no capsule was ever retested in different experiments (since they had to be discarded after every experiment). If additional experiments allow for the retest of the same capsule, this could allow for a multivariate analysis (i.e., one model assessing all assays as opposed to comparing many models for each assay as is the case in univariate analysis), which may result in a more accurate model.

7.4 Conclusion

This study designed, validated, and examined several methods to assess fibrotic responses *in vitro* (e.g., cell attachment/overgrowth and protein adsorption), and then explored their predictability through binomial logistic regression models. Although initially the assays explored were '2D', most of the assays which showed most promise for use as a screening tool were '3D' and utilized the same capsule compositions that are implanted into animals for further testing. This was done to more closely mimic *in vivo* conditions and hopefully be able to obtain similar responses *in vitro* for the purpose of simplifying the selection and screening processes of these capsules. Moreover, the assays' methodology and subsequent analysis described in this study have been optimized to the point that other cell lines (for cell attachment assays) and proteins (for protein adsorption assays) can be easily changed, with little additional optimization. For both NIH 3T3 and RAW 264.7 cell attachment assays, it was found that CA (0.1% PLL) capsules always

had a higher cell attachment than CA Uncoated capsules, making the former a reliable 'positive' calibrator and the latter a 'negative' calibrator. Protein adsorption assays had more distinct patterns. The simplicity of these assays creates an attractive and versatile approach to modify these experiments as desired.

Utilizing logistic regression offers a simple approach to test the potential of *in vitro* assays to predict more complicated *in vivo* responses such as PCO, making this study the first of its kind to predict the fibrotic response potential of hydrogel capsule compositions *in vivo* through direct and easily modifiable *in vitro* assays. Out of the NIH 3T3 cell attachment assay, the RAW 264.7 cell attachment assay, the fibrinogen protein adsorption assay, and the lysozyme protein adsorption assay, it was found that the RAW 264.7 cell line better predicted the results for *in vivo* PCO. Using this model, future *in vivo* PCO results with different capsule types can be best predicted based on the values obtained from the RAW 264.7 cell attachment assay, and likelihoods can be calculated to assess whether the capsule being assessed merits further testing in animals. For instance, if a value of ~32 cells/mm^2 was obtained, the calculated probability of that capsule achieving a PCO score higher than 2 (i.e., more than 50% cellular overgrowth) would be ~95%, and thus it would not be advisable to spend further time and resources to test that capsule *in vivo*. Of course, no model is perfect, and it is imperative to note that the remaining assays not significant in these models may still be useful if more capsule compositions are tested and more data is collected to enhance the model. Overall, the goal of this project was to develop *in vitro* assays to compare and select capsules that will better avoid fibrotic responses *in vivo*. The development and validation of these quick-to-

implement assays can help advance and lead to a more promising and long-term treatment of diabetes.

8 List of References

Agrawal, N. K. (2014). Targeting inflammation in diabetes: Newer therapeutic options. *World Journal of Diabetes*, *5*(5), 697–697. https://doi.org/10.4239/wjd.v5.i5.697

Agresti, A. (2013). *Categorical data analysis* (3rd ed). Wiley.

American Diabetes Association. (2004). Diagnosis and classification of diabetes mellitus. *Diabetes Care*, *27*(Supplement 1), S5–S10. https://doi.org/10.2337/diacare.27.2007.S5

American Diabetes Association. (2008). Economic costs of diabetes in the U.S. in 2007. *Diabetes Care*, *31*(3), 596–615. https://doi.org/10.2337/dc08-9017

American Diabetes Association. (2018). Economic Costs of Diabetes in the U.S. in 2017. *Diabetes Care*, *41*(5), 917–928. https://doi.org/10.2337/dci18-0007

Ashcroft, F. M., Harrison, D. E., & Ashcroft, S. J. H. (1984). Glucose induces closure of single potassium channels in isolated rat pancreatic β-cells. *Nature*, *312*(5993), 446–448. https://doi.org/10.1038/312446a0

Ashcroft, F. M., Proks, P., Smith, P. A., Ämmälä, C., Bokvist, K., & Rorsman, P. (1994). Stimulus-secretion coupling in pancreatic β cells. *Journal of Cellular Biochemistry*, *55*(S1994A), 54–65. https://doi.org/10.1002/jcb.240550007

Ballinger, W. F., & Lacy, P. E. (1972). Transplantation of intact pancreatic islets in rats. *Surgery*, *72*(2), 175–186.

Barkai, U., Rotem, A., & de Vos, P. (2016). Survival of encapsulated islets: More than a membrane story. *World Journal of Transplantation*, *6*(1). https://doi.org/10.5500/wjt.v6.i1.69

Barnard, K. D., Lloyd, C. E., & Skinner, T. C. (2007). Systematic literature review: Auality of life associated with insulin pump use in type 1 diabetes. *Diabetic Medicine*, *24*(6), 607–617. https://doi.org/10.1111/j.1464-5491.2007.02120.x

Bochenek, M. A., Veiseh, O., Vegas, A. J., McGarrigle, J. J., Qi, M., Marchese, E., Omami, M., Doloff, J. C., Mendoza-Elias, J., Nourmohammadzadeh, M., Khan, A., Yeh, C.-C., Xing, Y., Isa, D., Ghani, S., Li, J., Landry, C., Bader, A. R., Olejnik, K., … Oberholzer, J. (2018). Alginate encapsulation as long-term immune protection of allogeneic pancreatic islet cells transplanted into the

omental bursa of macaques. *Nature Biomedical Engineering*, *2*(11), 810–821. https://doi.org/10.1038/s41551-018-0275-1

Boden, G. (2005). Free fatty acids and insulin secretion in humans. *Current Diabetes Reports*, *5*(3), 167–170. https://doi.org/10.1007/s11892-005-0004-5

Boland, B. B., Rhodes, C. J., & Grimsby, J. S. (2017). The dynamic plasticity of insulin production in β-cells. *Molecular Metabolism*, *6*(9), 958–973. https://doi.org/10.1016/j.molmet.2017.04.010

Bornfeldt, K. E., & Tabas, I. (2011). Insulin resistance, hyperglycemia, and atherosclerosis. *Cell Metabolism*, *14*(5), 575–585. https://doi.org/10.1016/j.cmet.2011.07.015

Bretzel, R. G., Hering, B. J., Schultz, A. O., Geier, C., & Federlin, K. (1996). International islet transplant registry report. In R. P. Lanza & W. L. Chick (Eds.), *Yearbook of Cell and Tissue Transplantation 1996–1997* (pp. 153–160). Springer Netherlands. https://doi.org/10.1007/978-94-009-0165-0_15

Burks, D. J., & White, M. F. (2001). IRS proteins and beta-cell function. *Diabetes*, *50*(Supplement 1), S140–S145. https://doi.org/10.2337/diabetes.50.2007.S140

Carroll, L., Mridha, A. R., & Tuch, B. E. (2019). Encapsulation and transplantation of pancreatic progenitor cells. In M. V. Joglekar & A. A. Hardikar (Eds.), *Progenitor Cells* (Vol. 2029, pp. 93–102). Springer New York. https://doi.org/10.1007/978-1-4939-9631-5_8

Censi, S., Mian, C., & Betterle, C. (2018). Insulin autoimmune syndrome: From diagnosis to clinical management. *Annals of Translational Medicine*, *6*(17), 335–335. https://doi.org/10.21037/atm.2018.07.32

Cernea, S., & Dobreanu, M. (2013). Diabetes and beta cell function: From mechanisms to evaluation and clinical implications. *Biochemia Medica*, 266–280. https://doi.org/10.11613/BM.2013.033

Chatenoud, L. (2008). Chemical immunosuppression in islet transplantation—Friend or foe? *New England Journal of Medicine*, *358*(11), 1192–1193. https://doi.org/10.1056/NEJMcibr0708067

Chen, S., Du, K., & Zou, C. (2020). Current progress in stem cell therapy for type 1 diabetes mellitus. *Stem Cell Research & Therapy*, *11*(1), 275. https://doi.org/10.1186/s13287-020-01793-6

Chiasson, J.-L., & Rabasa-Lhoret, R. (2004). Prevention of type 2 diabetes: Insulin resistance and beta-cell function. *Diabetes*, *53*(Supplement 3), S34–S38. https://doi.org/10.2337/diabetes.53.suppl_3.S34

Cnop, M., Welsh, N., Jonas, J.-C., Jorns, A., Lenzen, S., & Eizirik, D. L. (2005). Mechanisms of pancreatic β-cell death in type 1 and type 2 diabetes: Many differences, few similarities. *Diabetes*, *54*(Supplement 2), S97–S107. https://doi.org/10.2337/diabetes.54.suppl_2.S97

Cook, D. L., & Hales, N. (1984). Intracellular ATP directly blocks K+ channels in pancreatic B-cells. *Nature*, *311*(5983), 271–273. https://doi.org/10.1038/311271a0

Corbett, J. A., & McDaniel, M. L. (1995). Intraislet release of interleukin 1 inhibits beta cell function by inducing beta cell expression of inducible nitric oxide synthase. *The Journal of Experimental Medicine*, *181*(2), 559–568. https://doi.org/10.1084/jem.181.2.559

Couriel, D. R., Saliba, R., Escalon, M. P., Hsu, Y., Ghosh, S., Ippoliti, C., Hicks, K., Donato, M., Giralt, S., Khouri, I. F., Hosing, C., Lima, M. J., Andersson, B., Neumann, J., & Champlin, R. (2005). Sirolimus in combination with tacrolimus and corticosteroids for the treatment of resistant chronic graft-versus-host disease. *British Journal of Haematology*, *130*(3), 409–417. https://doi.org/10.1111/j.1365-2141.2005.05616.x

Delaune, V., Berney, T., Lacotte, S., & Toso, C. (2017). Intraportal islet transplantation: The impact of the liver microenvironment. *Transplant International*, *30*(3), 227–238. https://doi.org/10.1111/tri.12919

Dias, A. D., Elicson, J. M., & Murphy, W. L. (2017). Microcarriers with synthetic hydrogel surfaces for stem cell expansion. *Advanced Healthcare Materials*, *6*(16). https://doi.org/10.1002/adhm.201700072

Diba, M., Spaans, S., Hendrikse, S. I. S., Bastings, M. M. C., Schotman, M. J. G., van Sprang, J. F., Wu, D. J., Hoeben, F. J. M., Janssen, H. M., & Dankers, P. Y. W. (2021). Engineering the dynamics of cell adhesion cues in supramolecular hydrogels for facile control over cell encapsulation and behavior. *Advanced Materials*, *33*(37), 2008111. https://doi.org/10.1002/adma.202008111

DiMaggio, P. A., Subramani, A., Judson, R. S., & Floudas, C. A. (2010). A novel framework for predicting in vivo toxicities from in vitro data using optimal methods for dense and sparse matrix reordering and logistic regression. *Toxicological Sciences*, *118*(1), 251–265. https://doi.org/10.1093/toxsci/kfq233

Dolgin, E. (2014). Encapsulate this. *Nature Medicine*, *20*(1), 9–11. https://doi.org/10.1038/nm0114-9

Dowarah, J., & Singh, V. P. (2020). Anti-diabetic drugs recent approaches and advancements. *Bioorganic & Medicinal Chemistry*, *28*(5), 115263. https://doi.org/10.1016/j.bmc.2019.115263

Dusseault, J., Langlois, G., Meunier, M., Menard, M., Perreault, C., & Halle, J. (2008). The effect of covalent cross-links between the membrane components of microcapsules on the dissemination of encapsulated malignant cells. *Biomaterials*, *29*(7), 917–924. https://doi.org/10.1016/j.biomaterials.2007.10.045

Efrat, S. (2002). Cell replacement therapy for type 1 diabetes. *Trends in Molecular Medicine*, *8*(7), 334–340. https://doi.org/10.1016/S1471-4914(02)02365-1

Eizirik, D. L., Pasquali, L., & Cnop, M. (2020). Pancreatic β-cells in type 1 and type 2 diabetes mellitus: Different pathways to failure. *Nature Reviews Endocrinology*, *16*(7), 349–362. https://doi.org/10.1038/s41574-020-0355-7

Elliott, A. D., Ustione, A., & Piston, D. W. (2015). Somatostatin and insulin mediate glucose-inhibited glucagon secretion in the pancreatic α-cell by lowering cAMP. *American Journal of Physiology-Endocrinology and Metabolism*, *308*(2), E130–E143. https://doi.org/10.1152/ajpendo.00344.2014

Erathodiyil, N., Chan, H.-M., Wu, H., & Ying, J. Y. (2020). Zwitterionic polymers and hydrogels for antibiofouling applications in implantable devices. *Materials Today*, *38*, 84–98. https://doi.org/10.1016/j.mattod.2020.03.024

Feau, S., Garcia, Z., Arens, R., Yagita, H., Borst, J., & Schoenberger, S. P. (2012). The CD4+ T-cell help signal is transmitted from APC to CD8+ T-cells via CD27–CD70 interactions. *Nature Communications*, *3*(1), 948–948. https://doi.org/10.1038/ncomms1948

Ferrannini, E., & Mari, A. (2004). Beta cell function and its relation to insulin action in humans: A critical appraisal. *Diabetologia*, *47*(5), 943–956. https://doi.org/10.1007/s00125-004-1381-z

Fielding, C. A., Jones, G. W., McLoughlin, R. M., McLeod, L., Hammond, V. J., Uceda, J., Williams, A. S., Lambie, M., Foster, T. L., Liao, C.-T., Rice, C. M., Greenhill, C. J., Colmont, C. S., Hams, E., Coles, B., Kift-Morgan, A., Newton, Z., Craig, K. J., Williams, J. D., … Jones, S. A. (2014). Interleukin-6 signaling drives fibrosis in unresolved inflammation. *Immunity*, *40*(1), 40–50. https://doi.org/10.1016/j.immuni.2013.10.022

Foretz, M., Guigas, B., & Viollet, B. (2019). Understanding the glucoregulatory mechanisms of metformin in type 2 diabetes mellitus. *Nature Reviews Endocrinology*, *15*(10), 569–589. https://doi.org/10.1038/s41574-019-0242-2

Freychet, L. (1988). Effect of intranasal glucagon on blood glucose levels in healthy subjects and hypoglycaemic patients with insulin-dependent diabetes. *The Lancet*, *331*(8599), 1364–1366. https://doi.org/10.1016/S0140-6736(88)92181-2

Fu, Z., R. Gilbert, E., & Liu, D. (2013). Regulation of insulin synthesis and secretion and pancreatic beta-cell dysfunction in diabetes. *Current Diabetes Reviews*, *9*(1), 25–53. https://doi.org/10.2174/157339913804143225

Fung, M., Thompson, D., Shapiro, R. J., Warnock, G. L., Andersen, D. K., Elahi, D., & Meneilly, G. S. (2006). Effect of glucagon-like peptide-1 (7–37) on beta-cell function after islet transplantation in type 1 diabetes. *Diabetes Research and Clinical Practice*, *74*(2), 189–193. https://doi.org/10.1016/j.diabres.2006.03.022

Gamble, A., Pepper, A. R., Bruni, A., & Shapiro, A. M. J. (2018). The journey of islet cell transplantation and future development. *Islets*, *10*(2), 80–94. https://doi.org/10.1080/19382014.2018.1428511

Gardner, C. M., Burke, N. A. D., Chu, T., Shen, F., Potter, M. A., & Stöver, H. D. H. (2011). Poly(methyl vinyl ether-alt-maleic acid) polymers for cell encapsulation. *Journal of Biomaterials Science, Polymer Edition*, *22*(16). https://doi.org/10.1163/092050610X535149

Gardner, C. M., Burke, N. A. D., & Stöver, H. D. H. (2010). Cross-linked microcapsules formed from self-deactivating reactive polyelectrolytes. *Langmuir*, *26*(7). https://doi.org/10.1021/la903540c

Gardner, C. M., Potter, M. A., & Stöver, H. D. H. (2012). Improving covalent cell encapsulation with temporarily reactive polyelectrolytes. *Journal of Materials Science: Materials in Medicine*, *23*(1), 181–193. https://doi.org/10.1007/s10856-011-4523-0

Ghofaili, K. A., Fung, M., Ao, Z., Meloche, M., Shapiro, R. J., Warnock, G. L., Elahi, D., Meneilly, G. S., & Thompson, D. M. (2007). Effect of exenatide on beta cell function after islet transplantation in type 1 diabetes. *Transplantation*, *83*(1), 24–28. https://doi.org/10.1097/01.tp.0000251379.46596.2d

Godek, M. L., Duchsherer, N. L., McElwee, Q., & Grainger, D. W. (2004). Morphology and growth of murine cell lines on model biomaterials. *Biomedical Sciences Instrumentation*, *40*, 7–12.

Gökçay Canpolat, A., & Şahin, M. (2020). Glucose lowering treatment modalities of type 2 diabetes mellitus. In Md. S. Islam (Ed.), *Diabetes: From Research to Clinical Practice* (Vol. 1307, pp. 7–27). Springer International Publishing. https://doi.org/10.1007/5584_2020_516

Goonoo, N., Fahmi, A., Jonas, U., Gimié, F., Arsa, I. A., Bénard, S., Schönherr, H., & Bhaw-Luximon, A. (2019). Improved multicellular response, biomimetic mineralization, angiogenesis, and reduced foreign body response of modified polydioxanone scaffolds for skeletal tissue regeneration. *ACS Applied Materials & Interfaces*, *11*(6), 5834–5850. https://doi.org/10.1021/acsami.8b19929

Goujon, L. J., Hariharan, S., Sayyar, B., Burke, N. A. D., Cranston, E. D., Andrews, D. W., & Stöver, H. D. H. (2015). Tunable hydrogel thin films from reactive synthetic polymers as potential two-dimensional cell scaffolds. *Langmuir*, *31*(20). https://doi.org/10.1021/acs.langmuir.5b00376

Grainger, D. W. (2013). All charged up about implanted biomaterials. *Nature Biotechnology*, *31*(6), 507–509. https://doi.org/10.1038/nbt.2600

Grant, J. S., & Graven, L. J. (2016). Progressing from metformin to sulfonylureas or meglitinides. *Workplace Health & Safety*, *64*(9), 433–439. https://doi.org/10.1177/2165079916644263

Grill, V., & Björklund, A. (2001). Overstimulation and beta-cell function. *Diabetes*, *50*(Supplement 1), S122–S124. https://doi.org/10.2337/diabetes.50.2007.S122

Gutch, M., Kumar, S., Razi, S., Gupta, K., & Gupta, A. (2015). Assessment of insulin sensitivity/resistance. *Indian Journal of Endocrinology and Metabolism*, *19*(1), 160. https://doi.org/10.4103/2230-8210.146874

Hastings, D. E., & Stöver, H. D. H. (2019). Crosslinked hydrogel capsules for cell encapsulation formed using amino/betaine dual-functional semibatch copolymers. *ACS Applied Polymer Materials*, *1*(8), 2055–2067. https://doi.org/10.1021/acsapm.9b00124

Hatziavramidis, D. T., Karatzas, T. M., & Chrousos, G. P. (2013). Pancreatic islet cell transplantation: An update. *Annals of Biomedical Engineering*, *41*(3), 469–476. https://doi.org/10.1007/s10439-012-0676-3

Health Quality Ontario. (2015). Pancreas islet transplantation for patients with type 1 diabetes mellitus: A clinical evidence review. *Ontario Health Technology Assessment Series*, *15*(16), 1–84.

Hering, B. J. (2005). Single-donor, marginal-dose islet transplantation in patients with type 1 diabetes. *JAMA*, *293*(7), 830. https://doi.org/10.1001/jama.293.7.830

Ishihara, K., Kitagawa, T., & Inoue, Y. (2015). Initial cell adhesion on well-defined surface by polymer brush layers with varying chemical structures. *ACS Biomaterials Science & Engineering*, *1*(2), 103–109. https://doi.org/10.1021/ab500048w

Ishikura, S., & Klip, A. (2008). Muscle cells engage Rab8A and myosin Vb in insulin-dependent GLUT4 translocation. *American Journal of Physiology-Cell Physiology*, *295*(4), C1016–C1025. https://doi.org/10.1152/ajpcell.00277.2008

Jacobs-Tulleneers-Thevissen, D., Chintinne, M., Ling, Z., Gillard, P., Schoonjans, L., Delvaux, G., Strand, B. L., Gorus, F., Keymeulen, B., & Pipeleers, D. (2013). Sustained function of alginate-encapsulated human islet cell implants in the peritoneal cavity of mice leading to a pilot study in a type 1 diabetic patient. *Diabetologia*, *56*(7), 1605–1614. https://doi.org/10.1007/s00125-013-2906-0

Jeon, H. B., Kang, D. H., Gu, J. H., & Oh, S. A. (2016). Delayed foreign body reaction caused by bioabsorbable plates used for maxillofacial fractures. *Archives of Plastic Surgery*, *43*(01), 40–45. https://doi.org/10.5999/aps.2016.43.1.40

Ježek, P., Jabůrek, M., Holendová, B., & Plecitá-Hlavatá, L. (2018). Fatty acid-stimulated insulin secretion vs. Lipotoxicity. *Molecules*, *23*(6), 1483. https://doi.org/10.3390/molecules23061483

Jiang, G., & Zhang, B. B. (2003). Glucagon and regulation of glucose metabolism. *American Journal of Physiology-Endocrinology and Metabolism*, *284*(4), E671–E678. https://doi.org/10.1152/ajpendo.00492.2002

Kahn, S. E. (2003). The relative contributions of insulin resistance and beta-cell dysfunction to the pathophysiology of type 2 diabetes. *Diabetologia*, *46*(1), 3–19. https://doi.org/10.1007/s00125-002-1009-0

Kahn, S. E., Hull, R. L., & Utzschneider, K. M. (2006). Mechanisms linking obesity to insulin resistance and type 2 diabetes. *Nature*, *444*(7121), 840–846. https://doi.org/10.1038/nature05482

Kahn, S. E., Prigeon, R. L., McCulloch, D. K., Boyko, E. J., Bergman, R. N., Schwartz, M. W., Neifing, J. L., Ward, W. K., Beard, J. C., & Palmer, J. P. (1993). Quantification of the relationship between insulin sensitivity and β-cell function in human subjects: Evidence for a hyperbolic function. *Diabetes*, *42*(11), 1663–1672. https://doi.org/10.2337/diab.42.11.1663

Kim, J., & Somorjai, G. A. (2003). Molecular packing of lysozyme, fibrinogen, and bovine serum albumin on hydrophilic and hydrophobic surfaces studied by infrared−visible sum frequency generation and fluorescence microscopy. *Journal of the American Chemical Society*, *125*(10), 3150–3158. https://doi.org/10.1021/ja028987n

King, A., Sandler, S., & Andersson, A. (2001). The effect of host factors and capsule composition on the cellular overgrowth on implanted alginate capsules. *Journal of Biomedical Materials Research*, *57*(3), 374–383. https://doi.org/10.1002/1097-4636(20011205)57:3<374::AID-JBM1180>3.0.CO;2-L

Kleinberger, R. M., Burke, N. A. D., Zhou, C., & Stöver, H. D. H. (2016). Synthetic polycations with controlled charge density and molecular weight as building blocks for biomaterials. *Journal of Biomaterials Science, Polymer Edition*, *27*(4), 351–369. https://doi.org/10.1080/09205063.2015.1130407

Klip, A., Sun, Y., Chiu, T. T., & Foley, K. P. (2014). Signal transduction meets vesicle traffic: The software and hardware of GLUT4 translocation. *American Journal of Physiology-Cell Physiology*, *306*(10), C879–C886. https://doi.org/10.1152/ajpcell.00069.2014

Komatsu, M., Schermerhorn, T., Noda, M., Straub, S. G., Aizawa, T., & Sharp, G. W. G. (1997). Augmentation of insulin release by glucose in the absence of extracellular Ca2+: New insights into stimulus-secretion coupling. *Diabetes*, *46*(12), 1928–1938. https://doi.org/10.2337/diab.46.12.1928

Kulseng, B., Skjåk-Bræk, G., Følling, I., & Espevik, T. (1996). TNF production from peripheral blood mononuclear cells in diabetic patients after stimulation with alginate and lipopolysaccharide. *Scandinavian Journal of Immunology*, *43*(3), 335–340. https://doi.org/10.1046/j.1365-3083.1996.d01-43.x

Lamos, E. L., Stein, S. A., & Davis, S. N. (2013). Sulfonylureas and meglitinides: Historical and contemporary issues. *Panminerva Medica*, *55*(3), 239–251.

Lang, J. (1999). Molecular mechanisms and regulation of insulin exocytosis as a paradigm of endocrine secretion. *European Journal of Biochemistry*, *259*(1–2), 3–17. https://doi.org/10.1046/j.1432-1327.1999.00043.x

Largiadèr, F., Kolb, E., & Binswanger, U. (1980). A long-term functioning human pancreatic islet allotransplant. *Transplantation*, *29*(1), 76. https://doi.org/10.1097/00007890-198001000-00017

Lavin, D. P., White, M. F., & Brazil, D. P. (2016). IRS proteins and diabetic complications. *Diabetologia*, *59*(11), 2280–2291. https://doi.org/10.1007/s00125-016-4072-7

Lebovitz, H. E., & Melander, A. (2015). Sulfonylureas and meglitinides: Insights into physiology and translational clinical utility. In R. A. DeFronzo, E. Ferrannini, P. Zimmet, & K. G. M. M. Alberti (Eds.), *International Textbook of Diabetes Mellitus* (pp. 615–640). John Wiley & Sons, Ltd. https://doi.org/10.1002/9781118387658.ch42

Lee, K. Y., & Mooney, D. J. (2012). Alginate: Properties and biomedical applications. *Progress in Polymer Science*, *37*(1), 106–126. https://doi.org/10.1016/j.progpolymsci.2011.06.003

Li, W., Lei, X., Feng, H., Li, B., Kong, J., & Xing, M. (2022). Layer-by-layer cell encapsulation for drug delivery: The history, technique basis, and applications. *Pharmaceutics*, *14*(2), 297. https://doi.org/10.3390/pharmaceutics14020297

Liu, Q., Chiu, A., Wang, L.-H., An, D., Zhong, M., Smink, A. M., de Haan, B. J., de Vos, P., Keane, K., Vegge, A., Chen, E. Y., Song, W., Liu, W. F., Flanders, J., Rescan, C., Grunnet, L. G., Wang, X., & Ma, M. (2019). Zwitterionically modified alginates mitigate cellular overgrowth for cell encapsulation. *Nature Communications*, *10*(1), 5262. https://doi.org/10.1038/s41467-019-13238-7

Lopez-Mendez, T. B., Santos-Vizcaino, E., Pedraz, J. L., Orive, G., & Hernandez, R. M. (2021). Cell microencapsulation technologies for sustained drug delivery: Latest advances in efficacy and biosafety. *Journal of Controlled Release*, *335*, 619–636. https://doi.org/10.1016/j.jconrel.2021.06.006

Ma, Z., Yue, Y., Luo, Y., Wang, W., Cao, Y., & Fang, Q. (2020). Clinical utility of the inflammatory factors combined with lipid markers in the diagnostic and prognostic assessment of ischemic stroke: Based on logistic regression models. *Journal of Stroke and Cerebrovascular Diseases*, *29*(4), 104653. https://doi.org/10.1016/j.jstrokecerebrovasdis.2020.104653

MacDonald, P. E., Ha, X. F., Wang, J., Smukler, S. R., Sun, A. M., Gaisano, H. Y., Salapatek, A. M. F., Backx, P. H., & Wheeler, M. B. (2001). Members of the Kv1 and Kv2 voltage-dependent K+ channel families regulate insulin secretion. *Molecular Endocrinology*, *15*(8), 1423–1435. https://doi.org/10.1210/mend.15.8.0685

MacDonald, P. E., Joseph, J. W., & Rorsman, P. (2005). Glucose-sensing mechanisms in pancreatic β-cells. *Philosophical Transactions of the Royal Society B: Biological Sciences*, *360*(1464), 2211–2225. https://doi.org/10.1098/rstb.2005.1762

Mackie, G., Gao, L., Yau, S., Leslie, D. C., & Waterhouse, A. (2019). Clinical potential of immobilized liquid interfaces: Perspectives on biological interactions. *Trends in Biotechnology*, *37*(3), 268–280. https://doi.org/10.1016/j.tibtech.2018.08.003

Major, M. R., Wong, V. W., Nelson, E. R., Longaker, M. T., & Gurtner, G. C. (2015). The foreign body response: At the interface of surgery and bioengineering. *Plastic and Reconstructive Surgery*, *135*(5), 1489–1498. https://doi.org/10.1097/PRS.0000000000001193

Maloy, M. H., Ferrer, M. A., & Parashurama, N. (2020). In vivo differentiation of stem cell-derived human pancreatic progenitors to treat type 1 diabetes. *Stem Cell Reviews and Reports*, *16*(6), 1139–1155. https://doi.org/10.1007/s12015-020-10018-5

McCullagh, P., & Nelder, J. A. (2019). *Generalized linear models* (2nd ed.). Routledge. https://doi.org/10.1201/9780203753736

McInnes, N., Hall, S., Sultan, F., Aronson, R., Hramiak, I., Harris, S., Sigal, R. J., Woo, V., Liu, Y. Y., & Gerstein, H. C. (2020). Remission of type 2 diabetes following a short-term intervention with insulin glargine, metformin, and dapagliflozin. *The Journal of Clinical Endocrinology & Metabolism*, *105*(8), 2532–2540. https://doi.org/10.1210/clinem/dgaa248

Moghissi, E., Korytkowski, M., DiNardo, M., Einhorn, D., Hellman, R., Hirsch, I., Inzucchi, S., Ismail-Beigi, F., Kirkman, M., & Umpierrez, G. (2009). American Association of Clinical Endocrinologists and American Diabetes Association consensus statement on inpatient glycemic control. *Endocrine Practice*, *15*(4), 353–369. https://doi.org/10.4158/EP09102.RA

Morin, E. A., & He, W. (2017). *In vitro* study of central nervous system foreign body response towards hydrogel particle modified planar substrate. *Journal of Biomedical Materials Research Part A*, *105*(12), 3242–3250. https://doi.org/10.1002/jbm.a.36180

Nanji, S. A., & Shapiro, A. M. J. (2004). Islet transplantation in patients with diabetes mellitus. *BioDrugs*, *18*(5), 315–328. https://doi.org/10.2165/00063030-200418050-00004

Nicholson, T., Church, C., Baker, D. J., & Jones, S. W. (2018). The role of adipokines in skeletal muscle inflammation and insulin sensitivity. *Journal of Inflammation*, *15*(1), 9. https://doi.org/10.1186/s12950-018-0185-8

Nifontova, G., Ramos-Gomes, F., Baryshnikova, M., Alves, F., Nabiev, I., & Sukhanova, A. (2019). Cancer cell targeting with functionalized quantum dot-encoded polyelectrolyte microcapsules. *Frontiers in Chemistry*, *7*, 34. https://doi.org/10.3389/fchem.2019.00034

Nir, T., Melton, D. A., & Dor, Y. (2007). Recovery from diabetes in mice by β cell regeneration. *Journal of Clinical Investigation*, *117*(9), 2553–2561. https://doi.org/10.1172/JCI32959

Ogurtsova, K., da Rocha Fernandes, J. D., Huang, Y., Linnenkamp, U., Guariguata, L., Cho, N. H., Cavan, D., Shaw, J. E., & Makaroff, L. E. (2017). IDF Diabetes Atlas: Global estimates for the prevalence of diabetes for 2015 and 2040. *Diabetes Research and Clinical Practice*, *128*, 40–50. https://doi.org/10.1016/j.diabres.2017.03.024

O'Neill, H. M. (2013). AMPK and exercise: Glucose uptake and insulin sensitivity. *Diabetes & Metabolism Journal*, *37*(1), 1. https://doi.org/10.4093/dmj.2013.37.1.1

Orci, L., Malaisse-Lagae, F., Ravazzola, M., Amherdt, M., & Renold, A. E. (1973). Exocytosis-endocytosis coupling in the pancreatic beta cell. *Science*, *181*(4099), 561–562. https://doi.org/10.1126/science.181.4099.561

Ørning, P., Hoem, K. S., Coron, A. E., Skjåk-Bræk, G., Mollnes, T. E., Brekke, O.-L., Espevik, T., & Rokstad, A. M. (2016). Alginate microsphere compositions dictate different mechanisms of complement activation with consequences for cytokine release and leukocyte activation. *Journal of Controlled Release*, *229*, 58–69. https://doi.org/10.1016/j.jconrel.2016.03.021

Otsuka, H., & Moskowitz, M. (1976). Arrest of 3T3 cells in G1 phase in suspension culture. *Journal of Cellular Physiology*, *87*(2). https://doi.org/10.1002/jcp.1040870209

Paez-Mayorga, J., Lukin, I., Emerich, D., de Vos, P., Orive, G., & Grattoni, A. (2022). Emerging strategies for beta cell transplantation to treat diabetes. *Trends in Pharmacological Sciences*, *43*(3), 221–233. https://doi.org/10.1016/j.tips.2021.11.007

Pansu, M., & Gautheyrou, J. (2006). *Handbook of soil analysis: Mineralogical, organic and inorganic methods*. Springer.

Petersen, M. C., & Shulman, G. I. (2018). Mechanisms of insulin action and insulin resistance. *Physiological Reviews*, *98*(4), 2133–2223. https://doi.org/10.1152/physrev.00063.2017

Pi, J., Zhang, Q., Fu, J., Woods, C. G., Hou, Y., Corkey, B. E., Collins, S., & Andersen, M. E. (2010). ROS signaling, oxidative stress and Nrf2 in pancreatic beta-cell function. *Toxicology and Applied Pharmacology*, *244*(1), 77–83. https://doi.org/10.1016/j.taap.2009.05.025

Piya, M. K., Tahrani, A. A., & Barnett, A. H. (2010). Emerging treatment options for type 2 diabetes. *British Journal of Clinical Pharmacology*, *70*(5), 631–644. https://doi.org/10.1111/j.1365-2125.2010.03711.x

Prasetyo, R. B., Kuswanto, H., Iriawan, N., & Ulama, B. S. S. (2020). Binomial regression models with a flexible generalized logit link function. *Symmetry*, *12*(2), 221. https://doi.org/10.3390/sym12020221

R Core Team. (2019). *R: A language and environment for statistical computing*. R Foundation for Statistical Computing. https://www.r-project.org/

Rachdaoui, N. (2020). Insulin: The friend and the foe in the development of type 2 diabetes mellitus. *International Journal of Molecular Sciences*, *21*(5), 1770. https://doi.org/10.3390/ijms21051770

Ramadan, J. W., Steiner, S. R., O'Neill, C. M., & Nunemaker, C. S. (2011). The central role of calcium in the effects of cytokines on beta-cell function: Implications for type 1 and type 2 diabetes. *Cell Calcium*, *50*(6), 481–490. https://doi.org/10.1016/j.ceca.2011.08.005

Rätzsch, M. (1988). Alternating maleic anhydride copolymers. *Progress in Polymer Science*, *13*(4). https://doi.org/10.1016/0079-6700(88)90001-9

Ravier, M. A., & Rutter, G. A. (2005). Glucose or insulin, but not zinc ions, inhibit glucagon secretion from mouse pancreatic α-cells. *Diabetes*, *54*(6), 1789–1797. https://doi.org/10.2337/diabetes.54.6.1789

Ros, S., Burke, N. A. D., & Stöver, H. D. H. (2015). Synthesis and properties of charge-shifting polycations: Poly[3-aminopropylmethacrylamide-co-2-(dimethylamino)ethyl acrylate]. *Macromolecules*, *48*(24). https://doi.org/10.1021/acs.macromol.5b02191

Ryan, J. G. (2009). Cost and policy implications from the increasing prevalence of obesity and diabetes mellitus. *Gender Medicine*, *6*, 86–108. https://doi.org/10.1016/j.genm.2009.01.002

Safley, S. A., Cui, H., Cauffiel, S., Tucker-Burden, C., & Weber, C. J. (2008). Biocompatibility and immune acceptance of adult porcine islets transplanted intraperitoneally in diabetic NOD mice in calcium alginate poly-L-lysine microcapsules versus barium alginate microcapsules without poly-L-lysine. *Journal of Diabetes Science and Technology*, *2*(5), 760–767. https://doi.org/10.1177/193229680800200503

Salib, A., Cayabyab, F., & Yoshihara, E. (2022). Stem cell-derived islets for type 2 diabetes. *International Journal of Molecular Sciences*, *23*(9), 5099. https://doi.org/10.3390/ijms23095099

Sano, H., Kane, S., Sano, E., Mîinea, C. P., Asara, J. M., Lane, W. S., Garner, C. W., & Lienhard, G. E. (2003). Insulin-stimulated phosphorylation of a Rab GTPase-activating protein regulates GLUT4 translocation. *Journal of Biological Chemistry*, *278*(17), 14599–14602. https://doi.org/10.1074/jbc.C300063200

Santos, E., Zarate, J., Orive, G., Hernández, R. M., & Pedraz, J. L. (2010). Biomaterials in cell microencapsulation. In J. L. Pedraz & G. Orive (Eds.), *Therapeutic Applications of Cell Microencapsulation* (Vol. 670, pp. 5–21). Springer New York. https://doi.org/10.1007/978-1-4419-5786-3_2

Sato, Y., & Henquin, J. C. (1998). The K+-ATP channel-independent pathway of regulation of insulin secretion by glucose: In search of the underlying mechanism. *Diabetes*, *47*(11), 1713–1721. https://doi.org/10.2337/diabetes.47.11.1713

Scharfmann, R., Staels, W., & Albagli, O. (2019). The supply chain of human pancreatic β cell lines. *Journal of Clinical Investigation*, *129*(9), 3511–3520. https://doi.org/10.1172/JCI129484

Scharp, D. W., Lacy, P. E., Santiago, J. V., McCullough, C. S., Weide, L. G., Falqui, L., Marchetti, P., Gingerich, R. L., Jaffe, A. S., Cryer, P. E., Anderson, C. B., & Flye, M. W. (1990). Insulin independence after islet transplantation into type I diabetic patient. *Diabetes*, *39*(4), 515–518. https://doi.org/10.2337/diab.39.4.515

Scharp, D. W., & Marchetti, P. (2014). Encapsulated islets for diabetes therapy: History, current progress, and critical issues requiring solution. *Advanced Drug Delivery Reviews*, *67–68*, 35–73. https://doi.org/10.1016/j.addr.2013.07.018

Schneider, G. B., English, A., Abraham, M., Zaharias, R., Stanford, C., & Keller, J. (2004). The effect of hydrogel charge density on cell attachment. *Biomaterials*, *25*(15), 3023–3028. https://doi.org/10.1016/j.biomaterials.2003.09.084

Shah, S. C., Malone, J., & Simpson, N. E. (1989). A randomized trial of intensive insulin therapy in newly diagnosed insulin-dependent diabetes mellitus. *New England Journal of Medicine*, *320*(9). https://doi.org/10.1056/NEJM198903023200902

Shapiro, A. M. J., Gallant, H. L., Hao, E. G., Lakey, J. R. T., McCready, T., Rajotte, R. V., Yatscoff, R. W., & Kneteman, N. M. (2005). The portal Immunosuppressive storm: Relevance to islet transplantation? *Therapeutic Drug Monitoring*, *27*(1), 35–37. https://doi.org/10.1097/00007691-200502000-00008

Shapiro, A. M. J., Lakey, J. R. T., Ryan, E. A., Korbutt, G. S., Toth, E., Warnock, G. L., Kneteman, N. M., & Rajotte, R. V. (2000). Islet transplantation in seven patients with type 1 diabetes mellitus using a glucocorticoid-free immunosuppressive regimen. *New England Journal of Medicine*, *343*(4), 230–238. https://doi.org/10.1056/NEJM200007273430401

Shapiro, A. M. J., Ryan, E. A., & Lakey, J. R. T. (2001). Islet cell transplantation. *The Lancet*, *358*, S21. https://doi.org/10.1016/S0140-6736(01)07034-9

Shaw, J. E., Sicree, R. A., & Zimmet, P. Z. (2010). Global estimates of the prevalence of diabetes for 2010 and 2030. *Diabetes Research and Clinical Practice*, *87*(1), 4–14. https://doi.org/10.1016/j.diabres.2009.10.007

Sheikh, Z., Brooks, P., Barzilay, O., Fine, N., & Glogauer, M. (2015). Macrophages, foreign body giant cells and their response to implantable biomaterials. *Materials*, *8*(9), 5671–5701. https://doi.org/10.3390/ma8095269

Shen, F., Mazumder, M. A. J., Burke, N. A. D., Stöver, H. D. H., & Potter, M. A. (2008). Mechanically enhanced microcapsules for cellular gene therapy. *Journal of Biomedical Materials Research Part B: Applied Biomaterials*, *90B*(1), 350–361. https://doi.org/10.1002/jbm.b.31292

Shoelson, S. E. (2006). Inflammation and insulin resistance. *Journal of Clinical Investigation*, *116*(7), 1793–1801. https://doi.org/10.1172/JCI29069

Sigler, E. J., Randolph, J. C., & Charles, S. (2014). Foreign body response within postoperative perfluoro-n-octane for retinal detachment repair: Clinical features, grading system, and histopathology. *Retina*, *34*(2), 237–246. https://doi.org/10.1097/IAE.0b013e31829d002e

Smith, D., Herman, C., Razdan, S., Abedin, M. R., Stoecker, W. V., & Barua, S. (2019). Microparticles for suspension culture of mammalian cells. *ACS Applied Bio Materials*, *2*(7), 2791–2801. https://doi.org/10.1021/acsabm.9b00215

Smyth, S., & Heron, A. (2006). Diabetes and obesity: The twin epidemics. *Nature Medicine*, *12*(1), 75–80. https://doi.org/10.1038/nm0106-75

Srinivasan, P., Huang, G. C., Amiel, S. A., & Heaton, N. D. (2007). Islet cell transplantation. *Postgraduate Medical Journal*, *83*(978), 224–229. https://doi.org/10.1136/pgmj.2006.053447

Steiner, D. F. (2011). On the discovery of precursor processing. In M. Mbikay & N. G. Seidah (Eds.), *Proprotein Convertases* (Vol. 768, pp. 3–11). Humana Press. https://doi.org/10.1007/978-1-61779-204-5_1

Stonehouse, A. H., Darsow, T., & Maggs, D. G. (2012). Incretin-based therapies: Incretin therapies. *Journal of Diabetes*, *4*(1), 55–67. https://doi.org/10.1111/j.1753-0407.2011.00143.x

Støy, J., De Franco, E., Ye, H., Park, S.-Y., Bell, G. I., & Hattersley, A. T. (2021). In celebration of a century with insulin – Update of insulin gene mutations in diabetes. *Molecular Metabolism*, *52*, 101280. https://doi.org/10.1016/j.molmet.2021.101280

Strand, B. L., Ryan, L., Veld, P. I., Kulseng, B., Rokstad, A. M., Skjåk-Bræk, G., & Espevik, T. (2001). Poly-L-Lysine induces fibrosis on alginate microcapsules via the induction of cytokines. *Cell Transplantation*, *10*(3). https://doi.org/10.3727/000000001783986800

Swartzlander, M. D., Barnes, C. A., Blakney, A. K., Kaar, J. L., Kyriakides, T. R., & Bryant, S. J. (2015). Linking the foreign body response and protein adsorption to PEG-based hydrogels using proteomics. *Biomaterials*, *41*, 26–36. https://doi.org/10.1016/j.biomaterials.2014.11.026

Tang, L., Ugarova, T. P., Plow, E. F., & Eaton, J. W. (1996). Molecular determinants of acute inflammatory responses to biomaterials. *Journal of Clinical Investigation*, *97*(5), 1329–1334. https://doi.org/10.1172/JCI118549

Thangavel, N., Al Bratty, M., Akhtar Javed, S., Ahsan, W., & Alhazmi, H. A. (2017). Targeting peroxisome proliferator-activated receptors using thiazolidinediones: Strategy for design of novel antidiabetic drugs. *International Journal of Medicinal Chemistry*, *2017*, 1–20. https://doi.org/10.1155/2017/1069718

Tomita, T. (2017). Apoptosis of pancreatic β-cells in type 1 diabetes. *Bosnian Journal of Basic Medical Sciences*. https://doi.org/10.17305/bjbms.2017.1961

Tuch, B. E., Keogh, G. W., Williams, L. J., Wu, W., Foster, J. L., Vaithilingam, V., & Philips, R. (2009). Safety and viability of microencapsulated human islets transplanted into diabetic humans. *Diabetes Care*, *32*(10), 1887–1889. https://doi.org/10.2337/dc09-0744

Unger, R. H., & Orci, L. (2010). Paracrinology of islets and the paracrinopathy of diabetes. *Proceedings of the National Academy of Sciences*, *107*(37), 16009–16012. https://doi.org/10.1073/pnas.1006639107

Vaithilingam, V., Kollarikova, G., Qi, M., Larsson, R., Lacik, I., Formo, K., Marchese, E., Oberholzer, J., Guillemin, G. J., & Tuch, B. E. (2014). Beneficial effects of coating alginate microcapsules with macromolecular heparin conjugates– *in vitro* and *in vivo* study. *Tissue Engineering Part A*, *20*(1–2), 324–334. https://doi.org/10.1089/ten.tea.2013.0254

Vegas, A. J., Veiseh, O., Doloff, J. C., Ma, M., Tam, H. H., Bratlie, K., Li, J., Bader, A. R., Langan, E., Olejnik, K., Fenton, P., Kang, J. W., Hollister-Locke, J., Bochenek, M. A., Chiu, A., Siebert, S., Tang, K., Jhunjhunwala, S., Aresta-Dasilva, S., … Anderson, D. G. (2016). Combinatorial hydrogel library enables identification of materials that mitigate the foreign body response in primates. *Nature Biotechnology*, *34*(3), 345–352. https://doi.org/10.1038/nbt.3462

Vegas, A. J., Veiseh, O., Gürtler, M., Millman, J. R., Pagliuca, F. W., Bader, A. R., Doloff, J. C., Li, J., Chen, M., Olejnik, K., Tam, H. H., Jhunjhunwala, S., Langan, E., Aresta-Dasilva, S., Gandham, S., McGarrigle, J. J., Bochenek, M. A., Hollister-Lock, J., Oberholzer, J., … Anderson, D. G. (2016). Long-term glycemic control using polymer-encapsulated human stem cell–derived beta cells in immune-competent mice. *Nature Medicine*, *22*(3), 306–311. https://doi.org/10.1038/nm.4030

Veiseh, O., Doloff, J. C., Ma, M., Vegas, A. J., Tam, H. H., Bader, A. R., Li, J., Langan, E., Wyckoff, J., Loo, W. S., Jhunjhunwala, S., Chiu, A., Siebert, S., Tang, K., Hollister-Lock, J., Aresta-Dasilva, S., Bochenek, M., Mendoza-Elias, J., Wang, Y., … Anderson, D. G. (2015). Size- and shape-dependent foreign body immune response to materials implanted in rodents and non-human primates. *Nature Materials*, *14*(6), 643–651. https://doi.org/10.1038/nmat4290

Verma, S., & Hussain, M. E. (2017). Obesity and diabetes: An update. *Diabetes & Metabolic Syndrome: Clinical Research & Reviews*, *11*(1), 73–79. https://doi.org/10.1016/j.dsx.2016.06.017

Vidnes, J., & Øyasaeter, S. (1977). Glucagon deficiency causing severe neonatal hypoglycemia in a patient with normal insulin secretion. *Pediatric Research*, *11*(9), 943–949. https://doi.org/10.1203/00006450-197709000-00001

Vlahos, A. E., & Sefton, M. V. (2018). Muted fibrosis from protected islets. *Nature Biomedical Engineering*, *2*(11). https://doi.org/10.1038/s41551-018-0316-9

Watad, A., Rosenberg, V., Tiosano, S., Cohen Tervaert, J. W., Yavne, Y., Shoenfeld, Y., Shalev, V., Chodick, G., & Amital, H. (2018). Silicone breast implants and the risk of autoimmune/rheumatic disorders: A real-world analysis. *International Journal of Epidemiology*, *47*(6), 1846–1854. https://doi.org/10.1093/ije/dyy217

Wermuth, P. J., & Jimenez, S. A. (2015). The significance of macrophage polarization subtypes for animal models of tissue fibrosis and human fibrotic diseases. *Clinical and Translational Medicine*, *4*(1). https://doi.org/10.1186/s40169-015-0047-4

White, M. F. (2006). Regulating insulin signaling and β-cell function through IRS proteins. *Canadian Journal of Physiology and Pharmacology*, *84*(7), 725–737. https://doi.org/10.1139/y06-008

Wild, S., Roglic, G., Green, A., Sicree, R., & King, H. (2004). Global prevalence of diabetes: Estimates for the year 2000 and projections for 2030. *Diabetes Care*, *27*(5), 1047–1053. https://doi.org/10.2337/diacare.27.5.1047

Witherel, C. E., Abebayehu, D., Barker, T. H., & Spiller, K. L. (2019). Macrophage and fibroblast interactions in biomaterial-mediated fibrosis. *Advanced Healthcare Materials*, 1801451. https://doi.org/10.1002/adhm.201801451

Xia, F., Xie, L., Mihic, A., Gao, X., Chen, Y., Gaisano, H. Y., & Tsushima, R. G. (2008). Inhibition of cholesterol biosynthesis impairs insulin secretion and voltage-gated calcium channel function in pancreatic β-cells. *Endocrinology*, *149*(10), 5136–5145. https://doi.org/10.1210/en.2008-0161

Yasuda, H., Jin, Z., Nakayama, M., Yamada, K., Kishi, M., Okumachi, Y., Arai, T., Moriyama, H., Yokono, K., & Nagata, M. (2009). NO-mediated cytotoxicity contributes to multiple low-dose streptozotocin-induced diabetes but not to NOD diabetes. *Diabetes Research and Clinical Practice*, *83*(2), 200–207. https://doi.org/10.1016/j.diabres.2008.11.029

Zelová, H., & Hošek, J. (2013). TNF-α signalling and inflammation: Interactions between old acquaintances. *Inflammation Research*, *62*(7), 641–651. https://doi.org/10.1007/s00011-013-0633-0

Zhang, J.-J., Hong, J., Ma, Y.-S., Shi, Y., Zhang, D.-D., Yang, X.-L., Jia, C.-Y., Yin, Y.-Z., Jiang, G.-X., Fu, D., & Yu, F. (2021). Identified GNGT1 and NMU as combined diagnosis biomarker of non-small-cell lung cancer utilizing bioinformatics and logistic regression. *Disease Markers*, *2021*, 1–14. https://doi.org/10.1155/2021/6696198

Zhang, Q., Gonelle-Gispert, C., Li, Y., Geng, Z., Gerber-Lemaire, S., Wang, Y., & Buhler, L. (2022). Islet encapsulation: New developments for the treatment of type 1 diabetes. *Frontiers in Immunology*, *13*, 869984. https://doi.org/10.3389/fimmu.2022.869984

Zheng, S., & Liu, Z. (2021). The machine learning embedded method of parameters determination in the constitutive models and potential applications for hydrogels. *International Journal of Applied Mechanics*, *13*(01), 2150001. https://doi.org/10.1142/S1758825121500010